ERROR COMPENSATION AND UNCERTAINTY EVALUATION OF CMMs BASED ON KINEMATIC ERROR MODELS AND GAUSSIAN PROCESSES

A thesis submitted for the degree of Master of Philosophy

by

Panadda Salacheep

Department of Mechanical, Aerospace &
Civil Engineering

Brunel University London

October 2016

Abstract

Given the increasing demand for precision engineering applications, the evaluation of measurement error and uncertainty has been the focus of intensive research to meet the requirements of precision manufacturing processes. Systematic errors of mechanical components affect the accuracy of the production parts. It is therefore best to analyse the geometric accuracy of machine tools before production processes begin. This proposed method is based on simulation in the MATLAB programme, which investigates the influence of the geometric errors of the Coordinate Measuring Machine (CMM) on the calibration. The advantages of this measurement procedure are reduced physical measuring times, reduced measurement uncertainties as well as volumetric measurement, and compensation for CMM geometric errors.

In this research, theoretical modelling of the local, kinematic error model and the Gaussian Process (GP) model are presented and explored in depth. These proposed methods are simulations providing an integrated virtual environment in which user can generate the inspection path planning for specific tasks and evaluate the errors and uncertainty associated with the measurement results, all without the need to perform a number of physical CMM measurements. The estimated errors and uncertainty can serve as rapid feedback for users before performing actual measurements or as a prior evaluation of the results of the CMM calibrations.

The estimation of CMM geometric errors are usually described using 21 kinematic errors which consist of three positional and three rotational error functions for each of the three axes, along with three squareness errors. This assumes that the method to estimate of these kinematic errors can be generated by performing an artefact measurement such as for a hole or a ball plate in the numbers of the positions of the CMM working region and then matching the kinematic errors to the measured changes in artefact geometry.

The process validation of a local, kinematic error model and a GP model has been determined with the design and analysis of CMM measurement using a ball plate as an artefact, calculating the percentage error to compare their effective results.

This research project has led to the following contribution to knowledge:

- Mathematical model development for making effective choices regarding the local, kinematic error model and GP model is performed and formulated; this is verified by particular kinematic errors of the CMM measurements, presenting high accuracy and reliability of the error and uncertainty evaluation performance.
- The improvement achieved by the proposed method over the traditional approaches between the simulated datasets and actual CMM data measurements has been demonstrated.
- The numerical simulations with a well-designed strategy providing accurate estimates of the CMM kinematic errors using only a nominal CMM calibration with a ball plate have been validated and evaluated in both approaches.
- The influences of kinematic errors affected through the measurement process of the CMM on the calibration have been investigated.

Acknowledgements

This thesis would not have been possible without the supervision from my supervisor, Dr QingPing Yang for providing me the opportunity to do MPhil at Department of Mechanical, Aerospace & Civil Engineering, Brunel University. His support has been invaluable on both an academic and a personal level.

I would like to express my deeply sincere gratitude to Prof. Alistair B. Forbes, National Physical Laboratory (NPL) for giving me the best opportunity to carry out this research. I am extremely grateful for his enthusiastic support and encouragement in all aspects.

The thanks are also extended to my lecturers in Department of Physics, Faculty of Sciences, Kasetsart University in Thailand for all the support for my study

I wish to express my warm and sincere thanks to Thammarat Somthong, Dr Narin Chanthawong, Dr Jariya Buajarern, Dr Wiroj Sudatham and Dr Ketsaya Vatcharanukul for their close support during the experimental work for developing laboratory skills, simulation techniques and discussions. Also, I would like to greatly thank all my seniors at National Institue of Metrology Thailand (NIMT). Their support and guidance have been of great value in this study.

My sincere thanks are due to friends and staffs in Advanced Manufacturing and Enterprise Engineering at Brunel University. Special thanks are also to my senior, Dr Worapong Sawangsri for the support and valuable discussions in this research.

I would like to thank to the Royal Thai Government, Ministry of Sciences and Technology and National Institute of Metrology Thailand (NIMT) for awarding me this scholarship. I also wish to extend my warmest thank to friends and colleagues in Thailand, friends in Brunel University, Gerrards Cross and Denham Green (UK) for their friendly and cheerful.

Finally, my special gratitude is due to my parents, my aunt, my sisters and all my relatives. Without their love and encouragement it would have been impossible for me to finish this work.

Table of Contents

Abbreviations

BIPM	Bureau International des Poids et Mesures
BS	The British Standard Institution
CAD	Computer Aided Design
CAM	Computer Aided Manufacturing
CG	Scientific Computing method
CIPM	Comité International des Poids et Mesures
CMM	Coordinate Measuring Machine
CNC CMM	Computer Numerical Control Coordinate Measurement Machine
CNC	Computer Numerical Control
DCC CMM	Direct Computer Control Coordinated Measurement Machine
DCC	Direct Computer Control
DEA	Digital Electric Automation
DMIS	Dimensional Measurement Interface Specification
GP	Gaussian Process
GPML	Gaussian Processes for Maching Learning Matlab code
GUM	Guide to the expression of uncertainty in measurement
IEC	the International Electrotechnical Commission
IFCC	the International Federation for Clinical Chemistry and Laboratory Medicine
ILAC	the International Laboratory Accreditation Cooperation
IMS	International Metrology System Institute of Germany
ISO	International Organisation for Standardization

IUPAC	the International Organization for Pure and Applied Chemistry
IUPAP	the International Organization for Pure and Applied Physics
JCGM	Joint Committee for Guides in Metrology
NPL	The National Physical Laboratory
OIML	the International Organization of Legal Metrolog
PTB	Physikalisch-Technische Bundesabstalt, The National Metrology
SPC	Statistical Process Control software

Nomenclature

δl_n	Correction due to reflective index of air
Δt_x	Correction due to the temperature different between the ball plate with reference standard
δt_d	Correction for distribution temperature of the ball plate
δt_m	Correction for temperature measuring device
$\delta\alpha$	Correction for the thermal expansion coefficient of the ball plate
l_x	Length of the ball plate observed
l_0	Nominal length of the ball plate considered
α	The thermal expansion coefficient of the ball plate
δl_{is}	Correction for the errors of indication of the CMM
δl_{Ax}	Correction due to miss-alignment of ball plate
δl_{RP}	Correction due to reproducibility of probe system
δl_{vm}	Deviation of verification measurement;
(x_i, y_i)	Data points
$R_x'(x_i)$	The capacitive probe reading in x-axis
$R_y'(x_i)$	The capacitive probe reading in y-axis
$R_z'(x_i)$	The capacitive probe reading in z-axis
(x_a , y_a)	The values of coordinate point A
(x_b , y_b)	The values of coordinate point B
d_i	The gradient
l_i , l_{in}	distance between the probe tip and the pivot point of the ball joint

l_{max}	Maximum extensions of the legs
l_{min}	Minimum extensions of the legs
p_0	The probe tip
p_i	The pivot point of the ball joint
s^*	The CMM measured point
x^*	Positional correction for x
y^*	Positional correction for y
z^*	Positional correction for z
δu_i	The *u* direction of the ball surface
δv_i	The *v* direction of the ball surface
$\delta_x(x_i)$	The position error of x motion
δ_{xx}	x-axis scale error
δ_{xy}	x-axis straightness error in y direction
δ_{xz}	x-axis straightness error in z direction
$\delta_y(x_i)$	The straightness error
$\delta_z(x_i)$	The straightness error
ε_{align}	Misalignment of the material standard of size
ε_{cal}	Calibration error of the material standard of size
ε_{fixt}	Error due to the fixturing of the material standard of size
ε_t	Error due to the input of the temperature of the material standard of size
ε_α	Error due to the input of the CTE of the material standard of size
θ_i	the angle between tetrahedron legs with the angles
σ_f^2	The maximum allowable covariance
a	The parameters
e(x, b)	A Gaussian distribution effect

F	The form error of the test sphere
$f(x + a)$	The response function from the known effects
J	The $m\ x\ n$ Jacobian matrix
L	The nominal length of the ball plate (mm.)
m	Mean function
p	The probe offset
P	Air pressure (Pascal)
R	Relative humidity (percent)
r	Rotational Deviations
$R_x(x, r)$	Rotation matrix
$R_x(x,y,z)$	Rotational error along x-axis
$R_y(x,y,z)$	Rotational error along y-axis
$R_z(x,y,z)$	Rotational error along z-axis
T	Temperature (degrees Celsius)
t	Straightness Deviations
$u(F)$	The standard uncertainty of the form error
$u(P_{cal})$	Uncertainty of air pressure from certificate of calibration
$u(P_{read})$	Uncertainty of air pressure from digital resolution
$u(R_{cal})$	Uncertainty of relative humidity from certificate of calibration
$u(R_{read})$	Uncertainty of relative humidity from resolution
$u(T_{cal})$	Uncertainty of thermometer from certificate of calibration
$u(T_{read})$	Uncertainty of thermometer from digital resolution
U_1	The average uncertainties associated with the ball centre coordinates of the ball plate
U_2	The average uncertainties associated with the CMM measurements at 200 random locations in the evaluated region

U_3	The average uncertainties associated with the CMM measurements at the whole working volume
v	Covariance function
X	A random function, distributed as a Gaussian Process
ypy	Positioning Deviation
yrx	Horizontal axis rotational deviation
yry	Moving axis rotational deviation
yrz	Vertical axis rotational deviation
ytx	Horizontal Straightness Deviation
ytz	Vertical Straightness Deviation
βin	The angles between leg l_i and legs l_{in}
βip	The angles between l_i leg and legs l_{ip}
ϒ	Vacuum wave number (mm^{-1})
ϕ	Squareness Deviations
ϕ_{xy}	Plane XY squareness deviation
ϕ_{xz}	Plane XZ squareness deviation
ϕ_{yz}	Plane YZ squareness deviation
GP	Gaussian Process
$k(x, x')$	The covariance function
$u(P)$	The standard uncertainty of the probing error
$\delta(x, x')$	The Kronecker delta function
ϵ	Random effects

List of Figures

List of Tables

Chapter 1 Introduction

1.1. Research background

1.1.1. Research background

Generally, due to the increasing emphasis on the evaluation of measurement uncertainty, Coordinate Measuring Machine (CMM) researchers have developed several techniques to evaluate the CMM measurement uncertainties and further enhance the measurement performance in both hardware and software. Among these uncertainties, CMMs software has been demonstrated to be an effective tool for both error compensation and uncertainty evaluation. Of course, there have been several different approaches taken in the evaluation of CMM errors and uncertainty. But they all can be seen as methods to exploit the computing power which has become increasingly available through a virtual CMM (Pahk, et al., 1998; Okafor & Ertekin, 2000; Van Dorp, et al., 2001; Trek, et al., 2004; Hu, et al., 2012).

The mechanical approach presented in this research is similar to those described in previously published papers in the sense that it measures a calibrated artefact using a ball plate to align precisely a reference object for machined tools (Cauchick-Miguel, et al., 1996; Phillips, et al., 1997). There is some work evaluating the errors by using a laser interferometer to measure ring gauges (Kim & Chung, 2001). These generally use the ball plate, providing that accurate spheres and the distance between the axes of the spheres are certified in a plane measured by a CMM (Knapp, 1988; Forbes, 1991; Balsamo, et al., 1997). Parametric errors of CMMs can be determined using conventional methods such as a laser interferometer (Trapet & Wiudele, 1991). However, these methods are time-consuming, and require skill and expensive equipment. To overcome these problems, reference artefacts have been introduced such as a ball plate (Kunzmann, et al., 1990; Trapet & Wiudele, 1991), a ball array (Zhang & Zang, 1991) and a device consisting of a ball plate (Kruth, et al., 1994; Bringmann, et al., 2005). To calibrate CMMs using 2D reference objects, National Metrology Institute – Physikalisch-Technische Bundesanstalt (PTB) (Kunzmann, et al., 1990; Trapet & Wiudele, 1991) proposed a method to determine the parametric errors by placing the reference object in vertically and horizontally different orientations with a multiple of probe styli. This method generates a set of grids in the MATLAB programme. Thus, parametric errors can be calculated. Ball plate-based (Balsamo, et al.,

1997) techniques were validated by the international comparison on CMM calibration. The results showed the benefit of ball plate-based techniques for determining the parametric errors.

1.1.2. Definition and scope of the CMM

1.1.2.1 Introduction

Figure 1.1CMM (PMM-C700P)

The CMM probing system is part of the coordinate measurement machine that senses all the coordinates of the surface needed for measurement calculation. Depending on the type and scale of measurement, appropriate probes need to be selected and placed on the CMM swindle based on the measurement application. First generation probes were usually solid or hard, for example tapered plugs used in locating holes. Such probes usually need to be manipulated manually in order to establish contact with the workpiece before the measurement can be read from the digital display output. Current generation probes, such as optical probes, transmission trigger-probes, cluster or multiple probes and motorised probes, do not require manual intervention during the measurement operation of the work piece. The second generation of probes, the touch trigger probe, invented by David McMurty in the 1970s, was vital to the development of

the probing technology in yielding high-precision measurements. The probe has a loaded steel ball stylus and comes with a precise micro-switch which responds to smaller order displacement. When it comes in contact with the surface of the shape to be measured, the stylus will deflect and then trigger an electronic signal to get the current coordinate of the probe to be recorded. The measurement method used a touch-trigger probe to greatly enhance the accuracy and precision of the CMM. It also reduces the errors as a result of measurements taken by different operators. CMMs usually utilise optoelectronic, electromechanical or electronic measuring systems. These include linear encoders or rotary encoders, inductive transducers or capacitive transducers, and interferometers (Yang 1992). Since the invention of the electronic touch trigger probe by David McMurty, many new types of probe have been developed. Probes can be generally classified as contact (tactile) or non-contact.

Some newer models of contact probing system have features that will enable the probe to be moved along the surface being measured and at certain intervals of points, information is collected. These types of probe are also known as scanning probes and are known to be more accurate and faster than the conventional contact probing system. There are new research interests in combing both the non-contact and contact probing system into one integrated CMM system. The combination of the distinct characteristics of both contact and non-contact probing system will be beneficial in improving inspection speed while retaining high precision, or will fit a wider range of usage (Shen, et al., 1997; and Qin, et al., 2008).

The errors of a CMM can be categorised into two types. Dynamic errors are effects that are associated with short timescales vibration for example. Quasi-static errors are systematic effects associated with the imperfect kinematic behaviour of the CMM, such as scale and squareness errors that are associated with much longer timescales. It is estimated that the quasi-static errors account for about 70% of the errors of the machine (Bryan, 1990).

1.1.3. Overview of CMM kinematic errors model simulation

One of the problems in using kinematic error components, such as translational errors, rotational errors, and squareness errors, is that they vary in their measurement position. The local kinematic error model solves this difficulty in that it can only operate to the particular location of the CMM working volume used for the measurement task and the ball plate probes being used. It seems like a dynamic task that can reuse the model next

time by updating it facilitated within the limited time period to perform this measurement task. Therefore, the effect of the measurement location offsets can be overlooked when using this local kinematic error model.

However, the specification in this research uses a local kinematic model to describe the error behaviour of the CMM. Through the repeated use of a simple artefact, a ball plate, the parameter kinematic error model has been determined using non-linear least-square, together with a total of 21 relevant and suitable configuration parameters: three positional and three rotational error functions for each of the three axes, along with three squareness errors. The general methodology to evaluate the 21 parameter kinematic error configurations into the volumetric error map of a CMM by using the rigid body model is described in other works (Hockwn, et al., 1977; Schultschik & Matthias, 1977; Knapp & Matthias, 1983; Zhang, et al., 1985; Jouy & Clement, 1986; Belforte, et al., 1987; Kruth, et al., 1994; Sartori & Zhang, 1995). This methodology allows the CMM measurement errors and uncertainty to be calculated based upon the local, simplified kinematic error model, the propagation of uncertainty, and numerical simulations. A comprehensive mathematical model has been estimated to investigate the CMM parameter kinematic errors (Zhang, et al., 1988; Soons, et al., 1992). These evaluation methods are based on the experimental uncertainty determination according to the ISO 10360 standard for CMMs (ISO 10360-2 2002). The aim of this research is to simulate a local, simplified kinematic error model and a Gaussian process (GP) model, which together form a powerful accurate numerical virtual CMM, to evaluate the error and uncertainty of an actual CMM. These approaches lead to the precise error modelling of coordinate measurements, take as little time as possible, estimate real measurement, and reduce costs by task-specific definitions.

1.1.4. Overview of the CMM GP model

The GP model is a distribution over functions, which is basically the joint distribution of all the infinitely random variables. In statistical modelling, GP is important due to the properties inherited from the normal methods. When a process is modelled as GP, its distribution of various derived quantities, such as the average value of the process over certain duration and the error in the estimation of the average, could be obtained explicitly. GP is determined by its mean and covariance function. In terms of notation, the GP could be written as:

$$X \sim GP(m, v) \tag{1.10}$$

Where X is a random function, distributed as a GP with a mean function, m, and a covariance function, v. The random variables are assumed to have a zero mean, which will simplify the calculations without loss of generality and the mean square of the process is entirely determined by the covariance function. These are computed quickly using a recursive formula. GP is used in analysing a geometric feature into three components:

- Designed geometric form – This is done by deciding the line function and approach direction and solving the intersection points between functions.
- Systematic manufacturing errors – This refers to the deviation from an ideal form that is identically independent distributed random.
- Random manufacturing errors – This refers to the deviation from an ideal form that is non-identically independent distributed random.

The method models the systematic manufacturing errors as a spatial model using a Gaussian correlation function. The random manufacturing errors are modelled as independent and identical distributed noises. With a small number of coordinated measurements, the GP model could reconstruct the part surface and assess the form error better than traditional methods. It also provides an empirical distribution of the form error the quantification of the decision risk in part acceptance which works for generic features. The authors, Dowling et al. (1993), Yang and Jackman (2000) and Xia et al. (2008) used a GP method to provide information on the error and uncertainties in deciding on CMM acceptance or rejection.

1.2 Aim and objectives of the research

The aim of this research is to achieve a cost-effective evaluation of CMM kinematic errors by a desirable approach using reference artefacts and thus further explore the mathematical understandings of the CMM kinematic errors.

The objectives of the research are as follows:

- To develop a mathematical model for making effective choices regarding the local kinematic error simulation and Gaussian Process model based upon the real physical CMM performance.

- To demonstrate the improvement achieved by the proposed method using simulated datasets over the traditional approaches based on actual CMM data measurements.
- To validate and evaluate the numerical simulations with a well-designed strategy providing accurate estimates of the kinematic errors using only a nominal CMM calibration and a ball plate.
- To investigate the influence of CMM kinematic errors on the CMM calibration.

1.3 Outline of the thesis

This work is outlined in eight chapters. The comprehensive details of the thesis are demonstrated as in figure 1.2.

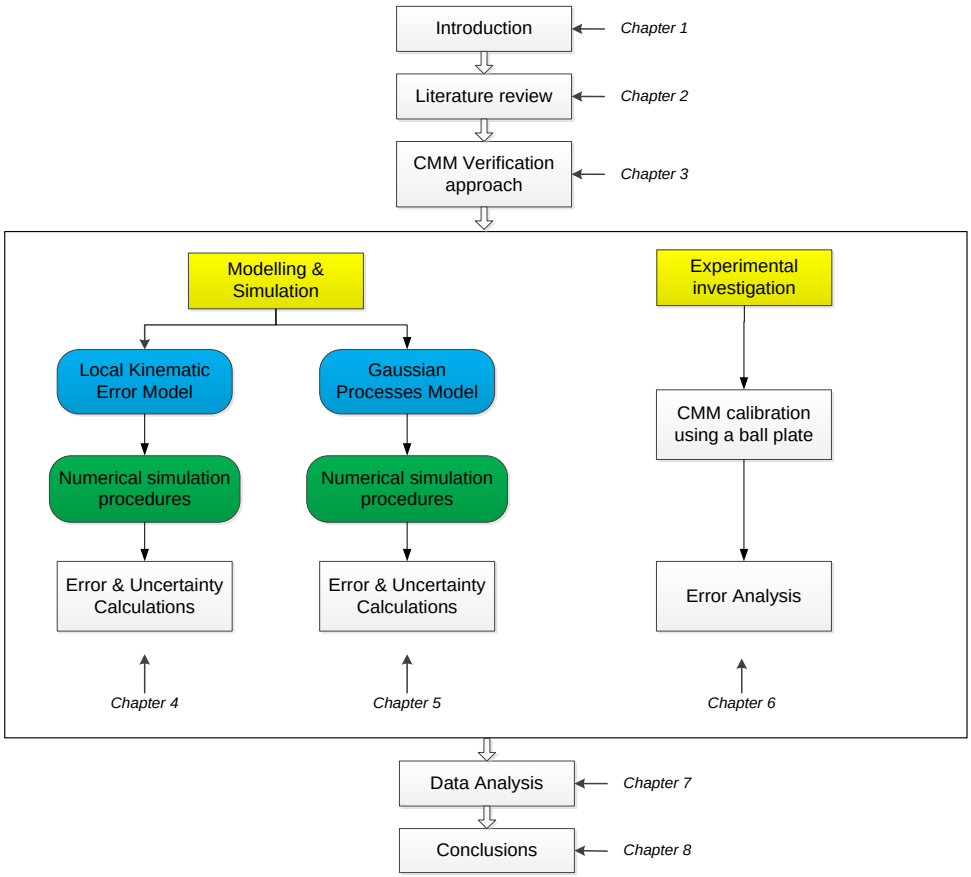

Figure 1.2 Chapter plan of the thesis

Chapter 1, the background, overview of CMM kinematic error model simulation and research aims/objectives to understand the body of the thesis are introduced.

Chapter 2, the state of the art of CMM, the systems, configurations and measuring methodologies will be reviewed. The errors and uncertainty of the CMM measurement will also briefly be emphasised. The discussion of the CMM kinematic errors model and the GP model for numerical simulation will be carried out to analyse the errors calculation and uncertainty evaluation of this model in the research area.

Chapter 3, the necessary theoretical backgrounds of the CMM, structures, systems and its measurement strategies will be explained. Also, the CMM measurement errors and uncertainty calculation will be introduced.

Chapter 4, the theoretical simulation procedures, including calculation of model parameters, errors calculation, and uncertainty evaluation, will be proposed. Then, the process of CMM kinematic errors model simulation presenting the local, kinematic errors model will be presented. The 21 kinematic errors parameters, including translational, rotational, and squareness errors, will be explained. The simulation processes used in this research, including locations of the artefact, probe qualification, and numerical procedures, will be implemented. Within this chapter, error compensation and uncertainty evaluation applying to the model will be assessed in the model of local, kinematic errors simulation. The mathematical model will be evaluated for uncertainty evaluation and the errors model using the local, simplified kinematic error model will be emphasised.

Chapter 5, GP simulation will be studied. In this chapter, the GP and its simulation, including the background theory in order to understand GP and its numerical simulation, will be investigated; errors that occur in the model will be compensated for.

Chapter 6, the experiment will be set up including preliminary operations: CMM calibration using a ball plate, measurement procedure and error analysis.

Chapter 7, the discussion of this work comparing the simulation between the local, kinematic errors model and the GP model will be analysed. The results from the CMM measurement using a ball plate as an artefact will be investigated, comparing it with the simulations.

Chapter 8, the results and conclusions from this work will be discussed. Further recommendations will be also provided at the end.

Chapter 2 Literature Review

2.1 Introduction

In this chapter, the literature reviews of coordinate measuring machine (CMM) and it related technologies are discussed. Sections 2.2 to 2.5 cover the following introduction to CMM which covers CMM system configuration, probing system, inspection planning, errors and uncertainty; CMM Kinematic errors model solution detailing Local Kinematic error model and Gaussian Process model; CMM numerical simulation calculation and its compensation strategies and the optimisation and control using Matlab programme.

2.2 Coordinate Measuring Machine (CMM)

2.2.1 Introduction

Coordinate Measuring Machine is a useful metrological instrument for measuring geometrical characteristics of a device. It is used in manufacturing and assembly processes, for testing parts with respect to their design specification. CMMs aid in the location of point coordinates on three dimensional structures or platforms. According to the International Organisation for Standard, CMM is a measuring system with means of moving a probing system and is capable of determining the spatial coordinates of an object on the workpiece surface. The measurements are conducted by a probe connected to the third moving axis of the machine. Probe used for CMM could be optical, laser, mechanical or white light. CMM simultaneously integrate both the dimension and orthogonal relationships. The machine could be operated by an operator in manual settings. When combined with computer systems, it becomes automated and could carry out complex analysis which could be useful in learning measurement routines and compares how a part conforms to the required specification. The measurement duration while using CMM is shorter compared to using traditional single axis instruments. One major advantage of using CMM for measuring is that it offers precision and speed for measuring complex objects. CMM takes its reading in six degree of freedom and these readings are displayed in mathematical form. It is composed of three axes which are orthogonal to one another just like the normal three-dimension coordinate system. With the three axes combined, the probe moves in a three dimensional space which makes it possible to conduct complex measurement with

high accuracy compared to single dimension instruments such as metre rule, tape rule etc. CMM uses the three coordinates (X, Y, and Z) of each of these points to calculate the size and position with a precision of micrometre. The probe of a CMM can rotate and tilt to varying degrees which makes it able to inspect objects with a great degree of access. After taking the correct reading of the three coordinates of the work piece, necessary points could be generated, which then could be analysed using a variety of regression algorithms to construct the features of the work piece. Coordinate points are collected via the CMM probe that is positioned either by an operator manually operating the machine or automatically through Direct Computer Control (DCC). Figure 2.1 showing two examples of CMM, FALCIO Apex G Series 355 High Accuracy Large CNC CMM and COORD3 Universal Bridge.

(a) (b)

Figure 2.1Showing (a) FALCIO Apex G Series 355 High Accuracy Large CNC CMM and (b) COORD3 Universal Bridge (Mitutoyo, 2016 and COORD3, 2016)

Though a CMM could be controlled either by an operator, manually or by using a computer system, modern CMM are generally computerised. Computerising CMM automated the measuring process and enabled it to have powerful computational capabilities. It could gather positional information through a number of points based on the coordinates system and then calculates geometrical characteristics of the object such as the radius for spherical objects. It could be used to determine relationship between characteristics such distance between the centre point of two spheres, angles between surface, distance and angles etc. When comparing CMM with most conventional

approaches, it has a number of benefits; some of these benefits are automation, precision, accuracy, efficiency and its universality. Using CMM enhances inspection greatly by introducing computer automated coordinate system and data fitting algorithms that help inspectors to set up the work piece in an orientation that is very convenient for inspection. With calibration in place, the data measured are corrected to remove any error due to the references. In conventional geometry inspection aligning the workpiece manually is difficult and to determine the right reference position can both labour intensive and time consuming (Gu 1994).

Performing measurement with high accuracy and precision is vital and CMM could be used to eliminate errors that were accumulated resulting from hard gauging inspection. With CMM, measurements are conducted in temperature controlled environment where the common procedure guidelines are followed and the operator influence in introducing errors could also be kept to a minimal value (Gu 1994). CMM could be used to measure any object, however there are few limitations to it. They are precise robots that effectively operate in the universal Cartesian coordinate system (Kurfess 2006 and Wang et al 2006). Today's CMMs are generally automated and integrated with control systems. Dimensional Measurement Interface Specification (DMIS) is a standard programming language designed for controlling CMM and also for communication between CMMs and Computer aided design (CAD) systems.

In 1963, an Italian company, Digital Electric Automation (DEA) designed and developed the first CMM with three dimensional coordinate systems and a hard probe. However, another company in Scotland, Ferranti Metrology also claimed to be the first inventors of the CMM, except that their design was for a measurement machine with only two axes. This makes the DEA the world first designer of CMM with a three dimensional frame work that currently is the standard frame work for CMM. Ferranti, which is now known as International Metrology System (IMS), introduced the first Direct Computer Control Coordinated Measurement Machine (DCC CMM). This could be programmed accurately and automatically measure identical parts of the workpiece, making it a specialized form of an industrial robot. DEA later developed the first Computer Numerical Control Coordinate Measurement Machine (CNC CMM). As with the saying, "necessity is the mother of invention," so the invention of CMM was done by the urgent need to develop instruments with very high measuring precision in the manufacturing industry in the late mid-20th century. The emergence of automated and computerised CMM could be linked to the rapid development of micro-electronics,

precision mining technology and manufacturing industry needs for reliable, flexible, efficient and fast measurement technology (Yang 1992).

It took over 10 years after the invention of CMM to achieve big success commercially, though industries were born almost immediately after its invention. CMM processes and techniques are still being enhanced to meet up with the challenges of the fast development of advanced manufacturing industry. With an increase in more complicated and aesthetic shapes on the rise, improvement of CMM for higher measurement qualities for such shapes are also being pursued. Nowadays, artificial intelligence is added to provide better measuring capabilities, increase reliability in inspection. This makes CMM measurement machines are one of the most accurate metrological instruments in manufacturing sector.

2.2.2 CMM system and configuration

A coordinate measurement machine basically consists of a platform and probe. A platform is the surface where the workpiece is placed and moved with linearity during measurement. The probe is normally attached to the head and it is capable of taking both horizontal and vertical measurement. The first generation of CMM probes were generally connected with a probe holder at the end of the spindle. They mostly consist of a hard ball tip connected to the end of stem. Other probes have their tips in other shapes and sizes. First generation probes were usually physically held by the operator and then carefully brought in contact with the points on the surface of the feature to be measured by hand. Spatial positional measurements were then read from the digital read out or digital display or simply stored on a computer. Using such method of taking measurements gives a wider room for errors and uncertainty.

Measurements conducted by such procedure were generally considered not reliable. The probe is susceptible to be damaged or the work piece deformed due to the excess pressure applied. In order to mitigate such damage from occurring, additional motors were added that drive each axis. With the addition of motors to the axes, the operators don't need to hold and move the probe by hand, instead a joystick could be used in controlling the movement of the probe.

2.2.2.1 CMM Design

When CMMs were first designed and developed, they were equipped with a direct digital display or equipped with a digital read out. With the innovation of computers,

CMM were equipped with a computer for data processing but manually operated by an operator. Currently, CMMs could be driven automatically using the CMM program. This development enabled modern CMMs to have new features compared to the first generation of CMMs. Some of these features are:

- Compensating temperature
- Crash Protection
- Reverse Engineering
- CAD model import capability
- Shop Floor Suitable
- SPC Software
- Offline programming

CMMs architecture and appearance have rapidly advanced since its invention in the early 1960s. Most modern designs are based on a Cartesian coordinate system. This is due to the simplicity and the universal arrangement of a three axes dimensional system (Yang, 1992). The International Organisation for Standardization in their guideline, ISO 10360-1, listed the configurations and types of CMMs which are:

(1) Fixed table cantilever Coordinate measurement machine

Most fixed table cantilever CMM are usually limited to small and medium sized machines. They offer easy access and occupy relatively small floor space where space requirement is important. This is one of the first CMM machines used in the manufacturing industry.

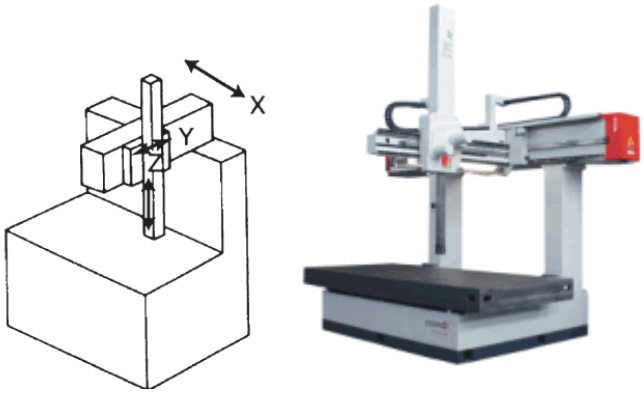

(a) (b)

Figure 2.2 Showing the Fixed table cantilever CMM structure and a typical Fixed table cantilever CMM product (Precision Engineering Specialization, 2012 and Bhagat, 2015)

(2) Moving bridge Coordinate measurement machine

This comprises of a CMM table which is normally produced from granite or steel; a bridge assembly and a Z-axis assembly. The CMM table has a grid pattern of threaded insert of either M8 or M10 size for easy clamping and is also used to support the object to be measured. For most manufacturers, the X-axis moves from left to right front view, Y-axis moves from front to back from a front view and the Z-axis moves vertically. Moving bridge CMM either use air bearing or mechanical bearing. Air bearing has its bridge mechanism sliding directly on the surface of the table while mechanical bearing has its bearing mechanism connected to either the side or top of the table. For improved performance when using air bearing, the air bearing ways machine directly into the granite plate.

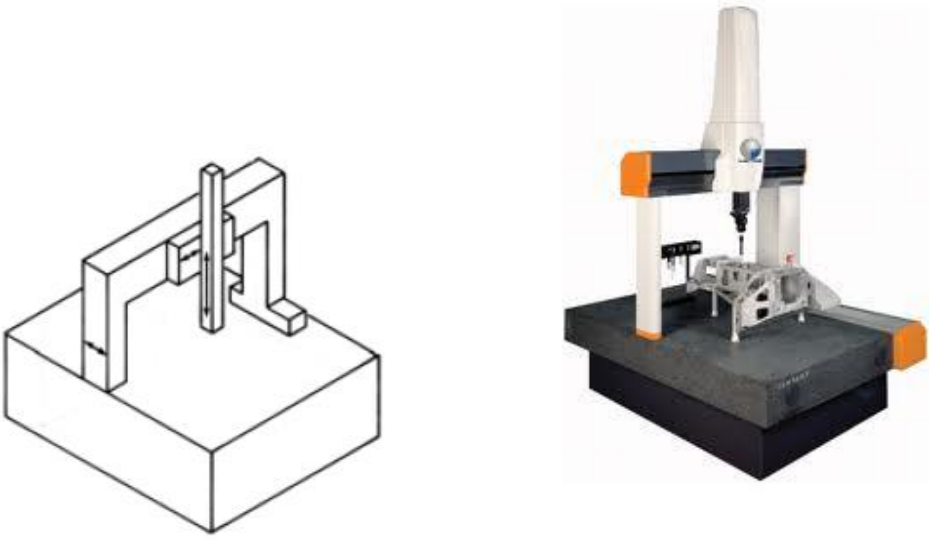

(a) (b)

Figure 2.3 Showing the moving bridge CMM structure and a typical moving bridge CMM product (Bhagat, 2015)

The X-axis of the air bearing CMM is mostly produced from steel, granite, aluminium or ceramic. The CMM machines were formerly produced from steel or granite but over the decades, CMM machines are produced from ceramic and aluminium. Granites generally have lower thermal coefficient of expansion and slow thermal diffusion rate which makes it slow to respond to changes in temperature. Aluminium has a high coefficient of expansion which makes it unsuitable material for the surface but it handles temperature change due to its high thermal diffusion rate. Ceramic is from glass. It is light and fragile but exhibits same metrological properties as the granite. Steel on the other hand has a low co-efficient of expansion and responds to changes to temperature. Materials used to build CMM are selected based on the operating environment. Moving Bridge CMM is the most common CMM due to its accurate design. This uses pneumatic counter balance system to maintain a balanced motion of the Z axis.

(3) Gantry Coordinate measurement machine

A Gantry Configuration CMM consists of its support pillars and horizontal beams, bridge assembly and Z axis Assembly. It has elevated horizontal beams which the bridge assembly slides upon. Gantry CMM has excellent dynamics because both X and Y axes are almost on the same height. Most Gantry CMM have their X-axis from the front view moving from left to right, Y-axis moving front to back when viewed from the

front and Z-axis is vertical. It could use either air bearing, with the bridge mechanism sliding on top of the horizontal beams or mechanical bearing, with the guide bearing mechanism attached to the side or top of the beams. They are mostly used for measuring large shape and could be used with monolithic base to remove the need of a foundation.

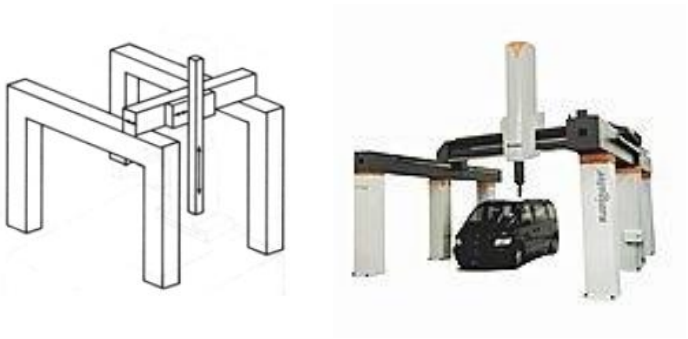

(a) (b)

Figure 2.4 Showing the fixed table cantilever CMM structure and a typical fixed table cantilever CMM product

(4) Fixed bridge Coordinate measurement machine,

Fixed bridge CMM supports only a unidirectional motion. This motion is linear only in the y-axis direction and it supports the weight of the part to be measured. Typically, the Fixed Bridge CMM supports lesser weight when compared to the Moving Bridge CMM. The Y-axis moves from left to right from a front view. Most Fixed Bridge CMMs use the air bearing structure as their bearing mechanism and have the best configuration in consideration that it has improved dynamics over the moving bridge CMM. It uses a pneumatic counter balance system to maintain a balanced motion of the object and Pneumatic Isolation System to remove any vibrations that could affect the measurement negatively. Fixed Bridge CMM is not common because of its high cost and is typically used for measuring complex applications where micro range tolerance is required. It is only available as a CNC CMM and uses a fixed head scanning probe.

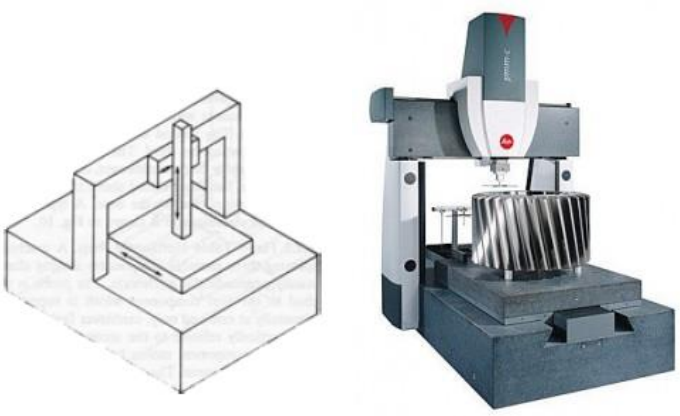

(a) (b)

Figure 2.5 Showing the Fixed Bridge CMM structure and a Fixed Bridge CMM product (Bhagat, 2015)

Other CMM configurations include L-shaped Bridge Coordinate Measurement Machine, Moving Table Cantilever CMM, Column CMM, Moving Ram Horizontal-arm CMM, Fixed Table Horizontal-arm CMM, and Moving Table Horizontal-arm CMM. Table 2.1 shows the typical accuracies for a number of configurations (Rodger et al., 2007).

Table 2.1 Showing the typical CMM accuracy

Configuration	Indicative errors
Bridge	±<5 µm
Gantry	±10 µm
Column	±10 µm
Cantilever	±10 - 50 µm
Articulated arm	±50 – 250 µm

2.2.2.2 Probing systems

In the late 1970s, the founder of Renishaw PLC, David McMurty, invented an electronic touch trigger probe. This invention was vital to the development of the probing technology in yielding measurement with high precision. The probe has a loaded steel ball stylus and comes with a precise micro switch which responds to smaller order displacement. When it comes in contact with the surface of the shape to be measured, the stylus will deflect and then trigger an electronic signal to get the

current coordinate of the probe to be recorded. The measurement method used trough-trigger probe to greatly enhance the accuracy and precision of CMM. It also reduces the errors as a result of measurements taken by different operators. CMMs usually utilize optoelectronic, electromechanical or electronic measuring systems. These include linear encoders or rotary encoders, inductive transducers or capacitive transducers and interferometers (Yang 1992).

Since the invention of the electronic touch trigger probe by David McMurty, many new types of probe were developed. Probes could be generally classified as contact (tactile) or non-contact types. The British Standard Institution (BS6808-1 1987) and the International Organisation for Standardization (ISO 2000) defined and classified the probing systems into the following:

- Contacting probe system: — Contact probes make contact with the surface that is being measured and are the most common probes used today. Though contact probes are slower when carrying out measurement as compared to non-contact probes, they are more accurate and very suitable when measuring rigid work pieces comprising of geometrical shapes that are primitive.
- Non-contacting probe system: — Non-contact probing system does not need any material contact with a surface being measured in order to function. For example, optical probe system is a non-contacting probing system that creates a connected measured point by probing via an optical system.
- Multi-probe system: — a multi probing system is a probing system having more than one probe attached to the coordinate measurement machine.
- Articulating probe system: — An Articulating probe system is probing system that could be rotated into various spatial angular positions through the use of manual position device or motorized positioning device.

Table 2.2 shows some of the most common probes used in coordinate measurement machine for both contact and non-contact probes.

Table 2.2 Showing some common probes used in coordinate measurement machine (contact and non-contact probes)

Probe	Type	Function
Touch-trigger probe	Contact	This probe outputs a binary signal as a result of the contact made with a workpiece.
Analogue contacting Probe	Contact	This probe generates and outputs a signal or series of signals in proportion to the displacement of the probe from the initial position. The displacement information is then mapped to coordinates.
Nulling contacting probe	Contact	This probe outputs a signal or series of signal that make the coordinate measuring machine to be driven to a position in referenced to a workpiece. It always gives a constant probe reading which is usually near zero output or a zero output. It does output values higher than zero.
Passive (solid) probe	Contact	This is a probe which locates the movable components of the CMM mechanically relative to the workpiece
Laser scanning optical probes	Non-contact	Laser scanning optical probe is a non-contact type of probe which uses laser scanning and technologies such as CCD (charge-coupled device) systems and machine vision (MV) systems.
White light scanning optical probes	Non-contact	White light scanning optical probe is a non-contact type of probe which uses white light scanning and utilizes technologies such as CCD (charge-coupled device) systems, machine vision (MV) systems.

Some newer models of contact probing system have features that will enable the probe to be moved along the surface being measured and at certain intervals of points, information are collected. These types of probe are also known as scanning probes and are known to be more accurate and faster than the conventional contact probing system. For non-contact probes, advance technologies are used in making it possible to collect huge amount of high density data containing information about the coordinate points in short time. The number of points could be thousands of points per inspection. These data could be used to recreate the 3D image of the shape and not only for checking its geometrical features. When integrated to CAD software, it makes it possible for the

software to create a 3D model of the workpiece from the millions of points taken per inspection. With this feature, non-contact scanning probe is ideal for reverse engineering for rapid prototyping of the workpiece, most especially for workpieces with complex geometrical features. Another benefit of non-contact probing system is that it could be used to measure delicate, soft or deformable workpieces since the probe will not touch the surface of the object. Currently, non-contact probing systems are less accurate when compared to contact probing systems but the accuracy margin is closing up due to rapid advancement in probing technology and electronics. There is new research interest in combing both the non-contact and contact probing system into one integrated coordinate measuring machine system. The combination of the distinct characteristics of both contact and non-contact probing system will be beneficial in improving inspection speed while retaining high precision or will fit a wider range of usage (Shen et al 200 and Qin et al 2008).

Microprobe is another area with new research interest. Microprobes are smaller than the regular probes in terms of their size and measurement scope. Microscale probing technologies are basically scaling down a number of the conventional probing technologies such as laser scanning probe, white light optical probe, standing wave optical probe, Touch-trigger probe, Analogue contacting Probe, Nulling contacting probe, and Passive (solid) probe. Despite the fact that there are a number of commercially available applications for micro probing system, it is still facing a number of critical challenges. Some of the challenges it is facing are lack of having a high aspect ratio probe with the capability of accessing deep or very narrow features, vulnerability to environmental influences such as humidity and surface interactions, maintain microscale contact in order to prevent damaging a high precision surface for example at nanometre level and unreliability during measurement (Bauza et al. 2005)

Optical and inductive Transmission Probes

Optical probe system is a non-contacting probing system that creates a connected measured point by probing via an optical system. Non-contact probing system does not need any material contact with a surface being measured in order to function. Optical and inductive Transmission Probes were developed for changing the tool automatically. The probe system receives power through the inductive link between the modules fitted to the machine structure and the probe system. The hard wired transmission probe is used mainly for tool setting and usually mounted in a fixed position on a machine

structure. Figure 2.6 shows the inductive probe system and automatic probe changing and figure 2.7 shows the optical transmission probe. The probe rotates between gaging moves which makes it very useful for datuming the probe. The probe wide angle gives it greater axial movement of the probe making it suitable for majority of the installation.

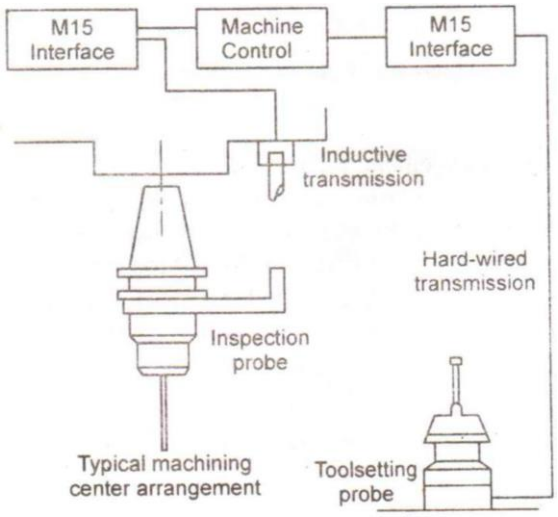

Figure 2.6 The inductive probe system and automatic probe changing (Bauza et al., 2005)

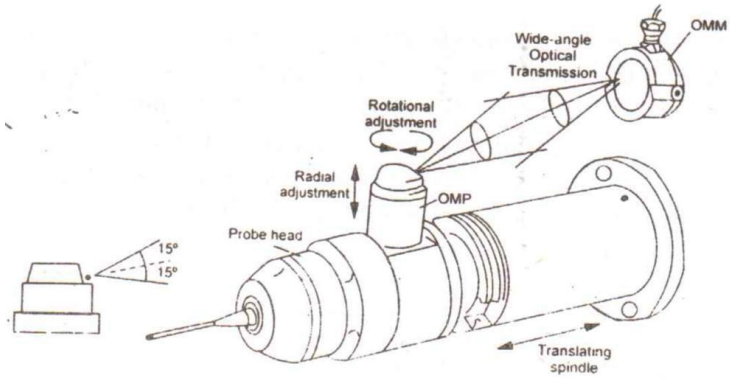

Figure 2.7 Showing the optical Transmission probe (Bauza et al., 2005)

Contacting probe system

Contact probes make contact with the surface that is being measured and are the most common probes used today. Though contact probes are slower when carrying out measurement as compared to non-contact probes, they are more accurate and very suitable when measuring rigid work pieces comprising of geometrical shapes that are primitive.

Motorised Probe

Motorised probe offers a total of 720 distinct probe orientations from it 48 position in the horizontal axis and it 15 position in the vertical axis. Figure 2.8 shows the motorised Probe system and Figure 2.9 show the typical application of motorised probe. The figures show that within the range of light weight extension, the probe head could reach into the deep holes and recesses. Figure 2.9 reveal the probe head is quite compact to be regarded as an extension of the machine quill. This architecture enables the inspection of complex components that would otherwise require complex or impossible setups.

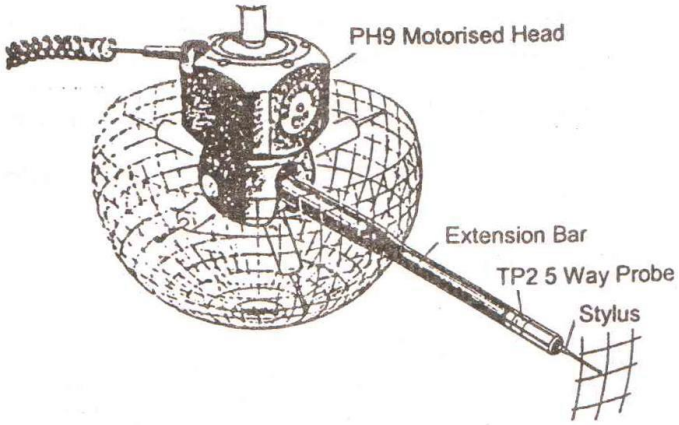

Figure 2.8 Motorized Probe head

Figure 2.9 Typical application of Motorised probe

Multiple Stylus Probe Heads

Multi probing system is a probing system having more than one probe attached to the coordinate measurement machine. Some of probe heads have wide ranges of styli which are developed to suit quite a number of different gaging applications. Figure 2.10 shows some of the different styli mounted on a multiple gaging head. The application for the usage of the probe determines the selection of stylus that will be mounted on the probe head.

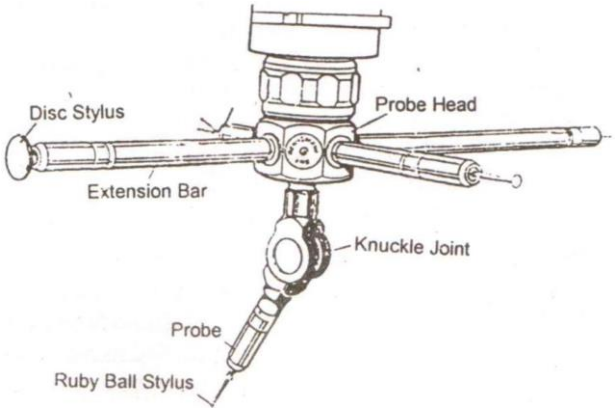

Figure 2.10 Multiple stylus probe head with variety of styli

Microprobe

Microprobes are used in both micro and nano CMM measurements with the form and the spacing of two reference spheres with diameters of two millimetres each. The application of the microprobes requires the probing system structures to be manufactured and assembled with very high precision in order to make the system function smoothly. Microprobes are smaller than the regular probes in terms of their size and measurement scope. Microscale probing technologies are basically scaling down a number of the conventional probing technologies such as laser scanning optical probe, white light optical probe, standing wave optical probe, Touch-trigger probe, Analogue contacting Probe, Nulling contacting probe, and Passive (solid) probe. Despite the fact that there are a number of commercially available applications for micro probing system, it is still facing a number of critical challenges. Some of the challenges it is facing are lack of having a high aspect ratio probe with the capability of accessing deep or very narrow features, vulnerability to environmental influences such as humidity and surface interactions, maintain mild contact in order to prevent damaging a high precision surface for example at nanometre level and unreliability during measurement (Bauza et al. 2005). Figure 2.11 shows Microprobe used in micro-nano CMM measurement. The Physikalisch-Technische Bundesanstalt (PTB) in Germany has developed a metrological scanning microprobe with capability of delivering micro and nano coordinate measurement. The PTB microprobe is able to meet the requirements for 3D measurements of both the micro and the nano structures.

Figure 2.11 Microprobe used in micro-nano CMM measurement (PTB, 2009)

Articulating probe system

An Articulating probe system is probing system that could be rotated into various spatial angular positions through the use of manual position device or motorized positioning device. Non-contact probing system does not need any material contact with a surface being measured in order to function. The probe head provides rotational movement on at least one axis and with at least one rotary measurement device for the measurement of the angular position of the surface sensing. Figure 2.12 shows an example of an articulating probe system.

Figure 2.12 Articulating probe system (Graywolfsensing, 2007)

2.2.3 CMM inspection planning

In the 21st century, manufacturing industries produce more workpieces that have very complicated geometrical features and aesthetic shape to meet both the functional and aesthetical environment. Due to the competition in the manufacturing industries, the ability and capability to rapidly design and produce these products with very high accuracy and precision is very important especially to a manufacturer who wants to thrive in the industry. Measuring the coordinate data with accuracy is another important procedure to be considered as sometimes it could be a bottle neck in the process of achieving short production cycle (Qin e al 2008).

Conducting CMM inspection is a requirement with more accurate and efficient operating procedure in order to fulfil the entire quality assurance standard with shorter cycle times. Coordinate measurement machines have become one of the widely accepted metrological instruments. Improving the measurement accuracy and increasing the speed of the inspection are two principal goals needed to improve the performance of CMM (Lu et al 1999). The inspection procedure of CMM could be divided into three parts

- Inspection planning
- Measuring program generation
- Actual inspection

Inspection planning is the key to achieve better CMM operational performance and it plays a vital role in the inspection procedure. The methodology and strategy used has direct impact on the safety of the equipment, safety of the workpiece, efficiency of the measurement and the accuracy of the inspection results. Over the last two decades, the study of inspection planning with the goal of improving CMM performance has evolved into a continuous developing research area and has attracted attention in a number research literature (Yang & Chen 2005 and Ziemian & Medeiros 1998). There are two aspect of planning when carrying out CMM inspection planning; low level planning and high level planning (Chen et al 2004).

Low level planning deals with the following:

1. Selecting measurement points on every surface
2. Accessibility evaluation for the measurement points
3. Sequencing and grouping of measurement points
4. Generation of collision free inspection path

And high level planning covers the following

1. Setting the work piece on the work table
2. Determination of the required features to measure in a particular setup.
3. Selection of the probes
4. orientation of the probe

Quite many researchers have been done in the areas listed above and new approaches are still being proposed. Measurement strategies and programs are regularly modified due to the different configurations and requirements of workpieces since the main characteristic of today's manufacturing industry is having production with low volume high-variety and products with close tolerance high-quality (Chen et al., 2004). In such scenario automating the inspection planning becomes highly desirable because of the following reasons:

- Every time there is a change in the workpiece or change in the measured features, there is also a need for the inspection to be planned again. When carrying out the inspection planning manually, the process could be very time consuming but when carrying out the inspection planning automatically, it the human workload and improve the inspection speed.
- Carrying out manual inspection planning on a CMM machine would cause more wear and risk collision damage considering that CMMs are expensive instruments. An alternative to manual inspection is to generate the measurement program offline and automatically which will greatly reduce cost and improve safety.
- By automating the inspection planning, it will maintain a certain standard of reliability thereby eliminating the human differences by different operators. When conducting the inspection manually, its validity and effectiveness is dependent on the operators' skills and experience.
- In a computer integrated manufacturing (CIM) environment, Coordinate measurement machines become involved in in-process inspection. The means CMMs are required to be closely integrated with both computers aided design and computer aided manufacturing. Automating inspection planning is vital in improving efficiency and for communication between the other components in the computer integrated manufacturing environment. Combining the two will make it possible to have a complete automated manufacturing system.

The concept of measurement and error analysis has always been in use since the existence of man, due to the need to assess the quality result of measurement. The application of error analysis hinges on two concepts, which are the actual value of the measurand and the measurement error. The values are difficult to be calculated exactly even when all components of the error have been evaluated and taken into consideration; an uncertainty on the correctness of the result will still remain (International Organization for Standardization, 2008). In the 1970s, metrologists discovered that it was more appropriate to use uncertainty while computing the characterisation of a measurement's reliability instead of using the word error. Uncertainty focuses on a measurement's dispersion which reasonably could be ascribed to the measurand.

Comité International des Poids et Mesures (CIPM) having seen the need of an agreement on the estimation of measurement, commissioned an organisation called Bureau International des Poids et Mesures (BIPM) to propose a recommendation that would be widely accepted. The organisation convened a working group to publish guidelines on the statement of uncertainties, of which in 1980 published the general recommendation INC-1. Based on this recommendation and CIPM Recommendation 1 (CI-1981) in 1981, the International Organization for Standardization (ISO) published guidelines the Expression of Uncertainty of Measurement in 1993. This guide was later corrected and reprinted in 1995. After over a decade of development and transformation, the GUM was revised current version in 2008, with the title 'Uncertainty of measurement – Part 3: Guide to the expression of uncertainty in measurement' (GUM 2008). This guide, ISO/IEC Guide 98-3:2008, is the current active ISO guide to the analysis of uncertainty. This was made possible by the Joint Committee for Guides in Metrology (JCGM) which comprises of leading experts selected by BIPM, the International Organization for Pure and Applied Chemistry (IUPAC), the International Organization for Standardization (ISO), the International Organization for Pure and Applied Physics (IUPAP) , the International Federation for Clinical Chemistry and Laboratory Medicine (IFCC), the International Electrotechnical Commission (IEC) , the International Laboratory Accreditation Cooperation (ILAC) and the International Organization of Legal Metrolog (OIML).

Uncertainty of measurement is defined by the International Organization for Standardization as a parameter associated with a measurement result that characterizes the dispersion of values which could reasonably be attributed to the measurand

(International Organization for Standardization, 2008). The GUM differentiated uncertainty from error stating that uncertainty of a measurement is as a result of lack of knowledge of the measurand value. When all the recognised systematic effects are corrected, the measurement value is an estimate of the measurand's true value, which is due to the imperfection of systematic effect correction and uncertainty form random effects. Some possible causes of uncertainty in a measurement are incomplete definition of the measurand, non-representative sampling, and insufficient knowledge of possible effects cause by the environmental conditions on the measurement or inaccurate measurements of the environmental conditions, personal bias in reading analogue instruments and Imperfect realization of the definition of the measurand. Other causes include the resolution of finite instrument, inaccurate values of the measurement standards and inexact reference materials, used of inaccurate values of constants and other parameters gotten from external sources in the data reduction algorithm, discrimination threshold, inaccurate assumptions and approximations incorporated in the measurement method and variations when repeated observations of the measurand is done under identical conditions.

2.2.4 Evaluation of CMM measurement errors and uncertainty

CMM physical structure is one of the identifiable sources of error as it comprises of numerous assembled parts which may provide from 1 micron to about 100-micron typical accuracy. Identifying these errors in order to compensate for them, quantifying the remaining errors and stating the errors in relation to their effect on results are vital. Broadly, CMM error could be classified as either geometric error, Kinematic error, stiffness error or thermal error.

i. Geometric error- Errors due to the manufacturing accuracy of component and mechanical adjustment after assembly of the components. This could be found by measuring the flatness, squareness, angular motion and straightness errors. Measuring CMM geometrical errors involves the use of laser interferometer which is characterised by good metrological features. Figure 2.13 shows a laser interferometer that measure with nanometer resolution and a feed rate of about 1m/s. Laser interferometer can determine the following errors; rotation errors, axial positional errors of particular machine, straightness errors and axial perpendicular errors. The device contains compensation system to compensate

the wavelength due the effect of environmental factors such as humidity, temperature and pressure.

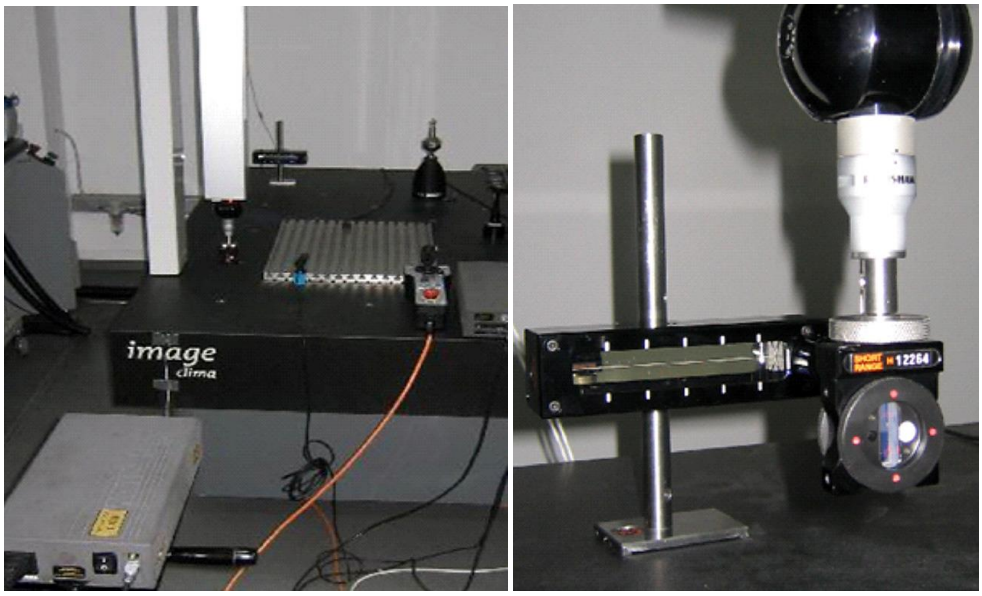

Figure 2.13 Showing the measurement of straightness errors using laser interferometer

ii. Stiffness error- Errors caused by the weight of moving parts and that depends on the stiffness, weight and configuration. Stiffness error could be reduced by the application of large centre distance between the slide bearing and also the implementation of the Abbe and Bryan principle.

iii. Thermal error- Error induced due the environmental temperature changes which cause CMM components to expand and bend. This has a complex non-linear nature making quite difficult to handle. some of the contributing components to the development of thermal errors are; the gradient of temperature, distribution of temperature of the CMM influence by external sources, uniform temperature changes, material of machine component and its thermal properties. Thermal error compensation could be done via the control of heat flows into the system, compensating the error through the controlled of relative motion amidst the frame.

iv. Kinematic error- Kinematic error is the inability for the coordinate measurement machine to accurately reach the specified position as directed by the controller. The authors Nawara et al (1989) and Veldhuis & Elbestawi (1995), in their studies on CMM presented and discussed the effect of change position on both the systematic and random components of the errors. This is mainly as a result of

the position of the machine slides, motors, couplers ball screws, controllers and gears do contribute to the error. Also backlash and hysteresis in the elements do have effect on the kinematic error.

2.3 CMM Kinematic errors model solution

2.3.1 Introduction

Considering a CMM with perfect geometry, the scale reading on each of the three machine axis will be considered as accurate for the coordinate measurement. However, in practice, the most improbable is that CMMs with perfect geometry in manufacturing or production line. CMMs, in practice have imperfect geometry in the following regards

- Straightness of each axis
- Squareness of pairs of axes
- Rotation describing the pitch, roll and yaw

It is vital these that these errors, also called systematic or parametric errors are taken in to account for in order to fully realise the accuracy potential of CMMs. Most manufacturers of CMMs ensure their CMM machines undergo a detailed and comprehensive calibration procedure as a final check before delivering them to their customers. On the customer site, an acceptance test is conducted to the customer by the manufacturer to show that the CMMs performance is within the international or national specification. Moreover, these standards include clauses that ensure other tests are conducted at certain intervals to maintain the CMM conformance to the specification. The 'other' tests are of two types:

Periodic re-verification test – This requires repeating the acceptance test yearly with the goal of identifying and compensating for the drift in CMM performance from the first acceptance testing. The re-verification measurement task is usually different from the routine measurement made with CMM.

Interim Checking - This is done between formal periodic re-verification test with the goal of ensuring that the CMM measurements are accurate, thereby giving the user confidence in the measurement results. The degree of measurement complexity varies between user and application of CMM machine. For some machine few test is carried to maintain measurement confidence while some require a complete re-calibration to maintain measurement confidence. NPL (1998) and Cox, Forbes and Peggs, (1997) have

classified the different level of checking on the degree of confidence which CMMs needed to be checked. Table 2.2 shows the listing.

Table 2.3 Showing classified level of the CMM degree of confidence (NPL 1998).

Class	**Degree of confidence**
Class 1	Verification of all degrees of freedom of the CMM accounting for any influence of temperature variations
Class 2	Verification of the entire working volume of the CMM using a standard artefact such as a ball- or hole-plate (a two-dimensional plate with regularly spaced features, usually holes or spheres);
Class 3	Verification of the space envelope of interest using a master artefact representing the work piece features measured in the user's usual application;
Class 4	Verification of just the working volume of interest using standard artefacts, for example, length bars

2.3.2 CMM kinematic error model and capabilities

This is based on the superposition of behaviours from the three coordinate axes with each describe as a function of the corresponding reading scale. For example, six functions of x could be used in describing the behaviour of a stylus assembly with the reading scale of y and z kept fixed. The six functions comprise of three stating the angle of rotation that describe the pitch roll and yaw of x axis and three giving the location of the fixed point on the housing. Similarly, keeping x and z fixed six function are generated for y axis and keeping, keeping x and y, six functions for z-axis. Kinematic model is used to describe the machine in terms of the six functions of each axis. Considering the x axis, which could be describe by

$$\begin{bmatrix} x_x \\ y_x \\ z_x \end{bmatrix} = \begin{bmatrix} x(1,0,0)^T + \delta_{xx}(x,a) \\ \delta_{xy}(x,a) \\ \delta_{xz}(x,a) \end{bmatrix} \tag{2.1}$$

and the orientation is described by a rotation matrix $R_x(x, r)$ defined as a product of plane rotations. The (δ_{xx}) term is sometimes described as the x-axis scale error while (δ_{xy}) and (δ_{xz}) give the x-axis straightness errors. Similarly, the location and orientation along the y-axis is described by

$$\begin{bmatrix} x_y \\ y_y \\ z_y \end{bmatrix} = \begin{bmatrix} \delta_{yx}(y,b) \\ y(0,1,0)^T + \delta_{yy}(y,b) \\ \delta_{yz}(y,b) \end{bmatrix} \tag{2.2}$$

and $R(y, s)$. This information can be combined to provide an estimate of location as a function of x and y

$$x_{xy} = x_x(x\ , a\ ) + R_x\ (x, r\ )\ x_y\ (y\ , b\ ) \tag{2.3}$$

This formulation supposes that the y-motion depends on (or is carried by) the x-motion and moreover that at x = y = 0 the axes are orthogonal and the two rotation matrices R_x and R_y are aligned. Adding the z-axis (assumed to be carried by the y-axis) and the probe offset under similar assumptions, the model takes the form

$$x = x_x(x\ , a\ ) + R_x\ (x, r\ )x_y\ (y, b\ ) + R_x\ (x, r\ )R_y\ (y, s\ )x_z(z, c) + R_x\ (x, r\ )R_y\ (z, t\ )P \tag{2.4}$$

Thus the kinematic model is specified in terms of 18 individual error functions, three positional and three rotational for each of the three axes. The basic components are therefore functions of a single variable and these can be specified using polynomials or splines, for example. The correct formulation depends on the architecture of the CMM, but the common CMM designs are covered by the model; see, for example, Zhang et al. (1988). If all three rotation matrices are set to the identity matrix, then x* is given by

$$x^* = x + P_x + [\delta_{xx}(x) + \delta_{yx}(y) + \delta_{zx}(z)] \tag{2.5}$$

Where the actual position of the probe in x-axis is P_x and similarly for y* and z*, showing that the positional correction for x includes a sum of functions of x, y and z. If each of these functions includes a constant term, there will be degrees of freedom in the model which cannot be determined from the data. The simplest way to resolve this is to

constrain $\delta_{yx}(0) = \delta_{xx}(0) = 0$. In fact, similar constraints have to be placed on all six types of component as will become clear when we consider a linearized version of the kinematic model. If we evaluate the kinematic model at points along each axis we obtain

$$x^*([x,0,0]^T) = x_x(x,a) + R_x(x,r)P \tag{2.6}$$

$$x^*([0,y,0]^T) = x_y(y,b) + R_x(y,s)P \tag{2.7}$$

$$x^*([0,0,z]^T) = x_z(z,c) + R_z(z,t)P \tag{2.8}$$

showing that each of the three sets of parameters can be determined by measurements along the three axes. Thus, a measurement strategy which includes measurements along or parallel to each of the three axes using three or more probe offsets will be sufficient to determine the model parameters, assuming that there are enough measurements along each axis. Often the kinematic model is used not as given above but in a simpler, linearized form. Employing the linearization, then *R* is given by:

$$\tilde{R}_{xyz} = \mathrm{R_x R_y R_z} = \begin{bmatrix} 1 & (\mathrm{w_x} + \mathrm{w_y} + \mathrm{w_z}) & -(\mathrm{v_x} + \mathrm{v_y} + \mathrm{v_z}) \\ -(\mathrm{w_x} + \mathrm{w_y} + \mathrm{w_z}) & 1 & (\mathrm{u_x} + \mathrm{u_y} + \mathrm{u_z}) \\ (\mathrm{v_x} + \mathrm{v_y} + \mathrm{v_z}) & -(\mathrm{u_x} + \mathrm{u_y} + \mathrm{u_z}) & 1 \end{bmatrix} \tag{2.9}$$

$$\mathrm{R_x x_y} = \begin{bmatrix} \delta_{\mathrm{yx}}(\mathrm{y}) + \mathrm{w_x}(\mathrm{x})\mathrm{y} \\ \delta_{\mathrm{yy}}(\mathrm{y}) + \mathrm{y} \\ \delta_{\mathrm{yz}}(\mathrm{y}) - \mathrm{u_x}(\mathrm{x})\mathrm{y} \end{bmatrix} \tag{2.10}$$

$$\mathrm{R_x R_y x_z} = \begin{bmatrix} \delta_{\mathrm{zx}}(\mathrm{z}) - (\mathrm{v_x}(\mathrm{x}) + \mathrm{v_y}(\mathrm{y})\mathrm{z}) \\ \delta_{\mathrm{zy}}(\mathrm{z}) + (\mathrm{u_x}(\mathrm{x}) + \mathrm{u_y}(\mathrm{y})\mathrm{z}) \\ \delta_{\mathrm{zz}}(\mathrm{y}) + \mathrm{z} \end{bmatrix} \tag{2.11}$$

With these linearisations, the expressions for the location of the probe stylus tip become:

$$x^* = x + P_x + [\delta_{xx}(x) + \delta_{yx}(y) + \delta_{zx}(z)] + w_x(x)y - (v_x(x) + v_y(y))z + (w_x(x) + w_y(y) + w_z(z))P_y - (v_x(x) + v_y(y) + v_z(z))P_z \quad (2.12)$$

$$y^* = y + P_y + [\delta_{xy}(x) + \delta_{yy}(y) + \delta_{zy}(z)] + (u_x(x) + u_y(y))z - (w_x(x) + w_y(y) + w_z(z))P_x - (u_x(x) + u_y(y) + u_z(z))P_z \quad (2.13)$$

$$z^* = z + P_z + [\delta_{xz}(x) + \delta_{yz}(y) + \delta_{zz}(z)] - u_x(x)y + (v_x(x) + v_y(y) + + v_z(z))P_x - (u_x(x) + u_y(y) + u_z(z))P_y \quad (2.14)$$

where x* is the positional correction for x, y* is the positional correction for y, and z* is the positional correction for z.

2.4 Selected technique

2.4.1 CMM Kinematic error model

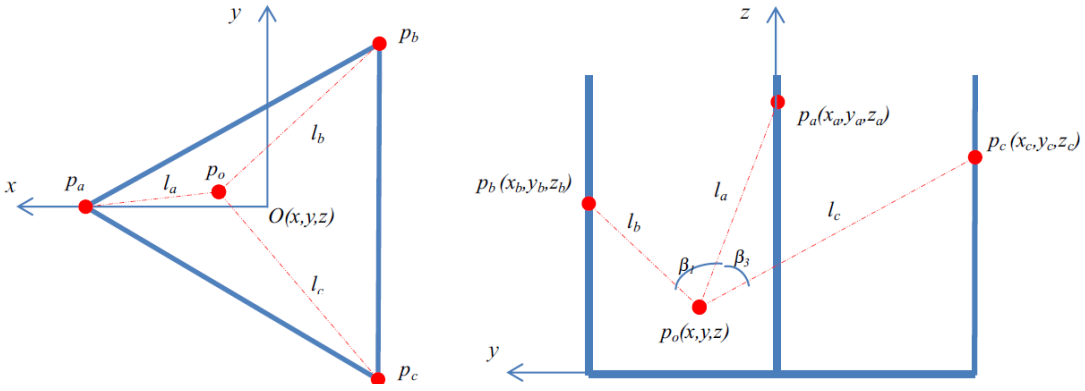

Figure 2.14 The coordinate system: top view x-y plane to the left while the front view y-z plane to the right (Ali R. and Kristiaan S., 2014)

The coordinate system of the coordinate measurement machine is shown in figure 2.14. The base of the CMM is placed at the origin O (0, 0, 0) and the joints intersect the base at points a (p_a), b (p_b) and c (p_c). The x-axis divides the angle at point an equally while the z-axis is perpendicular to the base plane (a, b, c). The geometric parameters are θ_i representing the angle between tetrahedron legs l_i , l_{in} with the angles $\theta_a = \theta_b = \theta_c = 68^o$ (Rugbani and Schreve, 2014). l_i is the distance between the probe tip p_0 and the pivot point of the ball joint p_i . l_{min} and l_{max} are maximum and minimum extensions of the legs. With the assumption that the probe tip (x, y, z) at the point of intersecting of the three legs, which is the main vertex of the moving tetrahedron. Due to the spherical joints, the legs equation of movement could be expressed suing the following equations:

$$l_a^2 = (x - x_a)^2 + (y - y_a)^2 + (z - z_a)^2 \quad (2.15)$$

$$l_b^2 = (x - x_b)^2 + (y - y_b)^2 + (z - z_b)^2 \quad (2.16)$$

$$l_c^2 = (x - x_c)^2 + (y - y_c)^2 + (z - z_c)^2 \quad (2.17)$$

The values of the moving motors (z_{i+1} and z_{i-1}) on the z coordinate could be computed relative to z component of the stationary motor (z_i), where distances dz_{i+1} and dz_{i-1}, i can be calculated provided that the legs l_a, l_b and l_c, as well as angels (β) between them are known. Let the subscript i and represent (a, b, c) when i rotates around z-axes in clockwise direction when seen from above, subscripts i_p and in refer to the previous and next points, respectively.

$$z_{in} = z_i - dz_{in} \quad (2.18)$$

$$z_{ip} = dz_{ip} - z_i \quad (2.19)$$

$$dz_{in}{}^2 = (d_{in})^2 - (b_{in})^2 \quad (2.20)$$

$$dz_{ip}{}^2 = (d_{ip})^2 - (b_{ip})^2 \quad (2.21)$$

$$d_{in}{}^2 = l_{in}{}^2 + l_{in}{}^2 - 2l_i l_{in} \cos(\beta_{in}) \quad (2.22)$$

$$d_{in}{}^2 = l_{ip}{}^2 + l_i{}^2 - 2l_i l_{ip}\cos(\beta_{ip}) \quad (2.23)$$

Where *i* is the pivot point of the *i*th joint, *i* = [a, b, c]. in and i_p are the pivot point of the next and previous pivot points, respectively, d_{in} and d_{ip} are the distance between ith pivot point and the next and previous pivots, respectively. D_z is the height difference between the pivot point of the joint on stationary motor and moving joints. βin and βip are the distance between p_1 and p_2 at $z_2 = z_1$ and $z_3 = z_1$, respectively.

βin and βip are the angles between leg l_i and legs l_{in} and l_{ip}, respectively. At the start of the operation, z is assumed to be equal to zero, or alternatively, the stationary point will have $z = -z_i$, and $z_i = 0$. The coordinate of the probe location can be found by solving Eqs. (2.24), (2.25) and (2.26) and replacing the values of zin and zip from Eq. (2.27). This yields explicit expressions for the x, y and z coordinates of the centre point of the probe as follows

$$y = \frac{-v \pm \sqrt{v^2 - 4uw}}{2u} \quad (2.24)$$

$$z = F + D\,(y) \quad (2.25)$$

$$x = A + B\,(y) \quad (2.26)$$

$$A = \frac{\left(\frac{c_{in}-c_i}{2z_{in}} - \frac{c_i-c_{ip}}{2z_{ip}}\right)}{\left(\frac{x_i-x_{ip}}{z_{ip}} - \frac{x_{in}-x_i}{z_{in}}\right)} \quad B = \frac{\left(\frac{y_{in}-y_{in}}{z_{in}} - \frac{y_{ip}-y_i}{z_{in}}\right)}{\left(\frac{x_i-x_{ip}}{z_{ip}} - \frac{x_{in}-x_i}{z_{in}}\right)} \quad D = \left(\frac{y_{in}-y_i}{z_{in}} - \mathrm{B}\,\frac{x_{in}-x_i}{z_{in}}\right) \quad F = \frac{x_{in}-x_i}{z_{in}} - \frac{c_{in}-c_i}{2z_{in}} \quad (2.27)$$

$$c_i = l_i^2 - x_i^2 - y_i^2 - z_i^2 \quad (2.28)$$

$$u = 1 + B^2 + D^2 \quad (2.29)$$

$$v = 2DF + 2\,x_i B - 2AB + 2y_i \quad (2.30)$$

$$\mathrm{W} = A^2 + F^2 - 2x_i A - c_i \quad (2.31)$$

2.4.2 Gaussian process model

Gaussian process (GP) is a time dependant statistical distribution where all points in some input space are associated with normal distributed random variable and a finite collection of the random variables do have a multivariate normal distribution. GP distribution is a distribution over functions which are basically the joint distribution of all the infinitely random variables. In statistical modelling, GP is important due to the properties inherited from the normal. When a process is modelled as GP, its distribution of various derived quantities such as the average value of the process over certain durations and the error in the estimation of the average could be obtained explicitly. GP is determined by its mean and covariance function. Notation wise, Gaussian process could be written as

$$X \sim GP(m, v) \tag{2.32}$$

Where X is a random function, distributed as a GP with a mean function, m, and a covariance function, v. when the random variables are assumed to have a zero mean which will simplify the calculations without loss of generality and the mean square of the process is entirely determined by the covariance function. These are computed quickly using recursive formula. GP is used in decomposing a geometric feature into three components

- Designed geometric form - This is done by deciding the line function and approach direction and solve the intersection points between functions.
- Systematic manufacturing errors- This refers to the deviation from an ideal form that are identically independent distributed random (i.i.d.).
- Random manufacturing errors - This refers to the deviation from an ideal form that is non-identically independent distributed random (non-i.i.d.).

The method models the systematic manufacturing errors as a spatial model using Gaussian correlation function. The random manufacturing errors are modelled as independent and identical distributed noises. With a small number of coordinated measurements, the Gaussian process model could reconstruct the part surface and assesses the form error better than traditional methods. It also provides an empirical distribution of the form error the quantification of the decision risk in part acceptance which work for generic features. The authors, Dowling et al. (1993), Yang and Jackman

(2000) and XIA et al (2008) used Gaussian process method to provide information on the error and uncertainties in deciding CMM acceptance or rejection.

2.5 CMM numerical simulation calculation

The international standard organisation in 2006 provided a set of general guideline and simplified equation for the calculation of CMM test uncertainty in ISO/TS 23165:2006 (International Organization for Standardization, 2006). In 2008, they provided another guideline, ISO/TS 15530-4:2008, which specifies the requirement for the application of simulation based uncertainty evaluation to CMM measurement. The guideline also contains description on testing methods for such simulation alongside various general testing procedures International Organization for Standardization, 2008). The International Organization for Standardization, in two other guidelines, ISO/TS 15530-3:2004 and ISO/DIS 15530-3:2009 (International Organization for Standardization 2004 and International Organization for Standardization 2009), describe an experimental approached when determining CMM measurement. This approach, instead of using an actual workpiece, it uses substituted measurements that are carried on calibrated work piece with similar shape and size. It then uses the obtained difference between the measured result and the known calibrated values to estimate the measurement uncertainty.

Empirical models are used to account for the unknown systematic effects of a GP model (Forbes, 2015). The GP model can be approximated by an empirical model with a prior correlation structure leading to a less computational expense. This approach is to fit a function $f(x)$ to data points (x_i, y_i) by assigning a suitable Gaussian prior to establish the response of a correlation structure.

The standard GP model:

$$y = f(x + a) + e \tag{2.33}$$

Where $f(x + a)$ is the response function from the known effects and a Gaussian distribution effect is described as e.

While the empirical model is:

$$y = f(x + a) + e(x, b) \tag{2.34}$$

An empirical function, such as a polynomial, spline, radial basis function, etc., has been concerned with fitting data that is subject *to systematic effects representing e(x, b)* as a correlation structure imposed by assigning a Gaussian prior to *b*. The applications included in the empirical models are such as liner least-squares regression, Gauss-Markov regression, spatially correlated empirical models, etc.

2.6 Optimisation and control

A number of tools are available for the optimisation and control of the coordinate machine measurement errors and uncertainty evaluation. For this project and in this section, Matlab software is used for evaluation and will be discussed in section.

Matlab programme

Matlab developed an optimization toolbox that could be used for optimisation of CMM error and uncertainty evaluation. The optimisation toolbox provides functions that search out parameters that either minimize or maximize specified objectives while satisfying constraint. The Matlab optimisation toolbox contains solvers for linear programming, mixed-integer linear programming, quadratic programming, non-linear optimisation and non-linear least square. The solvers could be used to obtained optimal solutions to continuous and discrete problem, conduct trade-off analysis, incorporation of optimisation methods into algorithms and applications. The Matlab optimisation toolbox using the following steps while obtain a satisfactory solution

- Solver Selection - Selecting the most appropriate solver and algorithm
- Writing Objective Function- Defining the required functions to minimize or maximize
- Writing Constraints -Giving details of the necessary bounds, linear constraints, and non-linear constraints of the problem.
- Set Options -Setting the optimization options
- Parallel Computing - Utilisation of parallel computing in Solving the constrained nonlinear minimization or multi-objective optimisation problems defined by the user.

2.7 Conclusions

In this chapter, the state of art of the CMM related technologies are reviewed with focus on system and configuration, measuring and probing system, inspection path planning, Evaluation of measurement errors and uncertainty, Kinematic errors model solution,

numerical simulation, Optimisation and control using Matlab programme. CMMs have high precision and accuracy due to their inherent characteristics of their measuring techniques. They are essentially universal measurement machines making them able to measure any dimensional characteristics of a part configuration. Combined with software control, most part could be inspected in a single setup, thereby eliminating the need to reorient the object. The accuracy and precision are improved as human errors and setup time are reduced. These advantages help make CMM more productive and the traditional inspection techniques. Both local kinematic error model and Gaussian process model were used to analyse the systematic measurement errors and measurement uncertainty. Local Kinematic error model only applies to a small region of the volume used for the measurement task and the limited time period it takes to conduct the task. The advantage of this approach is the compensation of medium term systematic effects due to thermal effect without the CMM needing full parametric compensation procedure. Gaussian process is a time dependant statistical distribution where all the points in some input space is connected with a normal distributed random variable. Combing both local kinematic modem and Gaussian model offers a novel approach in reducing the error and uncertainty characterisation process and compensating for them.

Chapter 3 CMM verification approach

3.1 Introduction

Right from the first Coordinate measurement machine over four decades ago, it certainly has revolutionised dimensional metrology while becoming an integral part of the industry quality systems. This advancement has resulted to increase in productivity and lower inspection cost (Miguel et al 1995). However, the machines require appropriate checks to be carried out on installation and periodically to the operational lifetime of the machine to maintain optimal performance. The development of techniques that are both accurate and efficient in checking the health of CMMs are necessary and still a priority in many research groups. Standards have been introduced to effectively obtain CMM performance and such standards include the international standard organisation, Coordinate Measuring Machine Manufacturers Association and other numerous national standard. The Coordinate Measuring Machine Manufacturers Association publish the first and second edition of the CMM Accuracy Specification in 1982 and 1989 respectively, the International Standard Organisation published its CMM standard, ISO 10360-2, for the acceptance test and interim machine checking in 1994. The British Standard Technical Committee published its standard for the verification of the coordinate measurement machine in three parts, titled BS 6808: Coordinate Measuring Machine, With the 1st, 2nd and 3rd parts published in 1987,1987 and 1989 respectively (ISO 1994, BS 1987, BS 1989).

The American standard, ANSI/ASME B89.1.12M was published in 1989 and a revised edition published in 1990 (ASNI/ASME 1989). Other commonly used standard are the French, German, Japanese and Austrian standards (VDI/VDE 2617 1991, NFE 1986, ONORM 1989, JIS 1987, CMMA 1982). Table 3.1 captures the different CMM specification. With the development of control system, CMM plays an important role in reducing the duration of the inspection process with some used as layout machine before machining and verifying feature location after machining.

Table 3.1 Showing some of the CMM Specification standards

Parameters	ISO 10360-2	BS 6808	B89.1.12M	VDI/VDE 2617	NF Ell 150	JISB 7440	CMMA
Measuring task	Length	Length	Various	Length	Various	Various	Various
Test Length	5	5 or 10	CMM dependant	5	8	5	3
Repeat	3	5 or 10	1	10	5	5	3
confidence interval	99.7%	95%	99.7%	95%	99.7%	95%	95%
Repeatability	No	Yes	Yes	No	Yes	No	Yes
Artefacts	Gauge blocks, step gauges	Gauge blocks, step gauges	Gauge blocks with ball-ended bars for volumetric accuracy	Gauge blocks, step gauges	Various. Geometrical elements in addition to gauge blocks.	Gauge blocks, step gauges	Gauge blocks,
Position	7	8	20-30	7	12	5	7
Thermal Drift	No	Yes	Yes	No	No	Yes	Yes
Probe Test	Yes	No	Yes	Optional	No	No	No

3.2 CMM measurement strategies

The CMM could be used to evaluate surfaces in 1, 2 or 3-dimensionsional coordinate systems depending on the required application and designated quality requirements. With a CMM, a single point data could be generated or numerous points could be generated with fitting routines for characterisation of part surfaces; these points could be measured by the probe on any surface that can be reached by the probe.

Prior to combining CMM and CAM, for decades CMM could be used off-line as quality evaluation tool in the manufacturing industry. However, this leaves no room for direct process control due to the time lag between the manufacturing machine and the offline CMM machine. Integrating the CMM directly with the manufacturing machine

allows immediate inspection that will enable a hundred percent inspection and a direct feedback to machine for other process control evaluation. This approach makes reconfiguring the machine an important aspect of this process-inspection integration because it must act both as material removal device in one instant and a measurement device the next instant.

Attaching a control unit enables manual measurements and programming in addition to CNC operation. A microprocessor is used to control the control unit. In a coordinate measurement machine, both the hardware and software are inseparable and they both represent one system. The CMM's software largely determines the effectiveness and efficiency of the CMM. Most CMM software includes the following features; measurement of plane and spatial curves, measurement of diameters, measurement of lengths, measurement of centre distance, measurement of geometrical and form errors in prismatic components, digital input and output commands for process integration, Interface to CAD software, Data communications, Parameter programming to minimize CNC programming time of similar parts, Measurement of plane and spatial curves, Program for the measurement of spur, helical, bevel and hypoid gears, and Online statistics for statistical information in a batch.

CMM has become an essential and useful tool in Computer aided manufacturing (CAM). Prior to using CMMs in CAM, it was difficult for designs to be checked if they conform to the specification. This was due to the fact that CAM old standards only used unidirectional communication which only translated data that was converted into design forms. With the addition of CMM to CAM, a new bi-directional standard was introduce known as Dimensional Measurement Interface System(DMIS) and it is used in communication of inspection data between the manufacturing machines and the inspection equipment to compare what has been made to what ought to be made. This approach generally improved the accuracy of the CAM machines.

CMM probe is the data collecting unit of a CAM machine. This means that the selection of the probe and its placement are very important. Instructions are sent to the CMM system with details that contain the positioning of the probe, the path the probe will follow and the angle that the probe will approach the machine. After production, the CMM is used to as part of the inspection to verify the part. The data of the checked part is the forwarded back to the system where the original geometry is kept. On the system, the produced part is the evaluated in relation to the design and the deviations are computed and identified. This approach has help in identifying and solving many

manufacturing issues that existed prior to the combination of CMM and CAM. Figure 3.6 showing the relationship between the CNC machine tool, CAD system and CMM. Implementing the right measurement strategies is vital in making metrologists make the best educated selections of the appropriate number of probing points and their equivalent distribution when measuring a work piece on coordinate measurement machine. It is imperative that the accuracy can be estimated and traceability demonstrated to ensure quality system. Having quality systems brings an increase in user awareness of the numerous benefits a provided by reliable and frequent check. Over the couple of decades' guidelines and standards were developed to enable metrologists make useful and appropriate comparison of different vendor's CMM and when purchased to be able to re-verify the CMM test specification results. It is of extreme importance that metrologists can demonstrate traceability to both international and national standards while estimating the accuracy of measurement carried out by a three dimensional CMM. The international Standard organisation detailed the necessary procedure for the acceptance, re-verification test and the interim checks requirement to ascertain if a CMM performance is within acceptable limits as indicated by the manufacture. However, due to the uncertainties associated with CMM, it is difficult to make concrete statement on the length measurement capability of a machine. This means that the length measurement gotten from a small sample of measurement could not be substantially considered as the representative of every possible length measurement task. In this regard the test results do not necessarily guaranty the traceability of the measurement foe all the measurement task that could be performed.

Being aware of this important fact, the metrologist need to develop task related measuring strategies for each set of measurement undertaken in order to provide the right level of measurement confidence on the entire result. There is an essential requirement of skill, relevant experience and attention to detail on the side of the metrologist when determine the right measurement strategies that offer an acceptable measurement result. The technological advancement of both hardware and software over the last two decades has produced machines that demonstrate high accuracy in measurement. The measurement accuracy is largely associated with the software and machine while the user is responsible for the sampling strategy for an inspection process.

The National Physics Laboratory (NPL) has identified keys tasks a user could follow and help in assisting the user to the uncertainties inherent in the CMM use and

suggesting the strategies will aid in ensuring confidence in the measuring results. Some of the recommended strategies include:

Definition the work piece datum feature(s) to be used within the co-ordinate system.

A datum feature could be defined as an actual feature of a part that is used to establish a datum. This could be an axis plane, median plane or surface of a component. It is very important to understand datum in order to prevent causing large error from using in inappropriate datum. Appropriate drawing should present all required manufacturing dimension that are related to datum information. Datum features are classified into the following:

1. The primary datum - Primary datum could be defined as feature(s) that are used for the levelling the component that are normally an axis or on a surface.
2. The secondary datum - Secondary datum could be defined as feature(s) used for the rotation of the component(s) that are relative to the primary datum.
3. The tertiary datum - Tertiary datum could be defined as a feature(s) that are used in completing the coordinate system in relation to both the primary datum and secondary datum.

Selection of the work piece orientation

The Selection of the work piece orientation within the measurement volume of the CMM come after both the measurement and datum features are determined. The key consideration is to verify accessibility of the surfaces and feature that are required for probing. During the measurement campaign, it is necessary that the datum features are free and not use to hold the work piece since the feature require probing. The user ought to be have knowledge of the work piece to enable the optimum measurement are taken. The National Physics Laboratory recommends aligning the critical features of length along any axis of the CMM, to ensure only an axis is utilising for measurement which will remove any uncertainty as a result of other axes. When selecting the work piece holding method, considering should be taken on the following; the measurement force, Heavy items, light items, Fixtures and adhesive.

For any measurement procedure, it is important that the work piece is not over constrained. Where possible let the clamping be done at only one point to minimise distortion even though clamping on one point may allow the work piece rotate during measurement. The use of a light clamp with materials such as cork or rubber placed

between the workpiece will help drive down distortion and avoid damage to the workpiece.

3.3 CMM calibration

Calibration of coordinate measuring machine is vital requirement in ensuring the authenticity of measurement results. Calibration is generally defined as a comparison between two measurement systems, with one from a known uncertainty also known as the standard and the other with unknown uncertainties referred as test equipment. Calibrated systems ensure appropriate measurement standards are maintained and are traceable to the value of stated references either national or international values.

Calibration of CMM must demonstrate accuracy and repeatability and must factor in external influences which include vibration, humidity, temperature, electrical power supply, humidity, radiated energy etc. In calibration, the sensitivity and stability of measurement instruments must be taken into account as the two parameters determine duration of a calibrated machine and the frequency of calibration. The Stability is generally expressed as the degree of change in the calibrated output of an instrument over a given duration of time. This is mostly measured in percentage and the duration could span from 90 days to 12 months in consideration of normal operating conditions. These results enable the performance of the instrument to be judge and rated.

Two popular standards used in calibrating are the U.S. standard, *American Society of Mechanical Engineers (*ASMEB89.4.1) and the international standard, (ISO 10360).

3.4 CMM Local Kinematic Model

Local Kinematic error model only applies to a small region of the volume used for the measurement task and the limited time period it takes to conduct the task. The advantage of this approach is the compensation of medium term systematic effects due to thermal effect without the CMM needing full parametric compensation procedure. This model only needs low but sufficient points in the region that are required to determine local kinematic model with the possibility of updating the local kinematic model continually. Figure 3.1 shows the schematic of the proposed approach with some examples of local evaluation tasks. The local evaluation task could be performed either through a physical CMM or simulation based on a physical CMM. The local kinematic model is based upon an axis-upon-axis build-up of the physical CMM concerned. The

calibration information, partial or full, of the reference artefact is also required. After acquiring the measurement, a best fit algorithm based on Gauss-Newton could be used to estimate the model parameters which include artefact parameters. This model will then be used to compute and compensate the systematic errors and evaluate the uncertainties associated with fitted parameters and the measurement in the area of interest.

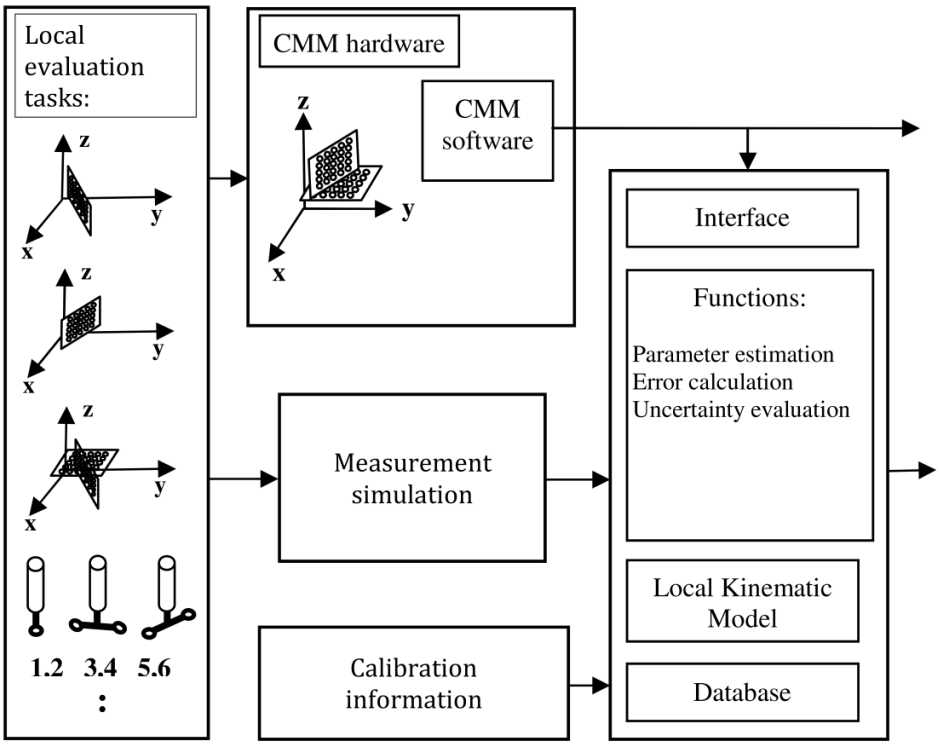

Figure 3.1 Schematic of the local kinematic error model measurement.

Reposted from (Yang, et al., 2008)

A model is used to evaluate the uncertainties and errors associated with the fitted parameters of the kinematic model in the measurement region interest. This was based on the law of propagation of uncertainty.

A numerical solution is used to investigate and determine the behaviour and performance of kinematic models as the following task:

I. Calculating the Model parameter

Each set of measurement data is applied to a Gauss-Newton method to calculate the model parameters. A QR approach is then used to solve the rank-deficiency problem and the parameters passed to another local evaluation.

II. Error calculation and simulation

The model that is now identified could be used to determine the errors in the evaluated region of the coordinate measuring machine volume based on the measurement results

III. Uncertainty calculation

The uncertainties from the model parameters and artefact are generated based on the Jacobean matrices. This is further extended to determine the uncertainties of the coordinated measurement machine in the entire working volume.

Other method used in calculating model parameters Least-Square method, Cheby-Chev, Monte-Carlo, Parametric model and polynomial model.

The specific details and further simulations and discussions on local kinematic error model are also included in Chapter 4.

3.5 CMM GP Model

The GP model is a distribution over functions, which is essentially the joint distribution of all the infinitely random variables. In statistical modelling, GP is important due to the properties inherited from the normal distribution. When a process is modelled as GP, its distribution of various derived quantities, such as the average value of the process over certain duration and the error in the estimation of the average, could be obtained explicitly. GP is determined by its mean and covariance function.

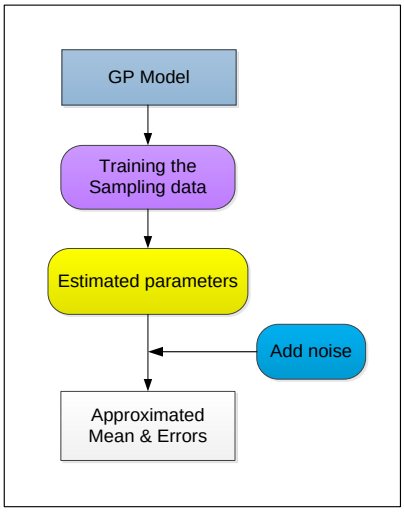

Figure 3.2 Illustrates the scheme of the GP model simulation

In the GP model, training data from the sampling points (in this case, using a ball plate position) is simulated to find the approximated parameters associated in the model using

likelihood estimation or GP function in the MATLAB programme etc. To simulate it as a real experiment, noise is added into the model. Then, mean and covariance functions are approximated and errors of the ball plate are also calculated.

More details and further analysis of GP regression model can be found in Chapter 5.

3.6 CMM measurement errors

CMM physical structure is one of the identifiable sources of error as it comprises of numerous assembled part which may provide from 1 micron to about 100-micron typical accuracy. Identifying these errors in order to compensate for them, quantifying the remaining errors and stating the errors in relation to their effect on results are vital.

3.6.1 Sources of CMM errors

3.6.1.1 Kinematics of CMM

Kinematic error is the inability for the coordinate measurement machine to accurately reach the specified position as directed by the controller. The authors Nawara et al (1989) and Veldhuis & Elbestawi (1995), in their studies on CMM presented and discussed the effect of change position on both the systematic and random components of the errors. This is mainly as a result of the position of the machine slides, motors, couplers ball screws, controllers and gears do contribute to the error. Also backlash and hysteresis in the elements do have effect on the kinematic error.

3.6.1.2 Form of work piece

Errors occur due to the manufacturing accuracy of components and mechanical adjustment after assembly of the components. This could be found by measuring the flatness, squareness, angular motion and straightness errors. Measuring CMM geometrical errors involves the use of laser interferometer which is characterised by good metrological features. Figure 2.6 shows a laser interferometer that measure with nanometre resolution and a feed rate of about 1m/s. Laser interferometer can determine the following errors; rotation errors, axial positional errors of particular machine, straightness errors and axial perpendicular errors. The device contains compensation system to compensate the wavelength due the effect of environmental factors such as humidity, temperature and pressure.

3.6.1.3 Environmental conditions

Error induced due the environmental temperature changes which cause CMM components to expand and bend. This has a complex non-linear nature making quite difficult to handle. some of the contributing components to the development of thermal errors are; the gradient of temperature, distribution of temperature of the CMM influence by external sources, uniform temperature changes, material of machine component and its thermal properties. Thermal error compensation could be done via the control of heat flows into the system, compensating the error through the controlled of relative motion amidst the frame.

Stiffness error- Errors caused by the weight of moving parts and that depends on the stiffness, weight and configuration. Stiffness error could be reduced by the application of large centre distance between the slide bearing and also the implementation of the Abbe and Bryan principle (Bryan J.B., 1979).

3.6.2 CMM kinematic errors

Considering a CMM with perfect geometry, the scale reading on each of the three machine axis will be considered as accurate for the coordinate measurement. However, in practice, it is most improbable that CMMs will have perfect geometry in the manufacturing or production line. CMMs in practice have imperfect geometry in the following regards

- Straightness of each axis
- Squareness of pairs of axes
- Rotation describing the pitch, roll and yaw

Positioning Deviation: *ypy* **Straightness Deviations:** *t* a) Horizontal: *ytx* b) Vertical: *ytz* **Rotational Deviations:** *r* a) Moving axis: *yry* b) Horizontal axis: *yrx* c) Vertical axis: *yrz*	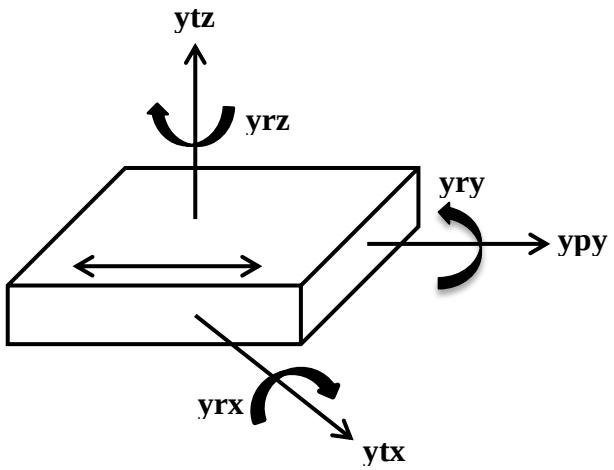
Squareness Deviations: ϕ a) Plane XY: ϕ_{xy} b) Plane XZ: ϕ_{xz} c) Plane YZ: ϕ_{yz}	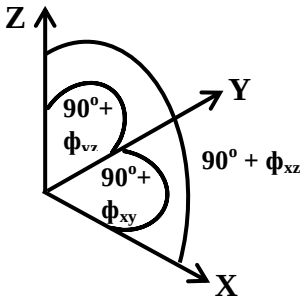

Figure 3.3 Errors of a CMM carriage. Reproduced from (Trapet and Waldele, 1991)

Figure 3.3 describes these component errors for a CMM carriage. Assuming the rigid body behaviour, the six error components are the positioning error, two straightness errors parallel to the axes, and three rotational errors (roll, pitch, and yaw). Thus, a three-axis machine has 18 errors and three squareness errors.

It is vital these that these errors, also called systematic or parametric errors are taken in to account for in order to fully realise the accuracy potential of CMMs. Most manufacturers of CMMs ensure their CMM machines undergo a detailed and comprehensive calibration procedure as a final check before delivering them to their customers. On the customer site, an acceptance test is conducted to the customer by the manufacturer to show that the CMMs performance is within the international or national specification. Moreover, these standards include clauses that ensure other tests are conducted at certain intervals to maintain the CMM conformance to the specification. The 'other' tests are of two types: Periodic re-verification test - This requires repeating the acceptance test yearly with the goal of identifying and compensating for the drift in

CMM performance from the first acceptance testing. The re-verification measurement task is usually different from the routine measurement made with CMM.

This is done between formal periodic re-verification test with the goal of ensuring that the CMM measurements are accurate, thereby giving the user confidence in the measurement results. The degree of measurement complexity varies between user and application of CMM machine. For some machines, few tests are carried out to maintain measurement confidence while some require a complete re-calibration to maintain measurement confidence. NPL (1998) and Cox, Forbes and Peggs, (1997) have classified the different level of checking on the degree of confidence which CMMs needed to be checked. Considering a CMM with perfect geometry, the scale reading on each of the three machine axis will be considered as accurate for the coordinate measurement. However, in practice, it is most improbable that CMMs will have perfect geometry in the manufacturing or production line. It is vital these that these errors, also called systematic or parametric errors are taken into account for in order to fully realise the accuracy potential of CMMs. On the customer site, an acceptance test is conducted to the customer by the manufacturer to show that the CMMs performance is within the international or national specification. Moreover, these standards include clauses that ensure other tests are conducted at certain intervals to maintain the CMM conformance to the specification. The 'other' tests are of two types. This requires repeating the acceptance test yearly with the goal of identifying and compensating for the drift in CMM performance from the first acceptance testing. The re-verification measurement task is usually different from the routine measurement made with CMM. This is done between formal periodic re-verification test with the goal of ensuring that the CMM measurements are accurate, thereby giving the user confidence in the measurement results. The degree of measurement complexity varies between user and application of CMM machine. For some machine few test is carried to maintain measurement confidence while some require a complete re-calibration to maintain measurement confidence. NPL (1998) and Cox, Forbes and Peggs, (1997) have classified the different level of checking on the degree of confidence which CMMs needed to be checked.

3.6.2.1 Translational errors

3.6.2.1.1 Positioning errors

The positioning errors of the Coordinate Measurement Machine in relation to its motion axis could be measured directly and comparing it with 3 non-contact capacitive probes.

The approach is suitable for CMM with either good or bad repeatability. When a CMM has good repeatability, it is also feasible to do the positioning measurement of the CMM on its moving axis while using an uncalibrated ball array though offer lesser accuracy compare to the former method. Two runs are required for a positional error measurement. The first run reads from the *X* channel of the capacitive probe with the following expression:

$$R_x(x_i) = l_i - \delta_x(x_i) \tag{3.1}$$

Where $\delta_x(x_i)$ is the position error of x motion when the carriage is moved to position x_i. After the first run, the ball array becomes shifted to a distance equal to the spacing between the two balls. The capacitive probe reading will now be

$$R_x'(x_i) = l_{i-1} - \delta_x(x_i) \tag{3.2}$$

Figure 3.4 shows the positional error found by intersecting regression lines with reference line through rows of measured points. The positional error is the deviation of the intersection from the ideal coordinate system intersections.

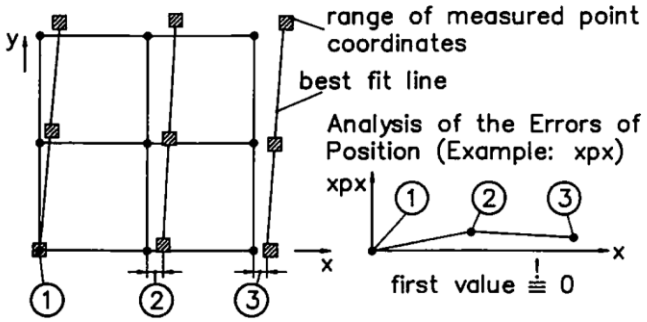

Figure 3.4 showing the positional error measurement (Trapet and Waldele, 1991)

3.6.2.1.2 Straightness errors

This is a deviation from the original line of travel perpendicular to the direction of travel in the horizontal plane. A deviation of straightness in the travel of X-axis stage will cause a positioning error in the Y direction while in the Y-axis stage will cause a positioning error in the X direction.

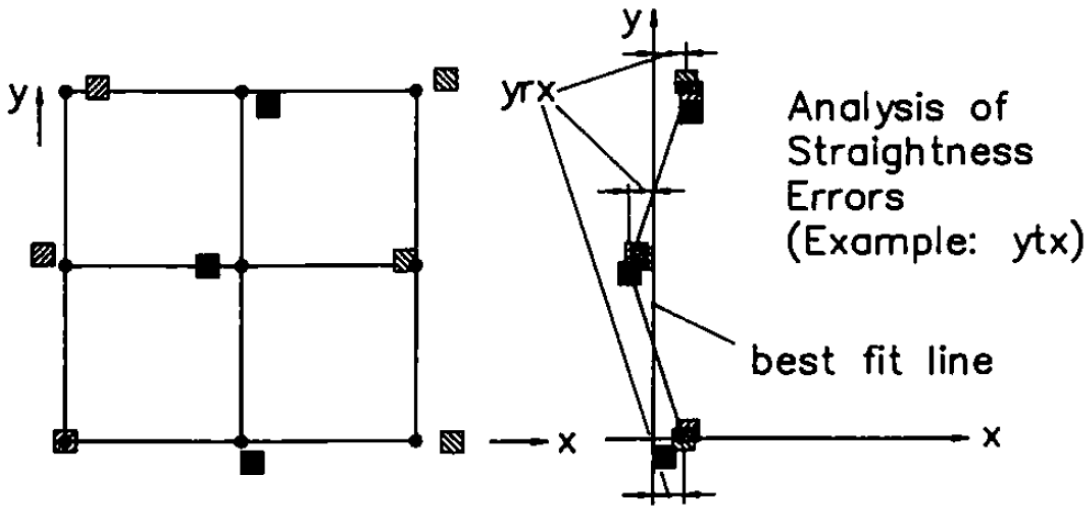

Figure 3.5 showing the straightness error measurement (Trapet and Waldele, 1991)

Figure 3.5 (Figure above) shows the measurement process of straightness error which is measured using the reversal method. *Y* and *Z* channel reading of the capacitive probe are expressed as

$$R_y(x_i) = \delta v_i + \delta_y(x_i) \tag{3.3}$$

$$R_z(x_i) = \delta u_i - \delta_z(x_i) \tag{3.4}$$

Where the y and z readings of the capacitive probe channel are $R_y(x_i)$ and $R_z(x_i)$. The straightness errors in the *u* and *v* direction of the ball surface are δu_i and δv_i. $\delta_y(x_i)$ and $\delta_z(x_i)$ represent the straightness errors. The ball array is then reversed 180 degrees about the *x* axis. The *y* and *z* will be as follows:

$$R_y'(x_i) = \delta v_i - \delta_y(x_i) \tag{3.5}$$

$$R_z'(x_i) = \delta u_i - \delta_z(x_i) \tag{3.6}$$

The straightness error could be computed by combining the four equations, this will yield to

$$\delta_y(x_i) = \left(R_y(x_i) - R_y'(x_i)\right) * 1/2 \tag{3.7}$$

$$\delta_z(x_i) = \left(R_z(x_i) - R_z'(x_i)\right) * 1/2 \tag{3.8}$$

3.6.2.2 Rotational errors

3.6.2.2.1 Roll errors

This is the rotation around an axis in the horizontal plane parallel to the direction of travel. Roll errors are calculated by measuring straightness errors of two parallel lines. The error is not essentially in the straightness measurements as the ball array slope in reference to moving axis is removed during data processing. The non-parallelism of the array in the measurements is necessary in computing the roll error. For best result, using only one mount of ball array with measurement done with extension rods mounted on both directions as linear components cannot be eliminated during data processing.

3.6.2.2.2 Pitch and Yaw errors

The rotation around an axis along the horizontal plane perpendicular to the direction of travel is called pitch and Yaw is the rotation around an axis in the vertical plane perpendicular to the direction of travel. Pitch and yaw errors of the CMM can be determined by measuring the positioning errors of two parallel lines separated at a distance z or y. Then the pitch and yaw errors are calculated from the differences between these two series of readings divided by the separation. When for certain axis the machine design complies with the Abbe principle an extension rod should be used in determining the errors.

3.6.2.3 Squareness errors

This is the displacement errors of either one or two diagonals on each of the 3 coordinate planes. Measuring two diagonals and taking their average will improve the accuracy of the measurement by eliminating random effects. The equation used to compute the squareness measurement is as follows:

$$d = 1 - \sqrt{(x_b - x_a)^2 + (y_b - y_a)^2} \qquad (3.9)$$

Where the calibrated distance from ball A to ball is l, the values of coordinate point A is (x_a , y_a) and for point B is (x_b , y_b).

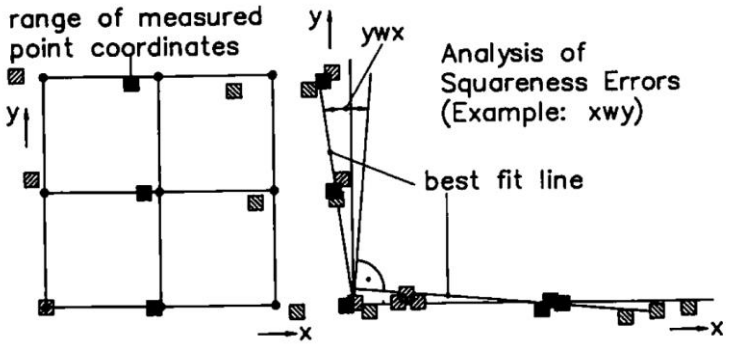

Figure 3.6 Showing the measurement of squareness errors (Trapet and Waldele, 1991)

3.6.3 CMM error calculation and compensation strategies

A good error calculation and compensation strategy will enhance the accuracy and effectiveness of a coordinate measurement machine. The international standard organisation in 2006 provided a set of general guideline and simplified equation for the calculation of CMM test uncertainty in ISO/TS 23165:2006 (International Organization for Standardization, 2006). In 2008, they provided another guideline, ISO/TS 15530-4:2008, which specifies the requirement for the application of simulation based uncertainty evaluation to CMM measurement. The guideline also contains description on testing methods for such simulation alongside various general testing procedures International Organization for Standardization, 2008). The International Organization for Standardization, in two other guidelines, ISO/TS 15530-3:2004 and ISO/DIS 15530-3:2009 (International Organization for Standardization 2004 and International Organization for Standardization 2009), describe an experimental approached when determining CMM measurement. This approach, instead of using an actual workpiece, it uses substituted measurements that are carried on calibrated work piece with similar shape and size. It then uses the obtained difference between the measured result and the known calibrated values to estimate the measurement uncertainty.

3.7 Mechanical artefacts based methods

Mechanical artefacts could be categorised according to the number of spatial coordinates associated with the principal calibrated features which could either be 1-dimensional, such as gauge block and ball bars or 2- dimensional such as ball plate or 3-dimensional artefacts such as space frame. Gauge blocks can be considered as the simplest method for testing coordinate measurement machines. The use of ball bars has been considered as a simple and economical method for determining volumetric errors

of coordinate measurement machine. The test procedure involves measuring the distance between spheres followed by repositioning and measuring the ball bar in a number of orientations throughout the working volume of the coordinate measurement machine. A space frame is a standard in which the co-ordinates of a number of points in 3-dimensional space within the work zone of a coordinate measurement machine are established by reference to points on the space frame.

3.8 CMM measurement uncertainty

3.8.1 Uncertainty of measurement

This is doubt pertaining to the result of a measurement. For every measurement, there is always a margin of doubt. Quite a number of factors introduce uncertainty in the measurement, ranging from the work piece to be measured, the operator and the strategy implemented for the measurement. The measurement strategy comprises the procedure of measurement, the location of workpiece in the CMM volume styli configuration and the probing strategy. The uncertainty of measurement will be estimated according to the ISO Guide to the Expression of Uncertainty in Measurement.

The uncertainty of coordinate measurements can be evaluated into two categories: 'Type A' and 'Type B'. The Type A uncertainty evaluation is based on the analysis of a series of observations by statistical uncertainty methods. The Type B evaluation of standard uncertainty is based on scientific knowledge other than statistical analysis.

3.8.2 CMM test uncertainty calculation

For the standard uncertainty of the probing error, the general equation is as follows

$$u(P) = \sqrt{\left(\frac{F}{2}\right)^2 + u^2(F)} \tag{3.10}$$

Where the form error of the test sphere is represented as *F* and it is usually reported on the calibration certificate. *u(F)* is the standard uncertainty of the form error stated on the certificate. The probing error equation is

$$u(P) = \sqrt{u^2(\varepsilon_{cal}) + u^2(\varepsilon_{\alpha}) + u^2(\varepsilon_t) + u^2\left(\varepsilon_{align}\right) + u^2(\varepsilon_{fixt})} \tag{3.11}$$

Where ε_{cal}, ε_{align},ε_{fixt}, ε_t, ε_α represent calibration error of the material standard of size, misalignment of the material standard of size, error due to the fixturing of the material standard of size, error due to the input of the temperature of the material standard of size and error due to the input of the CTE of the material standard of size respectively. The uncertainty *U*(*P*) or *U*(*E*) are obtained by the multiplication of a coverage factor k

$$U(P) = k \times u(P) \tag{3.12}$$

$$U(E) = k \times u(E) \tag{3.13}$$

In this research, mathematical model of this ball plate calibration is

$$l_x = \delta l_{vm} + \delta l_{is} + \delta l_{RP} + \delta l_n - \delta l_{Ax} - l_0\left[(\alpha \cdot \delta t_m) + (\alpha \cdot \delta t_d) + (\Delta t_x \cdot \delta\alpha)\right] \tag{3.14}$$

Where:

l_x : Length of the ball plate observed;

δl_{vm} : Deviation of verification measurement;

δl_{is} : Correction for the errors of indication of the CMM;

δl_{RP} : Correction due to reproducibility of probe system;

δl_n : Correction due to reflective index of air;

δl_{Ax} : Correction due to miss-alignment of ball plate;

l_0 : Nominal length of the ball plate considered;

α : The thermal expansion coefficient of the ball plate;

$\delta\alpha$: Correction for the thermal expansion coefficient of the ball plate;

δt_m : Correction for temperature measuring device;

δt_d : Correction for distribution temperature of the ball plate;

Δt_x : Correction due to the temperature different between the ball plate with reference standard;

1. Length of observation; l_x

The measurements are n times repeatability for ball plate calibration. The uncertainty evaluates from observed maximum standard deviation. Distribution is normal, so the standard uncertainty is:

$$u(l_x) = \frac{s(l_x)}{\sqrt{n}} \tag{3.15}$$

2. Deviation of verification measurement; δl_{vm}

In case of verification measurement, the results of measurements between each repeat measurement are not different more than x µm. calculating an uncertainty probability assuming to be a rectangular distribution($\sqrt{3}$).

$$u(\delta l_{vm}) = \frac{x}{\sqrt{3}} \text{ µm} \tag{3.16}$$

3. Correction for the error of indication of the CMM; δl_{is}

The resolution of the CMM is x µm and calculating an uncertainty probability assumes a rectangular distribution($\sqrt{3}$). The standard uncertainty is:

$$u(\delta l_{is}) = \frac{x}{2\sqrt{3}} \text{ µm} \tag{3.17}$$

4. Correction due to reproducibility of probe system; δl_{RP}

In the case of measurement stylus tip with standard ball, it has reproducibility of probe system less than x µm and calculating an uncertainty probability assume a rectangular distribution($\sqrt{3}$). The standard uncertainty is;

$$u(\delta l_{RP}) = \frac{x}{\sqrt{3}} \text{ µm} \tag{3.18}$$

5. Correction due to reflective index of air; δl_n

Ball plate is measured in a laboratory under ambient conditions. However, the metre is defined in terms of the distance that light travel in vacuum. The refractive index of air alters the wavelength according to $\lambda_v = n\lambda_{air}$. In most laboratories affecting the density

of the air, and then calculating the index of air by using a modified version of the Edlen equation.

$$(n-1)\times 10^{8} = \left(8342.54 + \frac{2406147}{130-\gamma^{2}} + \frac{15998}{38.9-\gamma^{2}}\right)\left(\frac{p}{96095.43}\right)\cdots$$
$$\times\left(\frac{1+10^{-8}(0.601-0.00972t)p}{1+0.0036610t}\right)\cdots$$
$$-R\left(8.753+0.036588..t^{2}\right)\left(0.037345-0.000401..\gamma^{2}\right) \qquad (3.19)$$

Where:

P	represents air pressure in Pascal units
T	represents temperature in degrees Celsius
R	represents relative humidity in percent
Υ	is the vacuum wave number in mm^{-1} units

6. Uncertainty of relative humidity from certificate of calibration; $u(R_{cal})$

The relative humidity device has an expanded uncertainty ± x % (k = 2) and multiplies by the sensitivity coefficient (a_1). The distribution is normal distribution (assume to be 2). The standard uncertainty is:

$$u(R_{cal}) = \left(\frac{x\,\%}{2}\right)\times(a_1) \qquad (3.20)$$

7. Uncertainty of relative humidity from resolution; $u(R_{read})$

The resolution of the relative humidity reading is x % and has a rectangular distribution with multiplying by the sensitivity coefficient (a_1). The distribution is rectangular distribution ($\sqrt{3}$). The standard uncertainty is:

$$u(R_{read}) = \left(\frac{1\,\%}{2\sqrt{3}}\right)\times(a_1) \qquad (3.21)$$

8. Uncertainty of air pressure from certificate of calibration; $u(P_{cal})$

The air pressure device has an expanded uncertainty ± x Pa (k = 2) and multiplies by the sensitivity coefficient (a_2). The distribution is normal distribution. The standard uncertainty is:

$$u(P_{cal}) = \left(\frac{x}{2}\right) \times (a_2) \tag{3.22}$$

9. Uncertainty of air pressure from digital resolution; *u(P_{read})*

The digital resolution of the pressure reading is x Pa and considered to have a rectangular distribution with multiplying by the sensitivity coefficient (a_3). The distribution is rectangular distribution ($\sqrt{3}$). The standard uncertainty is:

$$u(P_{read}) = \left(\frac{\mathrm{x}}{2\sqrt{3}}\right) \times (a_3) \tag{3.23}$$

10. Uncertainty of thermometer from certificate of calibration; *u(T_{cal})*

The thermometer device has an expanded uncertainty x °C (k = 2) and multiplies by the sensitivity coefficient (a_4). The distribution is normal distribution (assuming to be 2). The standard uncertainty is:

$$u(T_{cal}) = \left(\frac{x^{\circ}\mathrm{C}}{2}\right) \times (a_4) \tag{3.24}$$

11. Uncertainty of thermometer from digital resolution; *u(T_{read})*

The digital resolution of the thermometer reading is x °C and considered to have a rectangular distribution with multiplying by the sensitivity coefficient (a_5). The distribution is rectangular distribution ($\sqrt{3}$). The standard uncertainty is:

$$u(T_{read}) = \left(\frac{x^{\circ}\mathrm{C}}{2\sqrt{3}}\right) \times (a_5) \tag{3.25}$$

12. Correction due to miss-alignment of ball plate; δl_{Ax}

The cosine error is occurring from miss-alignment of the ball plate. In case of ball plate 620 mm length aligned parallelism with X-axis of the CMM, the deviation should less than 10 µm. An uncertainty probability assumes a rectangular distribution ($\sqrt{3}$). So,

$$u(\delta l_{\mathrm{cosine}}) = \frac{L(1-\cos(\theta))}{\sqrt{3}} \tag{3.26}$$

Where L: The nominal length of the ball plate: l_0 (mm)

13. Correction for temperature measuring device; δt_m

The thermometer device has an expanded uncertainty ± x °C (k = 2) multiply with thermal expansion coefficient (α), the distribution is normal distribution (assuming to be 2). The standard uncertainty is:

$$u(\alpha \cdot \delta t_m) = \frac{x\ ^{\circ}\mathrm{C}}{2} \times \alpha \tag{3.27}$$

14. Correction for distribution temperature of the ball plate; δt_d

The temperature distribution of the ball plate ± x °C multiply with thermal expansion coefficient (α). The distribution is rectangular distribution ($\sqrt{3}$). The standard uncertainty is:

$$u(\alpha \cdot \delta t_d) = \frac{x\ ^{\circ}\mathrm{C}}{\sqrt{3}} \times \alpha \tag{3.28}$$

15. Correction due to the thermal expansion coefficient; $\delta\alpha$

The uncertainty of thermal expansion coefficient multiplies (α) with temperature distribution of the ambient ± x °C. The distribution is rectangular distribution ($\sqrt{3}$). The standard uncertainty is:

$$u(\alpha \cdot \delta t_d) = \frac{\alpha}{\sqrt{3}} \times x\ ^{\circ}\mathrm{C} \tag{3.29}$$

3.9 Conclusions

Standards have been introduced to effectively obtain CMM performance and such standards include the international standard organisation, Coordinate Measuring Machine Manufacturers Association and other numerous national standard. CMMs have high precision and accuracy due to their inherent characteristics of their measuring techniques. They are essentially universal measurement machines making them able to measure any dimensional characteristics of a part configuration. The advantage of this approach is the compensation of medium term systematic effects due to thermal effect without the CMM needing full parametric compensation procedure. Gaussian process is a time dependant statistical distribution where all the points in some input space are connected with a normal distributed random variable. The First generation probe was usually solid or hard for example tapered plugs used in locating holes. Such probes

usually require to be manipulated manually in order to establish contact with the work piece before measurement could be read from the digital display output. The second generation of probes, touch trigger probe, are loaded with steel ball stylus and comes with a precise micro switch which responds to smaller order displacement. Currently generation probes don't require manual intervention during the measurement operation of the work piece, such as optical probes, transmission trigger-probes, Cluster or multiple probes and motorized probes.

Chapter 4 Simulation of CMM local, kinematic errors model

4.1 Introduction

With the high growth of rapid developments in various fields of precision technology, measurement uncertainties and errors are widely assessed not only in industry but also in scientific applications.

Many emerging products need ultra-precision positioning (nanometre-level) components with complex surface topography – while the manufacturing research is now being addressed, the metrology explanations are not. As many of the necessary metrology explanations do not exist, industry is currently using costly functional testing and trying to design such high-value components.

A prototype of proposed virtual CMM for the needs of metrological laboratories and industrial sections with high accuracy of uncertainty measurement has been developed. Its capability and performance could be greatly improved if there was a complete solution to simulate the measurement process and perform error analysis and uncertainty evaluation without the need to use a physical machine. Many approaches are permissible to integrate the many task-specific uncertainty and error measurements; however, it depends on a type of artefact and objectives of that measurement. High-precision simulation techniques always require greater performance when operating in industry. Therefore, there is a strong need for the development of an assessment method.

4.2 CMM kinematic error simulation procedure

The schematic diagram of CMM simulation is illustrated in figure 4.1. It can be seen that we assigned a 3x3 ball plate (a total of nine balls) to the positions of the spheres of a ball plate in order to simulate the data in the MATLAB programme. Constraint parameters are applied in this kinematic model to establish the frame of reference and probe qualification for the corrected positions of the ball plate using a Jacobian matrix. There are three positions of the ball plate locations to determine accurate results from the simulation. A random noise can be added to complete the data simulation procedures. The Gauss-Newton method is used to solve the model parameters. Error compensation and uncertainty evaluation for CMM would be drawn as the results.

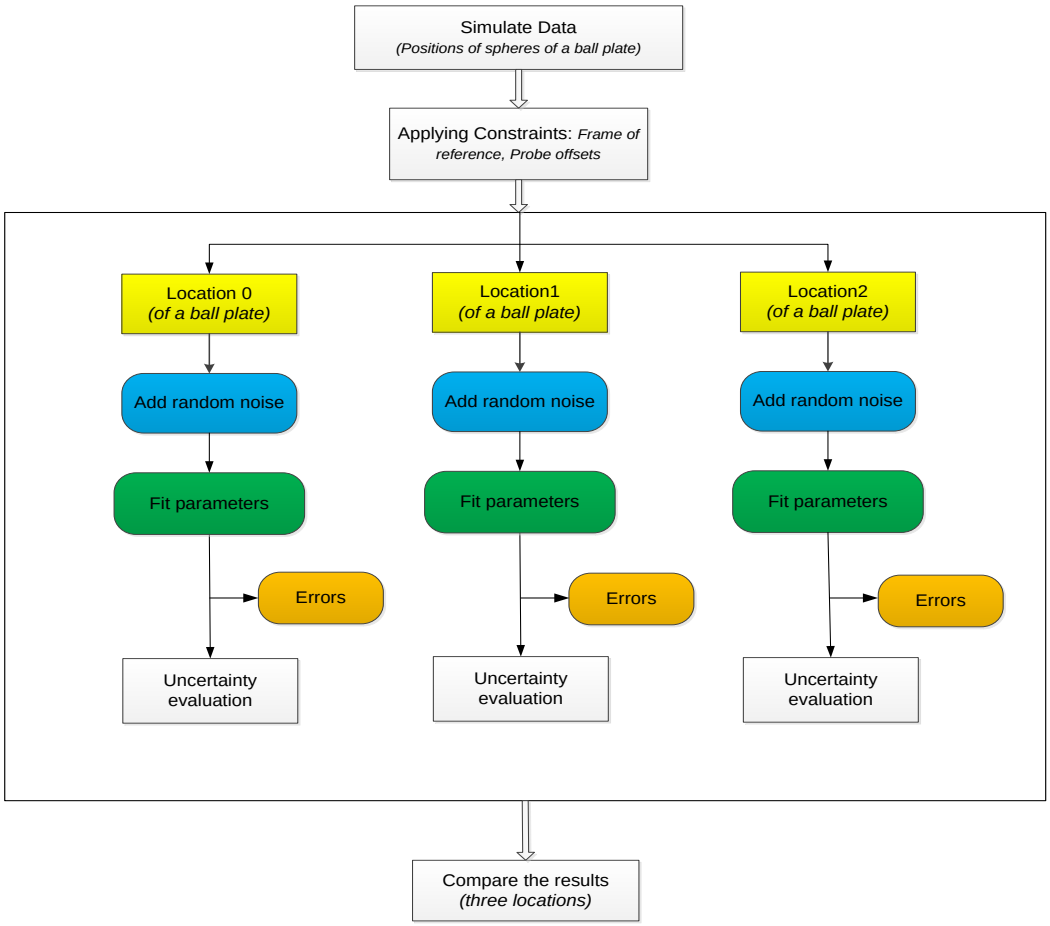

Figure 4.1 Schematic diagrams of CMM simulation procedures

4.3 Local, simplified kinematic errors model

The geometric errors associated with a CMM are relatively error motions between the tool and the work piece which show the mechanical imperfections of the CMM structure and the misalignment of the elements. Figure 4.2 shows the layout of the kinematic error components. The effect of the geometric errors are usually described by the 21 kinematic errors which consist of the positioning errors in each axis direction – $\delta_x(x,y,z)$, $\delta_y(x,y,z)$, and $\delta_z(x,y,z)$ – which are the linear displacement errors and vertical and horizontal straightness errors, the rotational errors along three axes: $R_x(x,y,z)$, $R_y(x,y,z)$, and $R_z(x,y,z)$, which are the roll, pitch and yaw angular errors, and three squareness errors: $Ø_{xy}$, $Ø_{yz}$, and $Ø_{zx}$ (Wang, 2003). The estimation of error correction and uncertainty evaluation can be determined by evaluating these kinematic errors using mathematical simulations.

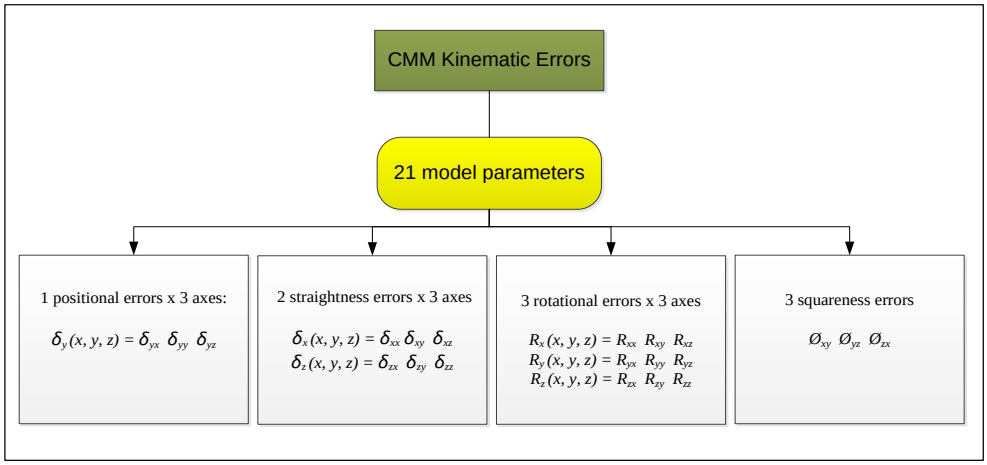

Figure 4.2 Details of the kinematic error components

Hunzmann et al. (1990) introduced a uniform approach to CMM calibration, acceptance and reverification tests. These suggested that applications still require precise experimental procedures and a number of datum points in the CMM working volume, which usually need a full calibration and long-term stability of the reference artefacts requirements (Sartori and Zhang, 1995). However, this approach requires much time and effort to establish.

The approach presented in this research is similar but it introduces a local, simplified kinematic error model specific to the measurement procedures. This kinematic error model is local in the sense that it applies only to the particular region of the CMM working volume used for the measurement task and the contact probes being used. Furthermore, it can be used in the sense that the model applies only during the limited time period it takes to perform the measurement task.

The advantages of this method are that, for example, the thermal effects, medium-term systematic effects associated with the CMM, can be compensated for without the requirement to conduct a full parametric error compensation measurement. Then, a low density of datum points in the entire CMM working region are performed, but still require a sufficient density of the datum in the working volume that matters to determine the local kinematic models. Moreover, it is also achievable to constantly update the local kinematic models. Figure 4.3 illustrates the proposed approach of the local kinematic error model.

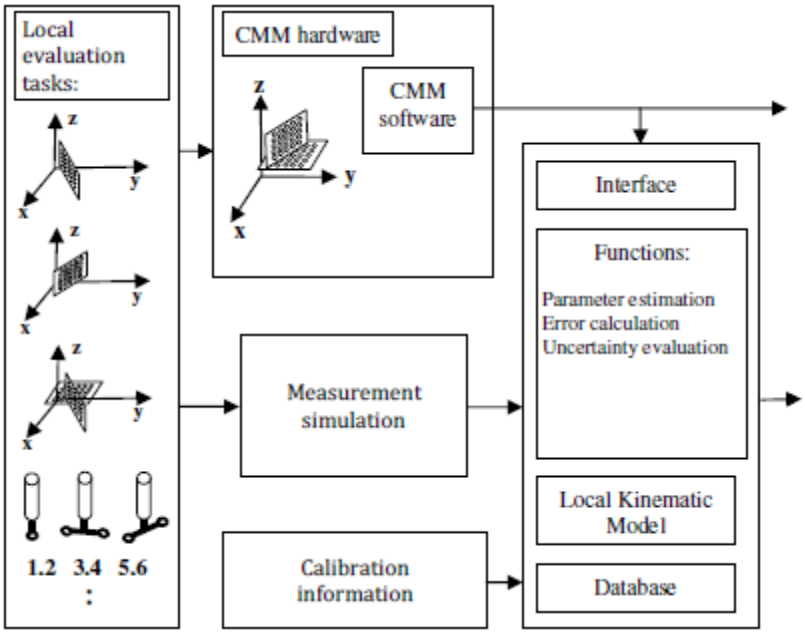

Figure 4.3 Schematic of the local kinematic error model measurement (Yang et al., 2008)

To begin with, the errors are determined by using a 2D ball plate in different orientations (three positions along x-, y-, and z-axis) and measuring probe offsets in six different orientations of both physical experiments, using CMM and simulation programming in MATLAB and recorded as a set of points coordinates. Then, the calibration data is included in the data, which includes results from the experiment and simulation to establish a model simulation. Among several local kinematic measurements, the model can be updated from its measurement data by matching the kinematic errors in a number of locations and probe qualifications in the CMM working volume. This local kinematic model requires a limited time period of iterative measurements without the need to perform a full parametric error compensation exercise. Thus, the accurate radius/diameter and the position in each axis (x, y, z) of the ball plate have been shown and the calculation of error compensation and uncertainty as well.

A physical CMM or CMM simulation can perform some examples of local evaluation tasks. The simulation should be performed and based on the real physical CMM, e.g. measuring range and measurement repeatability, etc. Furthermore, the probe qualifications simulation should be inserted in this model. While 2D ball plates are shown in the schematic, other reference artefacts (e.g. hole plates, ball plate, or step gauge, etc.) may also be used. The partial or full measurement for calibration information of the reference artefact is also required. The local kinematic model is based upon an axis-upon-axis build-up of the physical CMM.

After obtaining the measurement data, either through a physical CMM measurement or a simulation, a based fit algorithm based on the Gauss-Newton method is assigned to estimate the model parameters and additional related parameters (including the artefact parameters). The local kinematic model will subsequently be used to calculate and compensate for the systematic CMM errors. Based on the law of propagation of uncertainty, the model can also be used to evaluate the uncertainties associated with the fitted parameters (both the kinematic model and artefact parameters) and the CMM measurements in the working volume of interest.

Numerical simulation has been presented in this approach to analyse the behaviour and performance of the local kinematic error models, including the procedures and preliminary results described in the next section.

4.4 Numerical simulation procedure

4.4.1 Determination of kinematic errors parameters

The geometric errors associated with a CMM are usually described by the 21-parameter kinematic error model, which consists of three positional and three rotational error functions for each of the three axes, along with three squareness errors. As an indirect method, the estimation of these kinematic errors can be analysed by measuring a calibrated artefact such as a hole plate or ball plate in a number of datum positions in the CMM working volume and then matching the kinematic errors to the measured changes in artefact geometry.

4.4.1.1 Translational errors

$$x_x(x,a) = x(1,0,0)^T + \delta_x(x,a)\ ,\ \delta_x(x,a) = \begin{bmatrix}\delta_{xx}(x,a)\\ \delta_{xy}(x,a)\\ \delta_{xz}(x,a)\end{bmatrix} \tag{4.1}$$

$$x_y(y,a) = y(0,1,0)^T + \delta_y(y,a)\ ,\ \delta_y(y,a) = \begin{bmatrix}\delta_{yx}(y,a)\\ \delta_{yy}(y,a)\\ \delta_{yz}(y,a)\end{bmatrix} \tag{4.2}$$

$$x_z(z,a) = z(0,0,1)^T + \delta_z(z,a)\ ,\ \delta_z(z,a) = \begin{bmatrix}\delta_{zx}(z,a)\\ \delta_{zy}(z,a)\\ \delta_{zz}(z,a)\end{bmatrix} \tag{4.3}$$

4.4.1.2 Rotational errors

$$R_x(x,a) = R_z\left(e_{xz}(x,a)\right)R_y\left(e_{xy}(x,a)\right)R_x\left(e_{xx}(x,a)\right) \quad (4.4)$$

$$R_y(y,a) = R_z\left(e_{yz}(y,a)\right)R_y\left(e_{yy}(y,a)\right)R_x\left(e_{yx}(y,a)\right) \quad (4.5)$$

$$R_z(z,a) = R_z\left(e_{zz}(z,a)\right)R_y\left(e_{zy}(z,a)\right)R_x\left(e_{zx}(z,a)\right) \quad (4.6)$$

Then

$$e_x(x,a) = \left(e_{xx}(x,a), e_{xy}(x,a), e_{xz}(x,a)\right)^T \quad (4.7)$$

4.4.1.3 Squareness errors

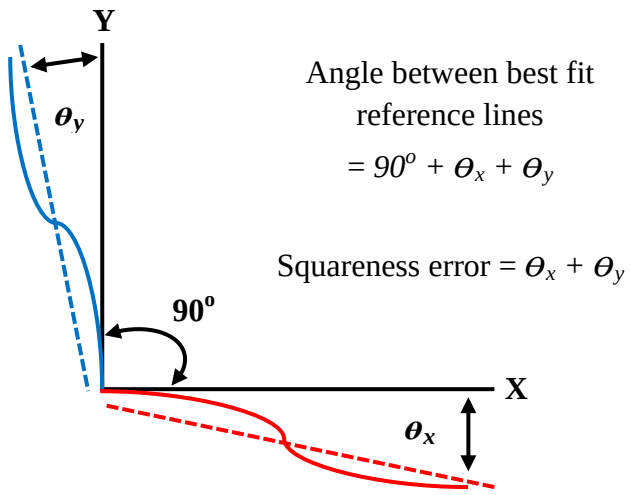

Figure 4.4 illustrates how the squareness error between two line axes of motion is calculated. The solid black lines represent the X and Y axes of the machine. The solid red and blue lines represent the variation in straightness deviation in the motion of the X and Y axes (i.e. their trajectories) recorded along the length of the axis. Reposted from (Chapman, 2013)

Then related squareness errors can be written in notation as:

$$\phi_{xy}, \phi_{yz}, \phi_{xz} \quad (4.8)$$

Axis-upon-axis build-up of the local kinematic model:

$$x^*(x,a) = x_x(x,a) + R_x(x,a)\left[x_y(y,a) + R_y(y,a)[x_z(z,a) + R_z(z,a)p]\right] \quad (4.9)$$

where p is the probe offset. This equation gives the modelled position of the probe centre as the function of the recorded scale reading x = $(x,y,z)^T$ and a is the parametric error coefficients. Thus the kinematic error behaviour is specified in terms of the 18 individual error functions, three positional and three rotational for each of three axes $\left(\delta_{xx},\delta_{xy},\delta_{xz},\delta_{yx},\delta_{yy},\delta_{yz},\delta_{zx},\delta_{zy},\delta_{zz},R_{xx},R_{xy},R_{xz},R_{yx},R_{yy},R_{yz},R_{zx},R_{zy},R_{zz}\right)$. Therefore, these functions of a single variable can be specified by polynomials or spline, for instance. It is suitable to include the probe qualifications to offset in this kinematic error model in order to evaluate the associated uncertainties. Up to six frame-of-reference constraints may need to be applied to fix the frame of reference of the probe geometry with that of the CMM.

We set:

$$e(x,a) = x - x^*(x,a) \quad (4.10)$$

If the CMM measures a point s^* then the measurement is modelled as:

$$x^*(x,a) = s^* + \epsilon \quad (4.11)$$

or the measurement equation is of the form:

$$x = s^* + e(x,a) + \epsilon \quad (4.12)$$

describing the observed scale readings x as a function of systematic $e(x,a)$ and random effects ϵ.

4.4.2 2D reference ball plate

The numerical simulations (in the MATLAB programme) are based upon the measurements of a 2D ball plate in three locations (positions and orientations) in the CMM working volume, including the measuring probes qualifications. This simulated

CMM is a moving-bridge type and has a volume of the working region of 1200 × 1000 × 700 mm. To allow possible comparison with physical CMM task measurements, a measurement repeatability of 0.5 μm is used in this simulation, which is close to the repeatability of the real CMM at National Institute of Metrology Thailand.

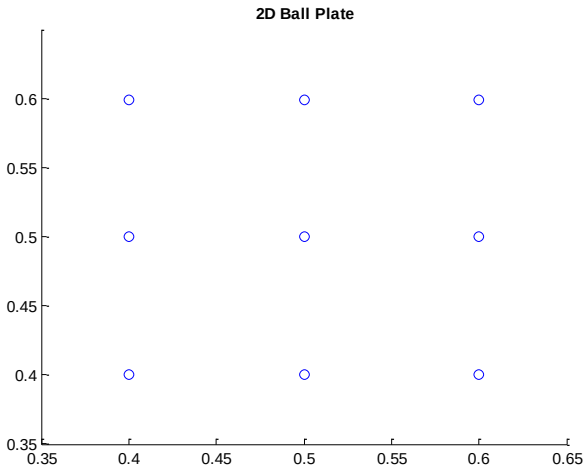

Figure 4.5 2D reference ball plate

4.4.3 Locations of the ball plate

The measurement of a ball plate is located in one local region of the CMM working volume where the actual measurement tasks will be calibrated. There are a number of suitable measurement approaches, e.g. using one or more of the three locations shown in figure 4.6.

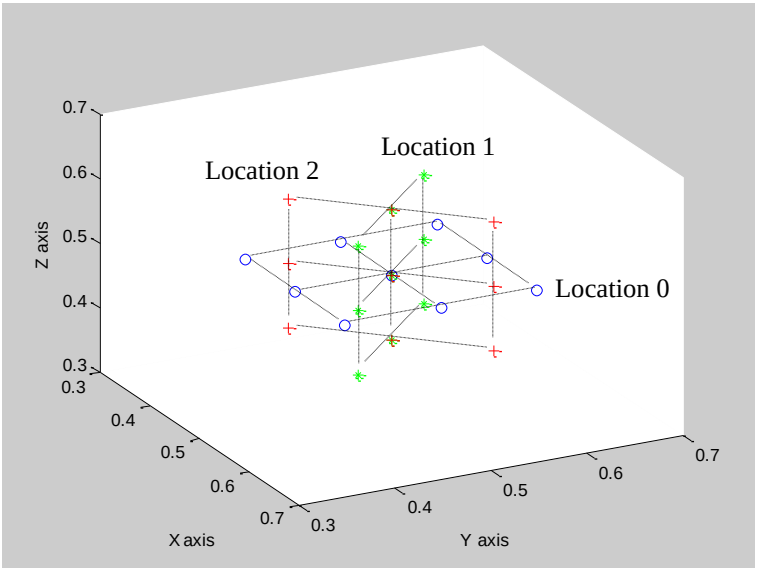

Figure 4.6 Three locations of a ball plate

- Location 0 is horizontal at z = 0.5 m, with the balls shown as circles.
- Location 1 is vertical, with the balls shown as stars.
- Location 2 is also vertical, with the balls shown as crosses.

4.4.4 Probe qualification measurements

The probe qualification measurements are also used in the modelled evaluation, with six probe offsets shown in figure 4.7. Offsets 1 and 2 are used in Location 0 measurements; other offsets may be used in the calibrations for Locations 1 and 2.

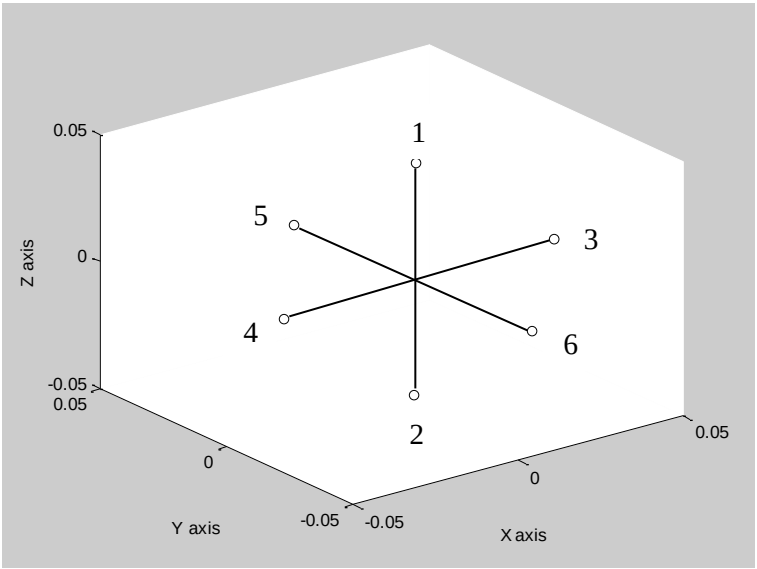

Figure 4.7 Six probe offsets

4.5 The performance of each local evaluation

The correct formulation depends on the architecture of the CMM, as the physical CMM is a moving-bridge type (FXYZ). Thus, the actual position of the probe tip relative to the workpiece is represented by the model equation as:

$$x^* = x_x + R_x\,(x_y + R_y\,(x_z + R_z p)) \qquad (4.13)$$

where x_x, x_y, x_z are the positions along x, y and z axes, respectively; they consist of the scale errors and straightness errors as well. The rotational matrices R_x, R_y, R_z are the orientations of x, y and z axes, respectively, including the rotational errors, pitch, roll and yaw. The model could encompass up to 21 parametric errors (three translational and

three rotational errors, plus three squareness errors); however, it may be simplified to just include 18 translational and rotational error components.

The Cheby-shev polynomial approach is used in this model to calculate each of these error components. Assuming that the required numerical stability for the local assessments (with low density of datum points) is achieved, it is necessary to simplify the model with a very low order of the polynomial (e.g. 2 or even 1).

For each local evaluation, the measurement data are simulated first, with an added repeatability error of 0.5 μm. Three tasks are then performed, as detailed below.

4.5.1 Calculation of model parameters

To calculate the model parameters, each set of measurement data is evaluated by using a Gauss-Newton algorithm for solving a non-linear, least-squares problem. QR factorisation approach is used to solve the problem of possible rank-deficiency. The estimated parameters can then be passed to and updated by another local evaluation.

Gauss-Newton algorithm can be started by minimise the function:

$$E(a) = \sum_{i=1}^{m} d_i^2(a) \tag{4.14}$$

as from n parameters $a_1, a_2, \dots, a_n$ where $m \geq n$. The solution of $a^*$is estimated to be a^e. First, the linear least-squares problem is solved from the equation:

$$Jp = -d \tag{4.15}$$

where *J* is the $m\ x\ n$ Jacobian matrix whose *ith* row is the gradient of d_i with respect to the parameter *a* evaluated at a^e as:

$$J_{ij} = \frac{\partial d_i}{\partial a_j}(a^e) \tag{4.16}$$

where *d* is a vector those *ith* component is $d_i(a^e)$. Thus, the estimation of a^* is updated by repeating as the equation:

$$a^e := a^e + p \tag{4.17}$$

These estimation and update are repeated until the approximates are judged to have converged.

4.5.2 Error calculations and compensation

The identified kinematic model can then provide productive predictions for analysing the geometric errors in the evaluated region of the CMM working volume, based on the nominal measurement results. This has been investigated with the kinematic errors simulation. In figure 4.8, a positioning error of 0.5 µm is proposed on the x-axis for the local evaluation using location 1, the nominal centres of the ball, shown as stars, the simulated centres (with positioning errors), shown as circles, and the centres predicted by the local kinematic model, shown as crosses, with all the errors magnified by 2000. Similarly, figure 4.9 shows straightness errors of 0.5 µm, introduced on the y-axis with a magnification of 2000 as well. Furthermore, figure 4.10 shows a yaw error of five arcseconds of the z-axis, magnified 2000 times. All of these plots have demonstrated the acceptable predictions of the local, kinematic error model using location 2. Other parametric error components and different local evaluations can be similarly investigated.

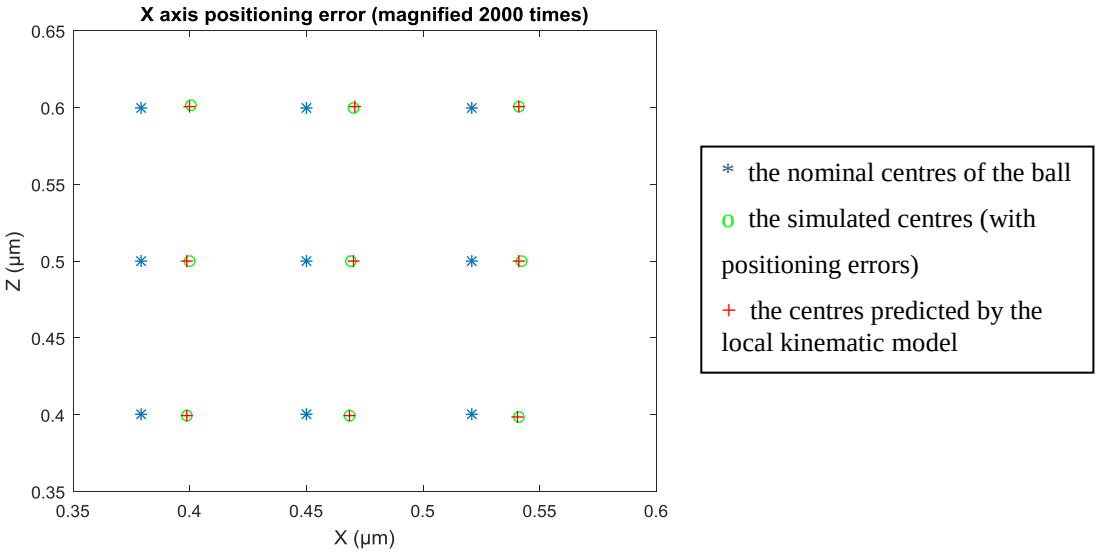

Figure 4.8 Simulation of positioning errors along X-axis and their prediction with local kinematic model

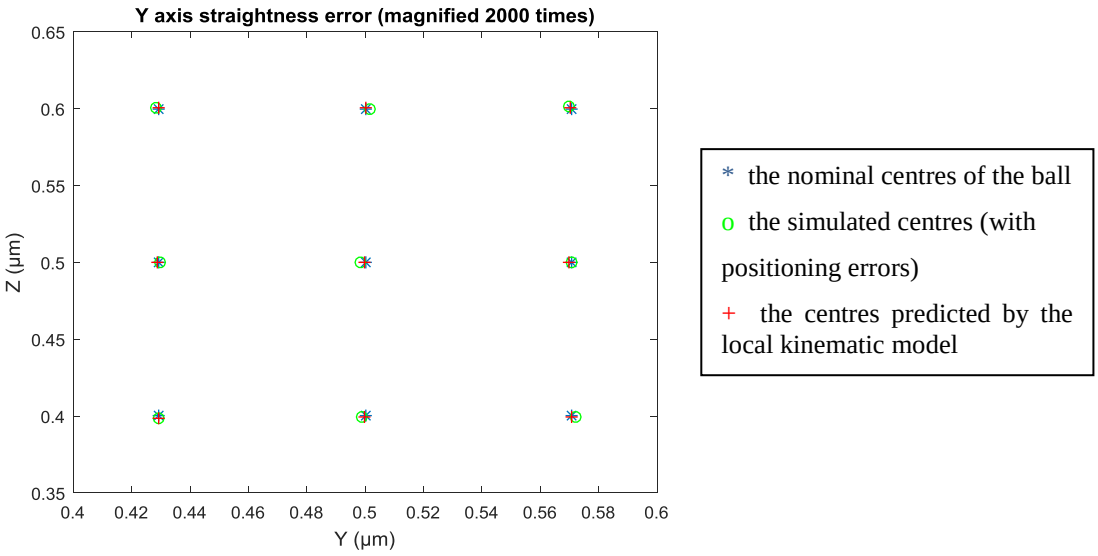

Figure 4.9 Simulation of Y-axis straightness errors and their prediction with local kinematic model

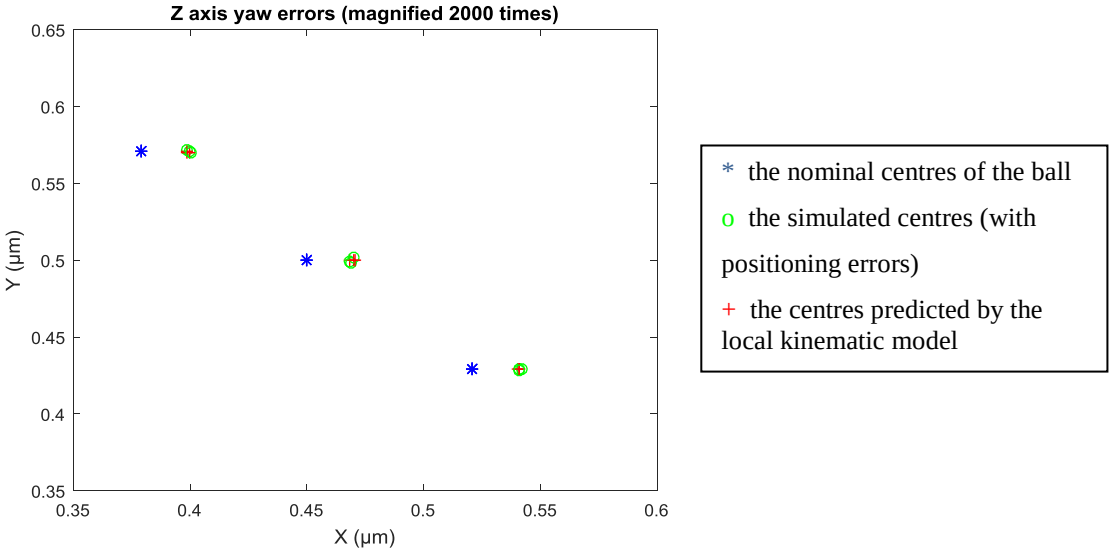

Figure 4.10 Simulation of Z-axis yaw errors and their prediction with local kinematic model

4.5.3 Uncertainty simulation calculation

The identified model parameters can be propagated based on the estimation of Jacobian matrices; the uncertainties associated with the model parameters and artefact parameters can be evaluated and further generated to assess the uncertainties associated with the CMM measurements in the measuring volume.

Table 4.1 The average uncertainties for locations 0 & 1 & 2 (unit: μm)

	Location 0			Location 1			Location 2		
	u_x	u_y	u_z	u_x	u_y	u_z	u_x	u_y	u_z
U_1	1.2122	0.8468	0.3935	0.2135	0.2567	0.2730	0.2152	0.2593	0.2673
U_2	1.7268	0.7908	0.2510	0.5563	0.3223	0.1123	0.5349	0.3039	0.5072
U_3	0.6631	1.8794	0.7217	0.7564	0.6223	0.7122	0.8028	0.7693	0.5721

Table 1 shows:

U_1 for the average uncertainties associated with the ball centre coordinates of the ball plate, based upon the local evaluation at locations 0, 1 and 2.

U_2 for the average uncertainties associated with the CMM measurements at 200 random locations in the evaluated region, based upon the local evaluation at locations 0, 1 and 2.

U_3 for the average uncertainties associated with the CMM measurements at the whole working volume, based upon the local evaluation at locations 0, 1 and 2.

The uncertainties U_1 are comparable to the repeatability of the CMM. As assumed, the average uncertainties associated with the CMM measurements in the evaluated region (U_2) are significantly lower than those in the whole working volume (U_3). It should be noted that while locations 1 and 2 can be used individually for local evaluation, location 0 alone will lead to the rank deficiency of the Jacobian matrix and numerical instability.

Table 2 shows the effects of a higher density of datum points on the measurement uncertainties. As expected, two location combinations result in all the average uncertainties U_1, U_2 and U_3 being smaller than the individual evaluation; the combined three local evaluations can further reduce the uncertainties U_1, U_2 and U_3.

Table 4.2 The average uncertainties for combined locations (unit: μm)

	Location 0 & 1			Location 0, 1 & 2		
	u_x	u_y	u_z	u_x	u_y	u_z
U_1	0.1123	0.2167	0.2535	0.1932	0.1283	0.1448
U_2	0.3364	0.2122	0.0803	0.1306	0.0872	0.1162
U_3	0.3271	0.4123	0.3308	0.2133	0.1202	0.1003

The higher density of datum points used in evaluation results in smaller uncertainties. It may also expand the measurement working volume at which the local kinematic model may be effectively implemented.

Different designs of ball plates (e.g. 3 × 3 and 5 × 5) with different plate sizes have been further investigated, and similar results were obtained, presented in table 3. The effects of different ball plate sizes on the average uncertainties U_1, U_2 and U_3 are obtained from location 1. It is important to note that as the size of the ball plate reduces, the average uncertainties associated with the measurements in the evaluated region or the whole measuring volume generally increase, but that the uncertainties associated with the plate parameters become somewhat smaller. More importantly, the results have shown that the local kinematic model approach presented may be applied with reference artefacts with different sizes.

Table 4.3 The average uncertainties for different ball plate sizes (unit: μm)

	Ball plate size 3 x 3			Ball plate size 5 x 5		
	u_x	u_y	u_z	u_x	u_y	u_z
U_1	0.2868	0.2597	0.2436	0.3138	0.3233	0.3642
U_2	0.4268	0.2023	0.0685	0.4664	0.4223	0.1184
U_3	0.5467	0.5113	0.5938	0.7112	0.6013	0.6693

The investigations have shown that the effects of different ball plate sizes on the uncertainty evaluation are quite small, similar to the results reported in M.G. Cox et al. (1998). Moreover, different ball plate designs can also be applied that show a similar performance. Therefore, this approach is very flexible, and can establish a uniform approach to different conditions and applications.

It is also apparent from these tables that the uncertainties associated with the ball plate and the physical CMM measurements in the region evaluated are independent of the previous evaluated locations, i.e. they are dependent only on the current location(s) of the evaluation.

4.6 Conclusions

An approach for CMM error compensation and uncertainty evaluation using artefacts (ball plate) and local, kinematic error models has been implemented.

The following conclusions can be drawn:

1) The numerical simulation results have shown that the proposed method allows a relatively small number of measurements to be used to determine the parameters of the local kinematic models, CMM parametric errors and uncertainties associated with both CMM measurements and the ball plate.

2) Suitable measurement strategies may be used to achieve a cost-effective evaluation of CMM systematic errors.

3) The proposed approach has good flexibility in terms of density of datum points in the evaluation and possible inclusion of probe qualifications and thermal errors, types of the artefacts, locations of artefacts along the measurement process, thus offering many potential benefits in CMM performance evaluation and enhancement.

Further verifications and experimental validations will be conducted and reported on in Chapter 6.

Chapter 5 Simulation of Gaussian Processes model

5.1 Introduction

Higher coordinate measurement precision and accuracy have become commercially important techniques and an active area of research in recent years. A simulation to maintain a high-quality, efficient operation is commonplace and is useful in many cases. From a Bayesian perspective, a choice of a neural network model can be viewed as defining a prior probability distribution over non-linear functions, and the neural network's learning process can be interpreted in terms of the posterior probability distribution over the unknown function.

In terms of the limit of large but otherwise standard networks, Neal (1996) has shown that the prior distribution over non-linear functions implied by the Bayesian neural network falls in a class of probability distributions known as Gaussian Processes (GP). GP have always been used to analyse the flexibility of the non-parametric model over the basis-function fitting approach. The hyperparameters of the neural network model determine the characteristic lengthscales of the GP. Neal's observation motivates the idea of discarding parameterized networks and working directly with GP.

Computations in which the parameters of the network are optimized are then replaced by simple matrix enumerating operations based on the mean function and covariance matrix of the GP. We have seen that a covariance function is an important component in a GP predictor, as it encodes the assumptions about the function with which we are concerned. The reliability of GP relates to how the suitable covariance functions are chosen. A GP approach for modelling and evaluating the kinematic errors is proposed in this chapter.

5.2 GP simulation

The GP method decomposes a geometric feature into these components: designed geometric form, systematic manufacturing errors and random manufacturing errors. The goal of the GP model is to study methods that can help assess the parametric errors of geometric features using ball plate measurements from a CMM.

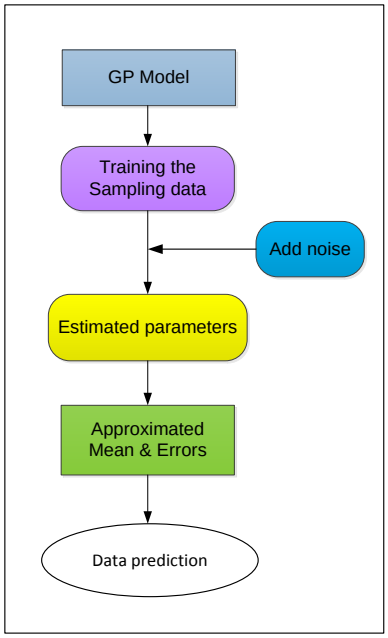

Figure 5.1 Scheme of the GP simulation

In a GP model, training data from the sampling points (in this case, using a ball plate position) is simulated to find the approximated parameters associated in the model when using likelihood estimation or GP function in the MATLAB programme. To simulate real physical CMM measurements, a random noise is assigned into the simulated input. Then the approximated initialization functions are generated; these consist of mean function, likelihood function, covariance function, and inference function. Finally, the predicted data is evaluated and errors of the ball plate are calculated as well.

It is normally assumed that the mean of the GP is zero everywhere. What relates one observation to another in such cases is just the covariance function, $k(x, x')$. A popular calculated method is the "squared exponential":

$$k(x, x') = \sigma_f^2 exp\left[\frac{-(x-x')^2}{2l^2}\right] \tag{5.1}$$

where σ_f^2 is defined as the maximum allowable covariance – this should be high for functions which cover a broad range on the y-axis. If $x \approx x'$, then $k(x, x')$ approaches this maximum, meaning $f(x)$ is nearly perfectly correlated with $f(x')$. If the function is to look smooth, then the neighbours must be alike. Now if x is distant from x', we have instead $k(x, x') \approx 0$, i.e. the two points cannot see each other. So, for instance, during

interpolation at new x values, distant observations will have a slight effect. How much effect this separation has will depend on the length parameter, l, so there is much flexibility built into (5.1).

However, the flexibility is not quite enough: the data is also often noisy, the result of measurement errors and so on. Each observation *y* can be thought of as related to an underlying function *f(x)* through a Gaussian noise model:

$$y = f(x) + N(0, \sigma_n^2) \tag{5.2}$$

something which should be familiar to those who carried out this type of regression before. Regression is the exploration for *f(x).* Purely for simplicity of exposition in the step, taking the approach of adding the noise into $k(x, x')$, by writing:

$$k(x, x') = \sigma_f^2 exp\left[\frac{-(x-x')^2}{2l^2}\right] + \sigma_n^2 \delta(x, x') \tag{5.3}$$

where $\delta(x, x')$ is the Kronecker delta function. (When many people use GP, they keep σ_n separate from *k(x, x')*. Given *n* observations y, the objective is to predict y_*, not the "actual" f_*; their expected values are identical according to (5.2), but their variances differ considering to the observation of a noise process. The expected value of y_*, and of f_*, is the dot at x_*.)

To prepare for Gaussian Process Regression, we calculate the covariance function, (5.3), among all possible combinations of these points, summarizing the findings in three matrices as:

$$K = \begin{bmatrix} k(x_1, x_1) & k(x_1, x_2) & \cdots & k(x_1, x_n) \\ \vdots & \ddots & & \vdots \\ k(x_n, x_1) & k(x_n, x_2) & \cdots & k(x_n, x_n) \end{bmatrix} \tag{5.4}$$

$$K_* = [k(x_*, x_1) \;\; k(x_*, x_2) \;\; \ldots \;\; k(x_*, x_n)] \tag{5.5}$$

$$K_{**} = k(x_*, x_*) \tag{5.6}$$

It can be confirmed that the diagonal elements of *K* are $\sigma_f^2 + \sigma_n^2$, and that its extreme off-diagonal elements tend to be zero when *x* spreads a large enough domain.

Since the key assumption in GP modelling is that the data can be represented as a sample from a multivariate Gaussian distribution, we have:

$$\begin{bmatrix} y \\ y_* \end{bmatrix} \sim N\left(0, \begin{bmatrix} K & K_*^T \\ K_* & K_{**} \end{bmatrix}\right) \tag{5.7}$$

where T indicates matrix transposition. Concentrating on the conditional probability $p(y_*|y)$: given the data, how likely is a certain prediction for y_*. The probability follows a Gaussian distribution:

$$y_*|y \sim N(K_* K^{-1} y, K_{**} - K_* K^{-1} K_*^T) \tag{5.8}$$

The best estimate for y_* is the mean of this distribution:

$$\overline{y_*} = K_* K^{-1} y \tag{5.9}$$

and the uncertainty in the estimate is calculated by its variance:

$$var(y_*) = K_{**} - K_* K^{-1} K_*^T \tag{5.10}$$

5.3 Numerical simulation procedure

This GP model simulation is based on the GPML toolbox as:
http://www.gaussianprocess.org/gpml/code/matlab/doc/

5.3.1 Calculation of model parameters

5.3.1.1 Zero mean regression

In a set of data of x-, y-, and z-axes of the GP model based on CMM:
- x is the 2D position of a ball plate (3 x 3 ball plate) (unit: mm)
- y is the positioning error of the CMM (unit: mm)
- z is the boundary of the CMM working volume (unit: mm)

In this case, the boundaries of the x- and y-axes are 0.400–0.600 mm of the CMM working volume. To generate the 3 x 3 ball plate position (x) in the x-axis and y-axis (unit: mm) as figure 5.2.

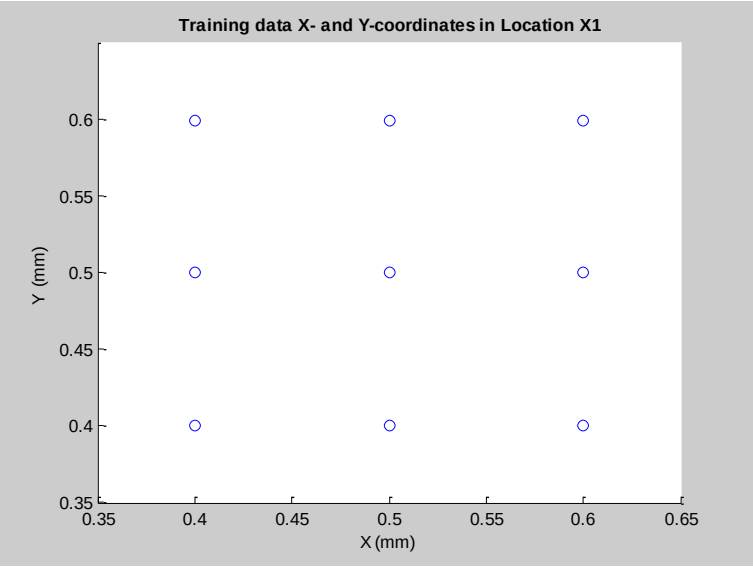

Figure 5.2 Shows the training data in the x- and y-coordinates

With the toolbox, we can simulate a random noise of the CMM (y) (unit: mm)

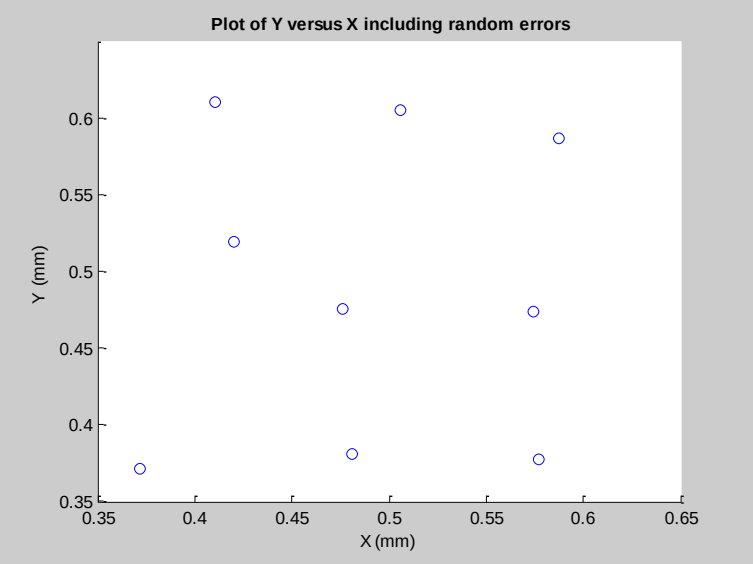

Figure 5.3 Shows the training data with random errors

It begins with four initialization steps, including four functions:

- Mean function: a cell array specifying the GP mean
- Covariance function: a cell array specifying the GP covariance function
- Likelihood function: the function specifying the form of the likelihood of the GP model and the terms needed for prediction and inference
- Inference function: a function computing the approximated posterior and its partial derivatives

Part of the code with zero mean;

```
% Mean function
   meanfunc= {@meanZero};
% Likelihood function
   likfunc = @likGauss;
% Covariance function
   covfunc=@covSEiso; % choosing SE covfunc
 % Inference function
   hyp.cov = [0; 0];
   hyp.mean = [];
   hyp.lik = log (0.1); % If we do not have the optimal parameter values,
                        % we employ the minimise function based on CG method
    hyp = minimize (hyp, @gp, -500, @infExact, meanfunc, covfunc, likfunc, x, y);
                       % to get the optimal parameters
```

To estimate the CMM working volume measuring a ball plate (z) (unit: mm)

```
z1= 0.4:0.01:0.6; z1 = z1';
   z2= 0.4:0.01:0.6; z2 = z2';
   z = zeros (441, 2);
   for i=1:1:21;
      for j=1:1:21;
         z ((i-1)*21+j, 1) =z1 (j);
         z ((i-1)*21+j, 2) =z2 (i);
      end
   end
```

With the gp function, we obtain the regression over z.

```
[m s2] = gp (hyp, @infExact, meanfunc, covfunc, likfunc, x, y, z);
                                    % m is the estimation
                                    % s2 is the variance
z_temp0=reshape (m, 21, 21);
i=0.4:0.01:0.6; j=0.4:0.01:0.6;
figure;
mesh (j, i, z_temp0)
```

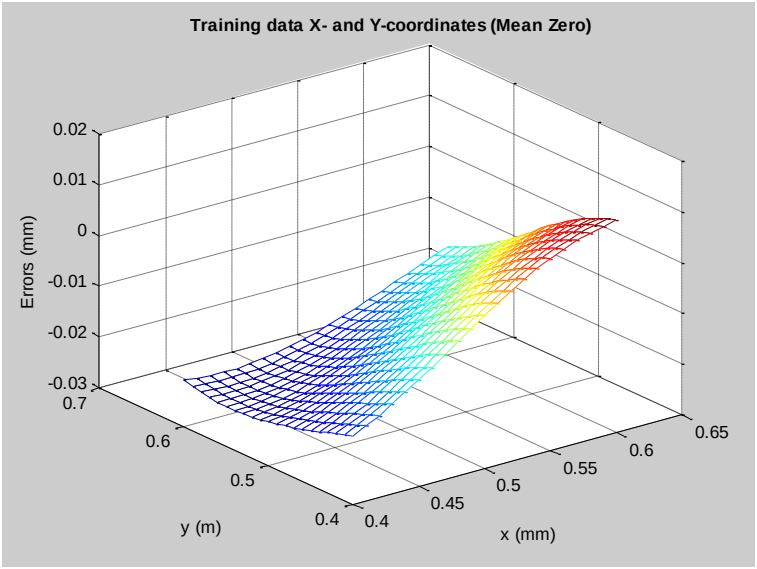

Figure 5.4 Shows the training data along x-axis and y-axis with zero-mean function

The initial functions have many types; from which we choose freely.

5.3.1.2 Regression with nonzero mean

Considering the nonzero mean, we have chosen a mean linear function because, in this case, we use a CMM as a linear measurement by taking the 'meanlinear.m' as an example (toolbox V34/mean/meanLinear.m). It contains two parts: one is for the mean estimation when the input parameters are 'hyp' and 'x'; the output is the mean evaluation. The other is for obtaining optimal mean function parameters in the case of the inputs 'hyp', 'x', and 'i'; the output is the derivative over the i-th parameter in the mean function.

Based on the above data, we define our own mean linear function according to the CMM: 'meanMylinear_2D.m'.

$$y = a_1 + a_2 x + a_3 x^2 \tag{5.11}$$

```
function A = meanMylinear_2D(hyp, x, i)
if nargin < 2, A = '3';
return;
end
[n,D] = size(x);
a = hyp(:);
h1 = zeros(n,3);
```

```
for k = 1:1:n;
   h1(k,1) = 1;
   h1(k,2) = x(k,1);
   h1(k,3) = x(k,1)^2;
end
A = zeros(n,1);                % allocate memory
if nargin == 2                 % compute mean vector
   A = h1*a;
else                        % compute derivative vector
 if i<=3;
    A = h1(:,i);             % derivative
 else
   A = zeros(n,1);
 end
end
```

We should note that as the parameters to be estimated are numerous, the initialization is vital. During the regression, we can set the initialization as follows:

1. Fit the data to the parametric model (integrant error model) to get the initialization of mean function parameters.

2. Establish regression by GP regression with zero mean to achieve the initialization of the parameters of covariance function and likelihood function.

Then continue the regression as follows:

```
meanfunc = {@meanMylinear_2D};
likfunc = @likGauss;
covfunc = {@covSEiso};
hyp.cov = [-2.013712762984104;-4.082864313671445];
hyp.mean = [-0.179669833204103;0.778362671986138;-0.863234577981942];
hyp.lik = -4.485943839204587;
hyp = minimize(hyp, @gp, -500, @infExact, meanfunc, covfunc, likfunc, x, y);
                % -500 can be changed to -5000 if necessary
                % get the optimal parameters
% Plot Figure 4: X-,Y-,Z-coordinates with nonzero mean
```

[m s2] = gp(hyp, @infExact, meanfunc, covfunc, likfunc, x, y, z);

z_tempmx = reshape(m,21,21);

i = 0.4:0.01:0.6; j = 0.4:0.01:0.6;

figure;

mesh(j,i,z_tempmx)

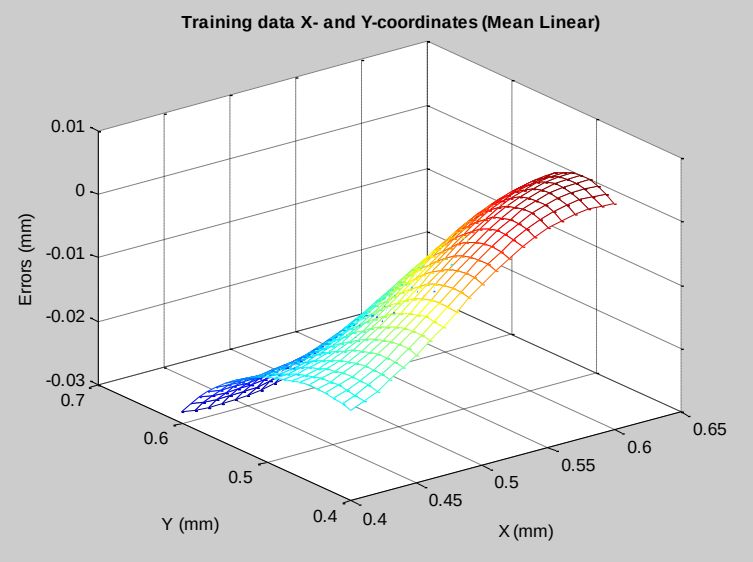

Figure 5.5 Shows the training data along x-axis and y-axis with specified mean function

5.3.2 Error calculations and compensation

The regression of a zero mean function is shown as figure 5.4 and the regression of a specified mean function compatible with the CMM integrant error model as figure 5.5. Therefore, the errors of the predicted data show as figure 5.6:

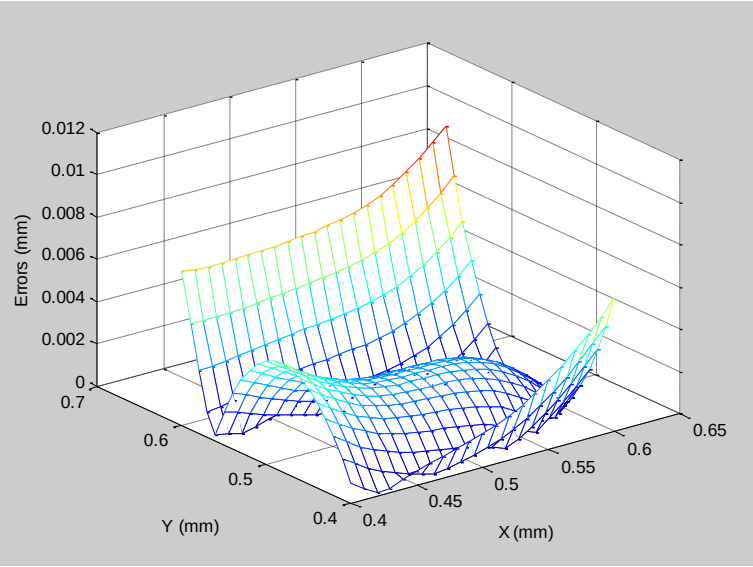

Figure 5.6 Shows errors along the x-axis and y-axis

5.4 Conclusions

The numerical simulation results have indicated that the evaluation of errors using a GP model based on CMM measurement is an achievable approach. The model is a collection of random variables, any finite number of which have joint Gaussian distributions and are completely specified by a mean function and a positive definite covariance function. With a sufficient number of evaluated measurements using a ball plate as an artefact, the hyperparameters associated with the covariance function can be accurately determined. They also indicated that the CMM systematic errors in the region in question can be assessed. As can be seen, the error evaluation from the GP model has appeared a very low number of errors (less than 0.011 μm). Thus, their flexible non-parametric nature and computational simplicity offer this proposed GP approach as one with a high measurement precision and accuracy method.

Chapter 6 CMM calibration using a ball plate

6.1 Introduction

In order to verify the local kinematic error model and Gaussian Process model as these case studies by experiment-based investigation, the CMM verifications were conducted. The details of experimental programme are presented and explained in this chapter consisting of CMM calibration using a ball plate as an artefact, measurement procedure, error analysis, and conclusion.

6.2 Preliminary Operations:

CMM

Specification of CMM (PMM-C 700) by Brown&Sharpe (Leitz):

Range: *X* x *Y* x *Z* (1200 x 1000 x 700) mm;

Accuracy: 0.6 µm + L/600;

Uncertainty ($k = 2$) = $\sqrt{(0.52)^2 + (1.4 * 10^{-3} * l)^2}$ µm;

l being indication length of the CMM in mm

Software: Quindos 6;

- Read entirely the operation instruction/operation manual of the CMM before beginning operation.
- Check the due date of the CMM. If the CMM is over the due date, it must be recalibrated before use.
- Clean the CMM by ethanol and wipe off with soft lint free cloth or appropriate wiper or chamois on moving part of CMM.
- Before using the CMM, check that the CMM is operated correctly as described in the manufacturer's operating instruction.
- Open the main electrical switch, air power and switch on the electronics cabinet.
- Setup the CMM probe for the measurement.
- Stabilize the CMM about 1 hour before start measurement.

Figure 6.1 CMM (PMM-C700P)

6.3 Verification procedure

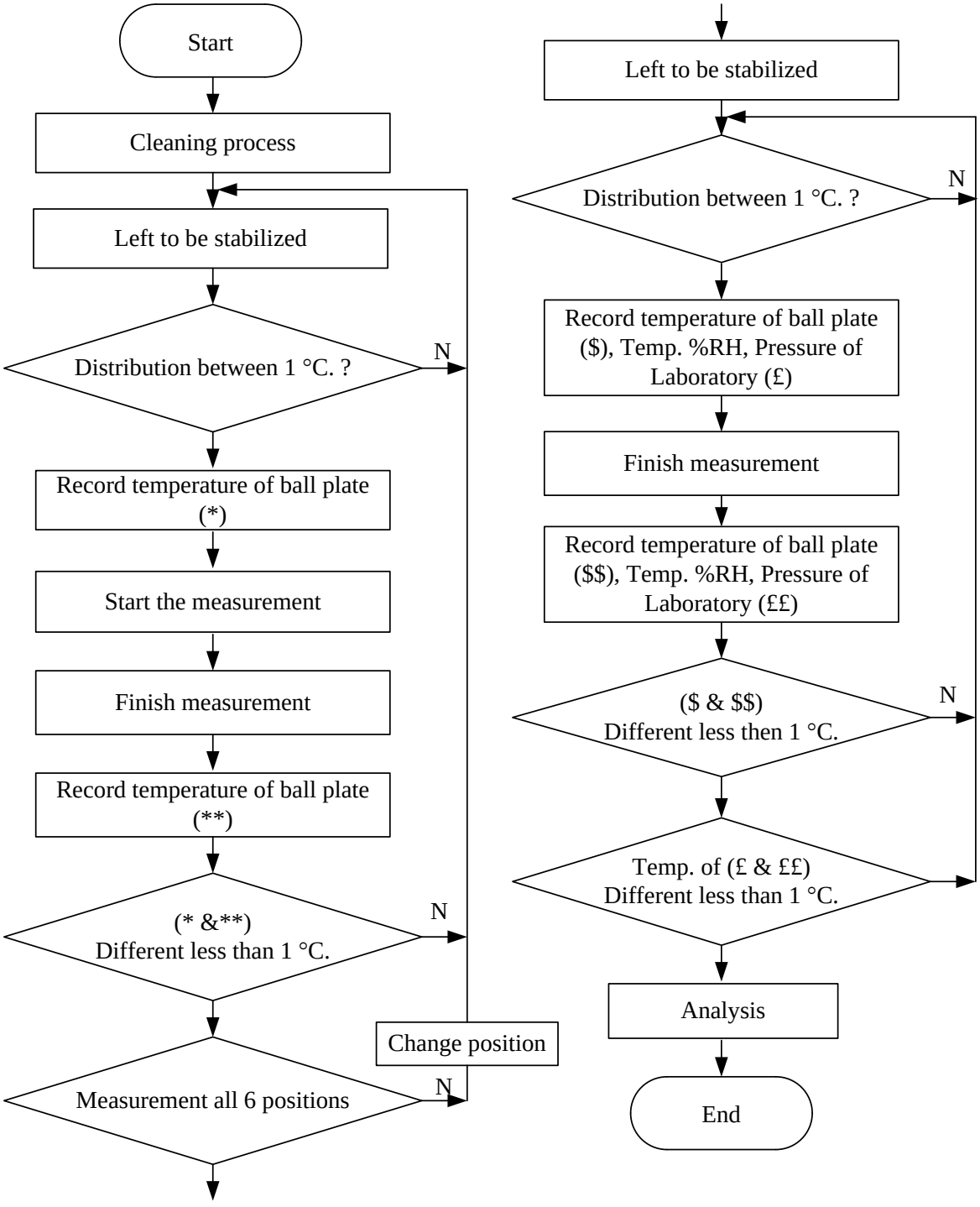

Figure 6.2 Verification flow chart

6.4 Ball Plate

- Clean the ball plate by ethanol and wipe off with soft lint free cloth or appropriate wiper or chamois in measuring faces.
- Place the ball plate in CMM table and align ball plate parallel to X-axis of CMM within 50 µm for 620*620 mm ball plate.
- Attach a digital thermometer to ball plate.
- Stabilize the ball plate about 3 hours before start measurement.

6.5 Locations of the ball plate

All CMM measurements should be performed in the same working volume of the CMM. The centres of the spheres (of the ball plate) have to coincide with the same points in the CMM's working space in all six plate positions. All spheres are measured with respect to the plate's reference coordinate system in all six positions.

- Measurement 1 (Location 0) is obtained in the basic ball plate position, where the X-axis of the plate points in the direction of the CMM's first cinematic axis, and the Z-axis of the ball plate is placed horizontal at z = 0 as figure 6.3

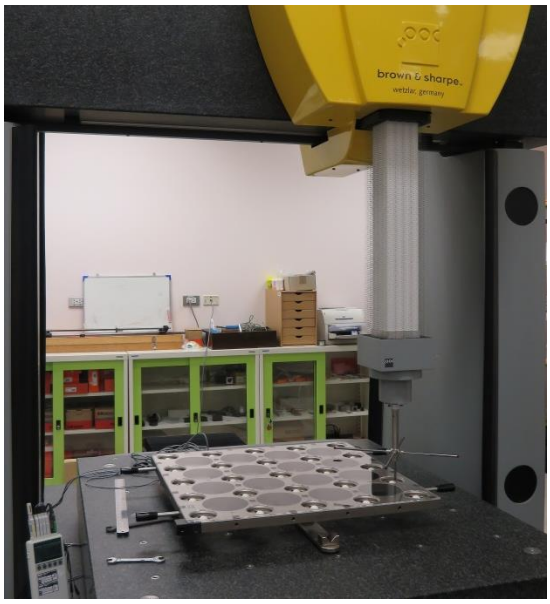

Figure 6.3 Location 0 of the ball plate (BP111)

- Measurement 2 (Location 0) is obtained by placing the ball plate in horizontal at z = 500 mm (BP112) with respect to the basic position (location 0).

- Measurement 3 & 4 (Location 1) is obtained by turning the ball plate in vertical, as figure 6.4

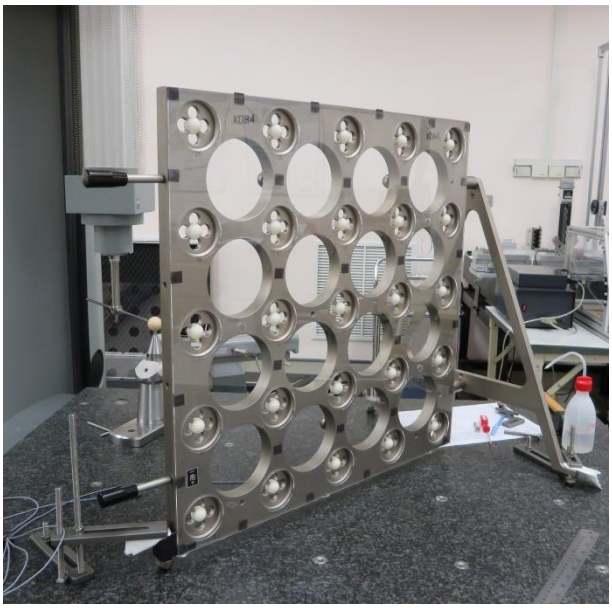

Figure 6.4 Location 1 of the ball plate (BP211 and BP212)

- Measurement 5 & 6 (Location 2) is obtained by also turning the ball plate in vertical, as figure 6.5

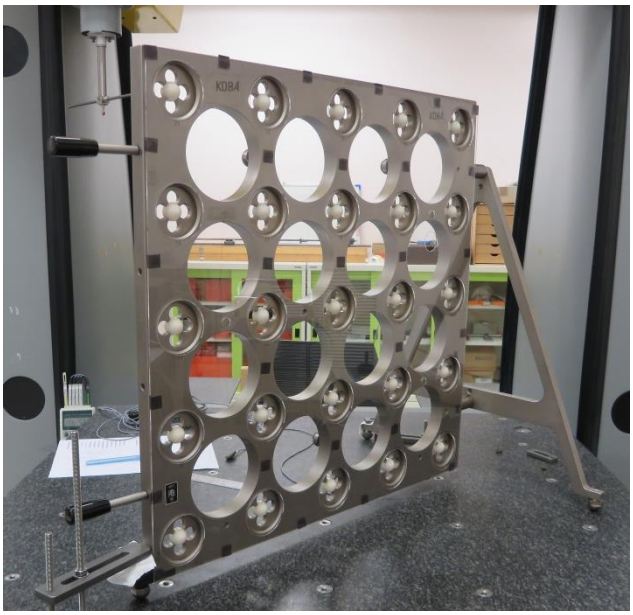

Figure 6.5 Location 2 of the ball plate (BP311 and BP312)

6.6 Setting the probe qualification measurements

Six probe offsets are also used in the evaluation shown in figure 6.6 and 6.7

- Offsets 1 and 2 are used in location 0 measurements
- Offsets 3 and 4 are used in location 1 measurements
- Offsets 5 and 6 are used in location 2 measurements

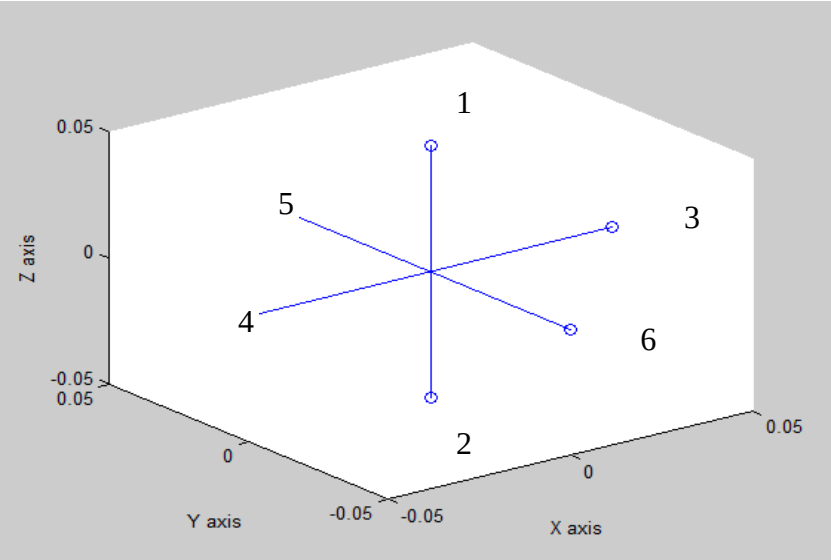

Figure 6.6 Six probe offsets

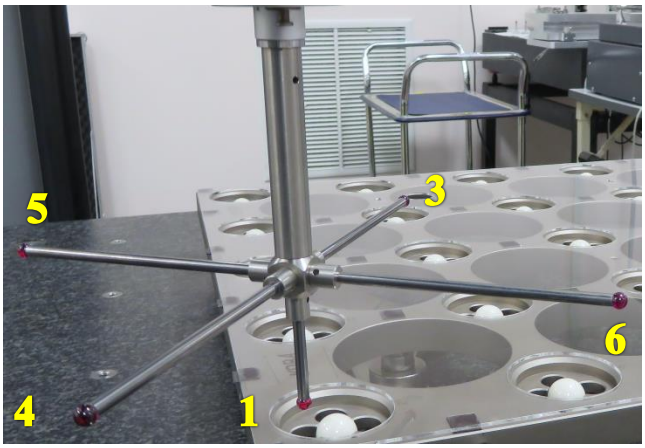

Figure 6.7 Six probe directions

6.7 Calibration of the CMM using a ball plate

- Place the ball plate on the CMM table. Let the XY-axis of ball plate follow with XY-axis of CMM (Location 0), following figure 6.3

- Use CMM probe touch on top of ball number 1, 5 and 21. Adjust height of three balls until the difference are less than 100 µm shown in figure 6.8

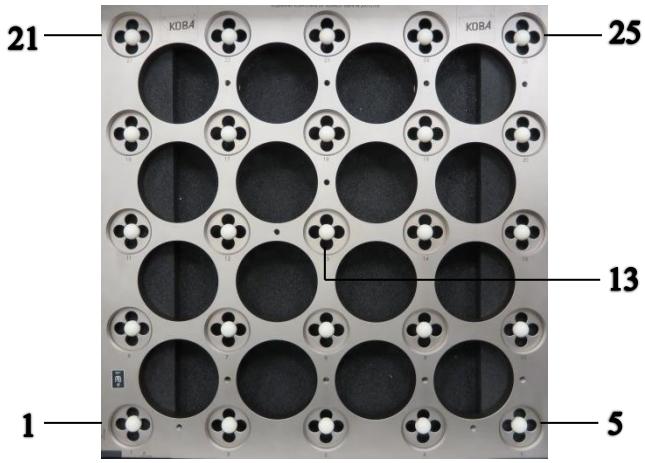

Figure 6.8 Ball numbers of the ball plate

The origin of object coordinate system is the centre of ball number 1.

- Align the ball plate to parallel with X-axis of CMM within 50 µm.
- Clamp ball plate support.
- Record X and Y positions of ball plate.
- Wait until temperature room distribution of ball plate between ± 1 °C
- Record temperature of ball plate to worksheet.
- Start ball plate measurement program.
- Calibrate CMM probe with sphere ball.
- Make manual coordinate system following the program.
- Start automatic measurements
- Program will measure forward following figure 6.9

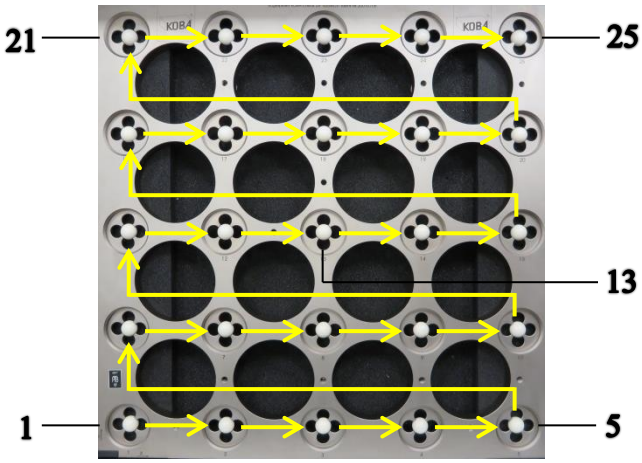

Figure 6.9 forward measurement

- Record the last temperature of ball plate to worksheet. Compare temperature with the first time. Measurement shall be rejected if temperature difference is more than ± 1 °C.
- Change ball plate position following figure 6.4 and 6.5
- Repeat 6.5.2 to 6.5.13 for other positions until finish.

6.8 Error Analysis

The geometric errors associated with a CMM are usually described by the 21 parametric errors which consist of:

- Three translational error functions for each of the three axes
- Three rotational error functions for each of the three axes
- Three squareness errors

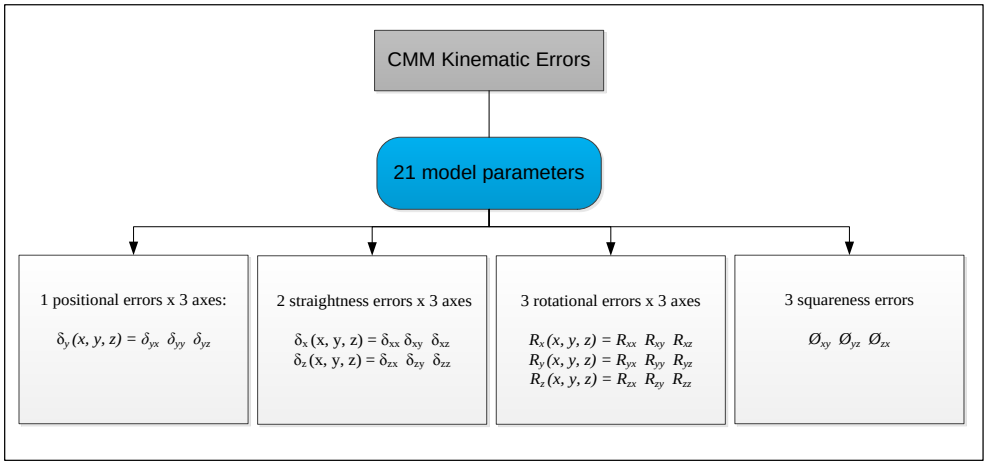

Figure 6.10 Details of the kinematic error components

6.9 Measurement Results

Environment	Start	Finish
Temperature (^{o}C)	20	21
Humidity (%RH)	52	52.5

Environment control
(20 ± 1) ^{o}C
(50 ± 10) %RH

CMM accuracy: 0.6 µm + L/600;

Table 6.1 Ball plate measurement: Location 0_BP111

Ball No.	X (mm)	Y (mm)	Z (mm)
1	0.00000	0.00000	0.00000
2	133.00493	-0.00302	0.03770
3	266.00861	-0.00185	0.05730
4	399.01683	-0.00148	0.03915
5	532.01957	0.00000	0.00000
6	-0.02317	133.01549	0.03071
7	132.98147	133.01424	0.04338
8	265.98752	133.01439	0.03205
9	398.99329	133.01453	0.02391
10	531.99398	133.01734	0.00855
11	-0.02928	266.02834	0.02127
12	132.97423	266.02270	0.05500
13	265.97911	266.02539	0.02536
14	398.98417	266.02573	0.02331
15	531.98564	266.02907	0.01283
16	-0.05183	399.04046	0.02567
17	132.95186	399.03848	0.04559
18	265.95342	399.04214	0.02934
19	398.95562	399.04332	0.03533
20	531.95767	399.04371	0.02794
21	-0.06035	532.04858	0.00000
22	132.94312	532.04635	0.03618
23	265.94425	532.04760	0.06559
24	398.94494	532.05017	0.05904
25	531.94582	532.05398	0.03377

Measurement Results (Continued)

Environment	Start	Finish
Temperature (^{o}C)	20	20.5
Humidity (%RH)	52.5	52

Environment control
(20 ± 1) ^{o}C
(50 ± 10) %RH

CMM accuracy: 0.6 µm + L/600;

Table 6.2 Ball plate measurement: Location 0_BP112

Ball No.	X (mm)	Y (mm)	Z (mm)
1	0.00000	0.00000	0.00000
2	133.00353	-0.00348	0.02870
3	266.00771	-0.00172	0.04371
4	399.01293	-0.00116	0.03774
5	532.01942	0.00000	0.00000
6	-0.02445	133.01395	0.03657
7	132.92887	133.01331	0.04224
8	265.97764	133.01337	0.02305
9	398.99020	133.01442	0.02788
10	531.97664	133.01655	0.00977
11	-0.03098	266.02284	0.02212
12	132.97112	266.01894	0.05513
13	265.97854	266.02447	0.02467
14	398.98001	266.02546	0.02667
15	531.97664	266.02965	0.02459
16	-0.05432	399.03866	0.02449
17	132.94288	399.03325	0.04416
18	265.95445	399.04416	0.02839
19	398.95007	399.04572	0.04481
20	531.95000	399.04982	0.04225
21	-0.06422	532.03225	0.00000
22	132.94227	532.04616	0.03522
23	265.94895	532.04358	0.06504
24	398.93294	532.05574	0.06330
25	531.94089	532.04392	0.04227

Measurement Results (Continued)

Environment	Start	Finish
Temperature (^{o}C)	21	21
Humidity (%RH)	51	50

Environment control
(20 ± 1) ^{o}C
(50 ± 10) %RH

CMM accuracy: 0.6 µm + L/600;

Table 6.3 Ball plate measurement: Location 1 (Front) _BP211

Ball No.	X (mm)	Y (mm)	Z (mm)
1	0.00000	0.00000	0.00000
2	133.00450	-0.00224	0.02751
3	266.00758	-0.00103	0.04234
4	399.01493	-0.00103	0.03086
5	532.01569	0.00000	0.00000
6	-0.02435	133.01294	0.03243
7	132.97987	133.01251	0.03571
8	265.98533	133.01264	0.02297
9	398.99030	133.01216	0.02288
10	531.98894	133.01489	0.01761
11	-0.03168	266.02445	0.02525
12	132.97152	266.01955	0.05418
13	265.97593	266.02213	0.02380
14	398.98025	266.02178	0.02981
15	531.97962	266.02472	0.03236
16	-0.05538	399.03547	0.02824
17	132.94817	399.03420	0.04412
18	265.94920	399.03745	0.02943
19	398.95087	399.03776	0.04393
20	531.95108	399.03790	0.05231
21	-0.06583	532.04230	0.00000
22	132.93754	532.04058	0.03110
23	265.93823	532.04147	0.06405
24	398.93849	532.04315	0.06685
25	531.93805	532.04654	0.05930

Measurement Results (Continued)

Environment	Start	Finish
Temperature (^{o}C)	21	20.8
Humidity (%RH)	51	50

Environment control
(20 ± 1) ^{o}C
(50 ± 10) %RH

CMM accuracy: 0.6 µm + L/600;

Table 6.4 Ball plate measurement: Location 1 (Back) _BP212

Ball No.	X (mm)	Y (mm)	Z (mm)
1	0.00000	0.00000	0.00000
2	133.00332	-0.00262	0.02750
3	266.00628	-0.00114	0.04147
4	399.01385	-0.00129	0.03008
5	532.01562	0.00000	0.00000
6	-0.02297	133.01361	0.03160
7	132.98021	133.01262	0.03515
8	265.98580	133.01218	0.02173
9	398.99094	133.01182	0.02058
10	531.99073	133.01421	0.01684
11	-0.02919	266.02464	0.02517
12	132.97326	266.01937	0.05283
13	265.97775	266.02147	0.02198
14	398.98231	266.02110	0.02700
15	531.98251	266.02366	0.03089
16	-0.05049	399.03545	0.02940
17	132.95221	399.03372	0.04487
18	265.95364	399.03660	0.02922
19	398.95527	399.03695	0.04266
20	531.95621	399.03676	0.05064
21	-0.05942	532.04208	0.00000
22	132.94344	532.03991	0.02976
23	265.94452	532.04054	0.06062
24	398.94473	532.04211	0.06237
25	531.94474	532.04535	0.05485

Measurement Results (Continued)

Environment	Start	Finish
Temperature (^{o}C)	21	21
Humidity (%RH)	50	50

Environment control
(20 ± 1) ^{o}C
(50 ± 10) %RH

CMM accuracy: 0.6 µm + L/600;

Table 6.5 Ball plate measurement: Location 2 (Front) _BP311

Ball No.	X (mm)	Y (mm)	Z (mm)
1	0.00000	0.00000	0.00000
2	133.00448	-0.00265	0.02815
3	266.00805	-0.00097	0.04188
4	399.01653	-0.00094	0.03037
5	532.01837	0.00000	0.00000
6	-0.02181	133.01300	0.03285
7	132.98223	133.01201	0.03562
8	265.98810	133.01245	0.02152
9	398.99394	133.01215	0.02129
10	531.99358	133.01478	0.01651
11	-0.02756	266.02430	0.02581
12	132.97519	266.01879	0.05382
13	265.97978	266.02151	0.02191
14	398.98483	266.02164	0.02737
15	531.98519	266.02462	0.02990
16	-0.04861	399.03520	0.02871
17	132.95440	399.03341	0.04382
18	265.95549	399.03701	0.02727
19	398.95748	399.03756	0.04114
20	531.95841	399.03772	0.04774
21	-0.05706	532.04199	0.00000
22	132.94569	532.04008	0.03016
23	265.94638	532.04127	0.05993
24	398.94682	532.04296	0.06215
25	531.94652	532.04650	0.05336

Measurement Results (Continued)

Environment	Start	Finish
Temperature (^{o}C)	20.5	20.6
Humidity (%RH)	50	50

Environment control
(20 ± 1) ^{o}C
(50 ± 10) %RH

CMM accuracy: 0.6 µm + L/600;

Table 6.6 Ball plate measurement: Location 2 (Back) _BP312

Ball No.	X (mm)	Y (mm)	Z (mm)
1	0.00000	0.00000	0.00000
2	133.00425	-0.00219	0.02836
3	266.00808	-0.00100	0.04260
4	399.01636	-0.00100	0.03161
5	532.01916	0.00000	0.00000
6	-0.02235	133.01381	0.03225
7	132.98164	133.01282	0.03644
8	265.98780	133.01268	0.02264
9	398.99361	133.01215	0.02157
10	531.99476	133.01447	0.01550
11	-0.02891	266.02539	0.02556
12	132.97395	266.02014	0.05380
13	265.97895	266.02232	0.02218
14	398.98426	266.02165	0.02644
15	531.98576	266.02455	0.02779
16	0.05007	399.03634	0.02800
17	132.95296	399.03451	0.04350
18	265.95479	399.03758	0.02696
19	398.95694	399.03789	0.03903
20	531.95869	399.03768	0.04437
21	-0.05778	532.04306	0.00000
22	132.94532	532.04074	0.02929
23	265.94666	532.04154	0.05895
24	398.94720	532.04298	0.05917
25	531.94792	532.04644	0.04919

Measurement Results (Average)

Environment	Start	Finish
Temperature (^{o}C)	20.6	20.8
Humidity (%RH)	51.1	50.8

Environment control
(20 ± 1) ^{o}C
(50 ± 10) %RH

CMM accuracy: 0.6 µm + L/600;

Table 6.7 Ball plate measurement: All Locations (average)

Ball No.	X_{ave} (mm)	Y_{ave} (mm)	Z_{ave} (mm)
1	0.00000	0.00000	0.00000
2	133.00425	-0.00219	0.02836
3	266.00808	-0.00100	0.04260
4	399.01636	-0.00100	0.03161
5	532.01916	0.00000	0.00000
6	-0.02235	133.01381	0.03225
7	132.98164	133.01282	0.03644
8	265.98780	133.01268	0.02264
9	398.99361	133.01215	0.02157
10	531.99476	133.01447	0.01550
11	-0.02891	266.02539	0.02556
12	132.97395	266.02014	0.05380
13	265.97895	266.02232	0.02218
14	398.98426	266.02165	0.02644
15	531.98576	266.02455	0.02779
16	0.05007	399.03634	0.02800
17	132.95296	399.03451	0.04350
18	265.95479	399.03758	0.02696
19	398.95694	399.03789	0.03903
20	531.95869	399.03768	0.04437
21	-0.05778	532.04306	0.00000
22	132.94532	532.04074	0.02929
23	265.94666	532.04154	0.05895
24	398.94720	532.04298	0.05917
25	531.94792	532.04644	0.04919

6.10 Error Calculations

CMM accuracy: 0.6 µm + L/600;

Table 6.8 Error calculations between the real CMM experiment and a standard of a ball plate calibration.

Ball No.	X_{ave} (mm)	Y_{ave} (mm)	Z_{ave} (mm)
1	0.00000	0.00000	0.00000
2	0.00127	0.00043	0.00534
3	0.00265	0.00024	0.00841
4	0.00391	0.00020	0.00830
5	0.00620	0.00000	0.00000
6	0.00003	0.00044	0.00064
7	0.00708	0.00070	0.00549
8	0.00133	0.00074	0.00744
9	0.00433	0.00025	0.00796
10	0.00362	0.00057	0.00123
11	0.00012	0.00083	0.00080
12	0.00155	0.00081	0.00393
13	0.00336	0.00033	0.00734
14	0.00447	0.00319	0.00804
15	0.00535	0.00111	0.00684
16	0.00319	0.00023	0.00075
17	0.00077	0.00256	0.00404
18	0.00386	0.00200	0.00753
19	0.00462	0.00271	0.00035
20	0.00599	0.00101	0.00216
21	0.00018	0.00284	0.00000
22	0.00209	0.00225	0.00595
23	0.00454	0.00188	0.00913
24	0.00378	0.00164	0.00150
25	0.00664	0.00257	0.00321

The ball plate was measured in six orientations on Coordinate Measuring Machine (PMM-C700P). By average these six measurements systematic geometry errors of CMM were calculated. The comparisons between the measurements from the real physical CMM and the standard CMM measurement certificate are evaluated in Matlab programme as figure 6.11

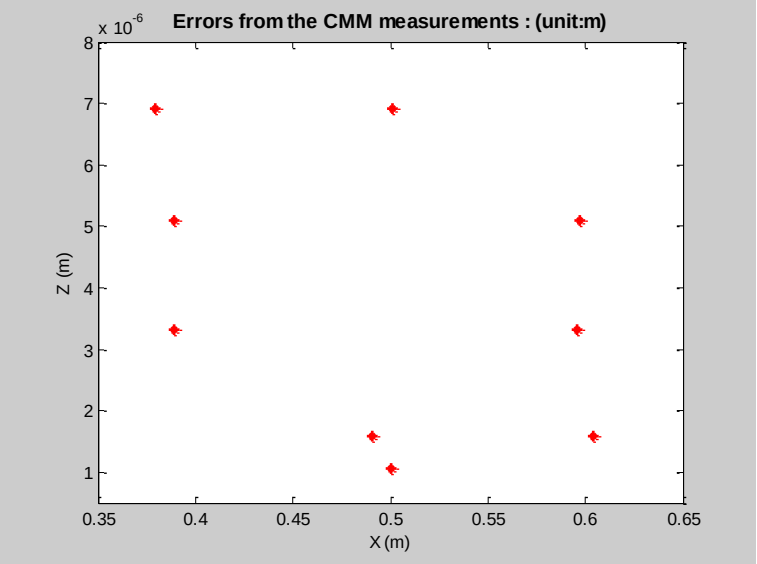

Figure 6.11 Shows the positioning errors of the ball plate measurement

6.11 Conclusions

In this research, the validation of the CMM measurement using a ball plate as an artefact is generated. The measurement positions of a ball are using CMM (PMM-C700P) with traditional calibration (from ball no. 1 to no. 25). The standard and unit under calibration had been stabilised in the ambient environment before calibration. The results of the errors calculation indicate a good performance for the CMM measurement due to the low density of errors (less than 0.01 µm).

Chapter 7 Data Comparisons

7.1 Introduction

Simulation results provide significant information for decisions and actions in many areas of physical experiments and investigation. The process of verification and validation can help to ensure that the simulated models are correct and reliable. In this chapter, the analysis of the simulations, local kinematic error model and a GP model are conducted on the validation through a real physical experiment by measuring a ball plate based on CMM in the real machine environment setup.

7.2 Comparison results between a local kinematic errors model and a GP model

The experimental data is validated by measurement and inspection of CMM using a ball plate as an artefact and, in addition, simulation approaches. All data obtained from the simulations and experimentation is presented through graphs to show the trends and to check the consistency of the results.

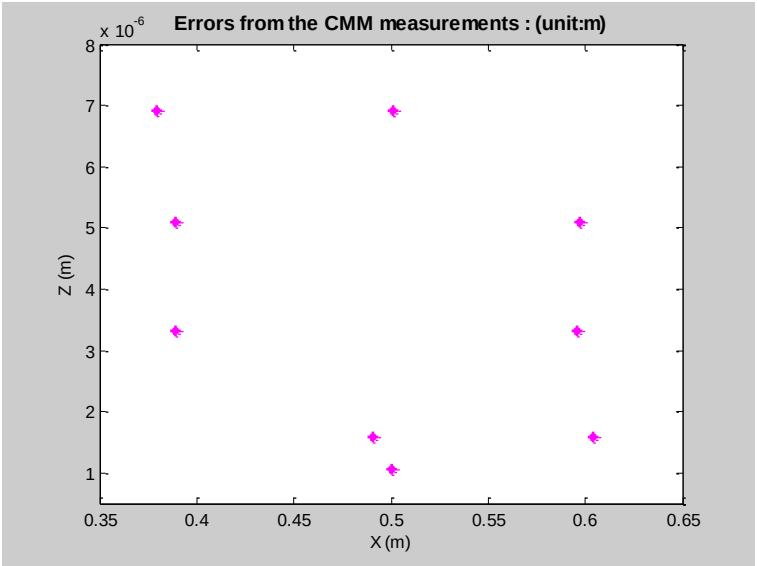

Figure 7.1 The graphical trends of errors from the physical CMM measurements

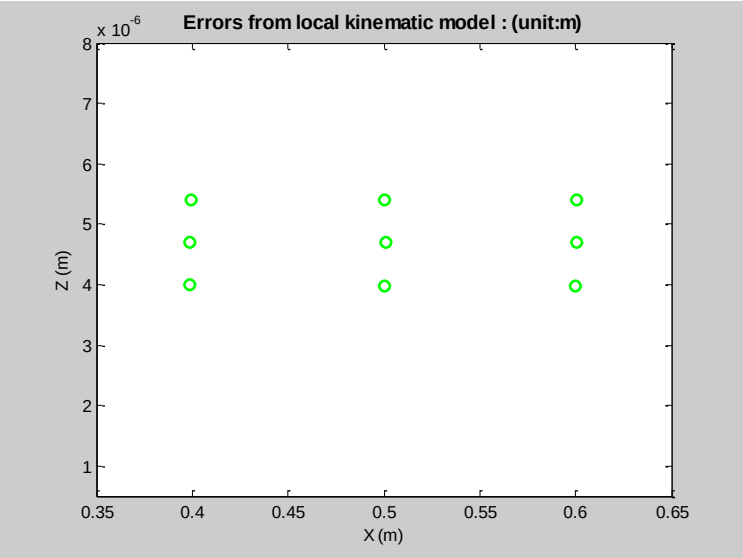

Figure 7.2 The graphical trends of errors from the local kinematic errors model

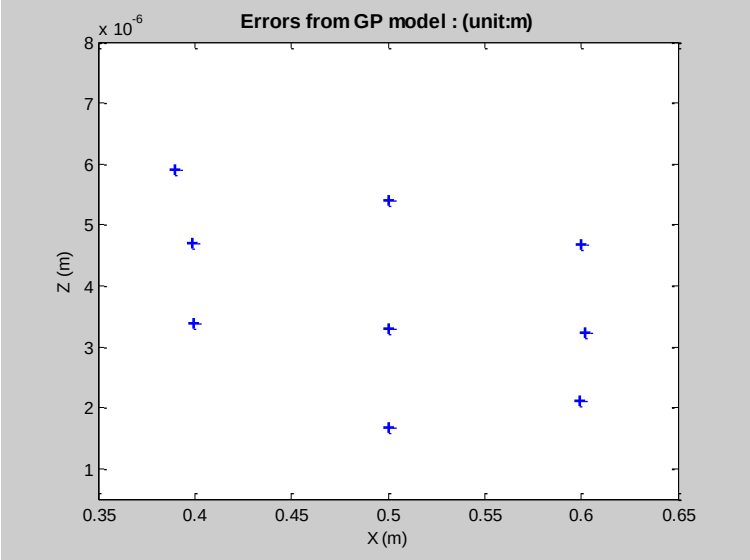

Figure 7.3 The graphical trends of errors from the GP model

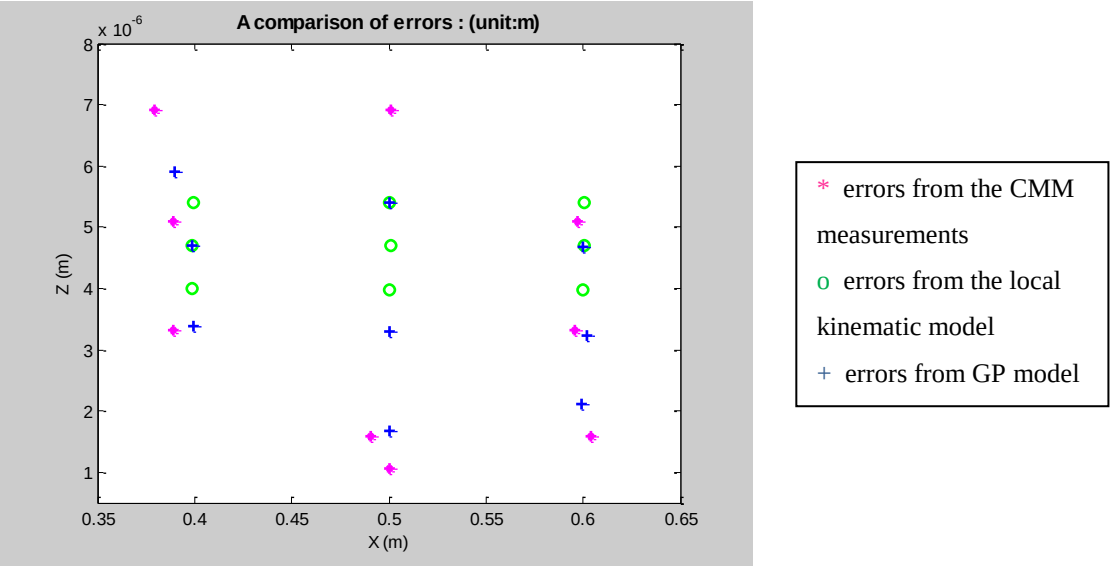

Figure 7.4 A comparison of the graphical trends of errors

These generated errors results show a significant performance in terms of errors evaluations of both the local kinematic error model and the GP method. From the evaluated errors results in figure 7.4, it is apparent that the error simulations from approaches, the local kinematic error model and the GP model, give actually similar results to the physical CMM measurements.

We can compare the both models (the local kinematic error model and the GP model) and the CMM measurement results by calculating the percentage error. The formula is given by:

$$\frac{|Simulated\ Value - Experimental\ Value|}{Experimental\ Value}\ x\ 100\% \qquad (7.1)$$

Table 7.1 The percentage error comparison between the local kinematic error model and the GP model based on the real physical CMM measurements

Ball plate No.	Percentage error	
	Local kinematic error model	GP model
1	0.0422 %	0.0148 %
2	0.0057 %	0.0058 %
3	0.0302 %	0.0010 %
4	0.0348 %	0.0012 %
5	0.0527 %	0.0324 %
6	0.0217 %	0.0218 %
7	0.0161 %	0.0060 %
8	0.0198 %	0.0015 %
9	0.0552 %	0.0075 %

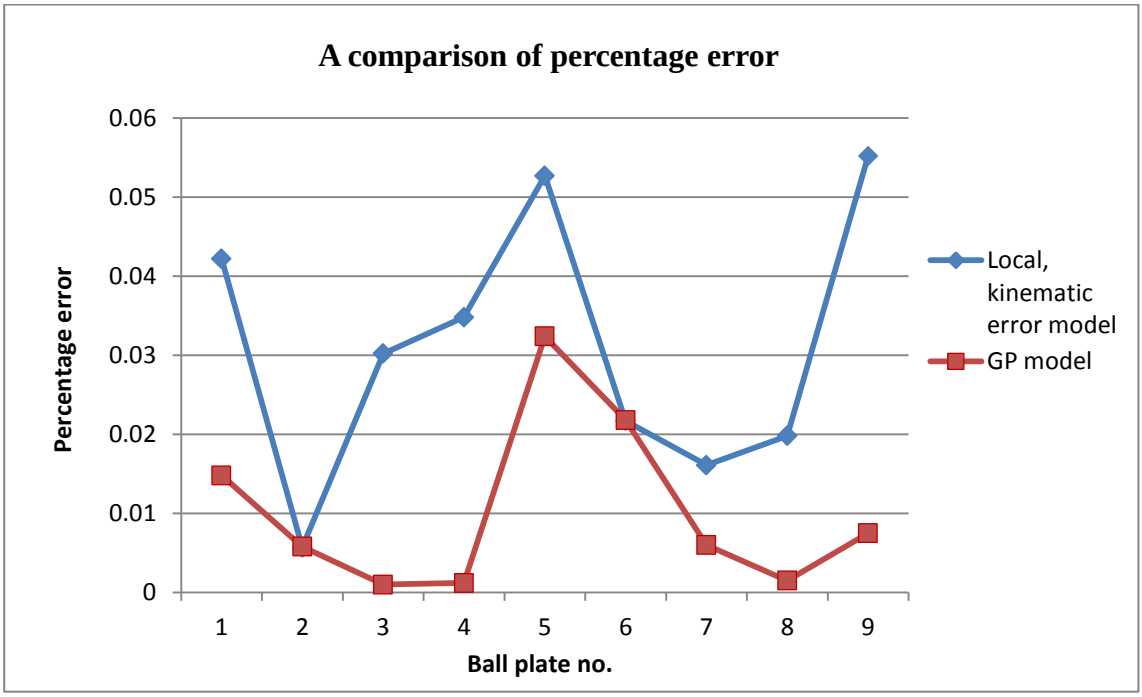

Figure 7.5 A comparison of the percentage errors of the two approaches

As can be seen from the data above, the comparative percentage errors between the local kinematic error model and the GP model, based on comparing to the real physical

CMM calibration, show that the GP model generated error evaluations that are much more similar to the real CMM measurements than to the local kinematic error model. The results of the percentage errors, through the ball plate location No. 1-9, illustrate that the GP model has the average percentage of the errors less than 0.034% in all positions of the ball while the local kinematic error model has the percentage errors more than 0.034% in some ball locations. However, these differences are differentiated only to a low degree. Therefore, both of these methods still show good performances for simulated estimators.

7.3 Conclusions

From the numerical simulation results, estimates of the systematic errors can be determined by the local kinematic error model and the Gaussian Process model. The results obtained from the preliminary simulation analysis of both simulations presented above show that the evaluated errors give similar results to those from the real physical CMM measurements. The reliability of the local kinematic error model and GP model depend on the validity of the assumptions used in the underlying theory and on the accuracy of the mathematical simulations. By means of the evaluation of error compensations and the development of fast precision performance, therefore, the local kinematic error model and the GP model can be applicable with high precision and accuracy simulators for coordinate measurements.

7.4 Discussions

This study set out with the aim of assessing the kinematic errors of the CMM in the part of numerical simulations designing as a real physical CMM performance. For comparison purposes, the most interesting finding is that the error evaluations from the local kinematic error model, the GP model and the actual physical CMM measurements using a ball plate as an artefact are different at the low degree.

It can therefore be assumed that the GP model and the local kinematic error model generate the errors compensation similarly to the real physical CMM calibrations. In accordance with the percentage error results based on the physical CMM measurements, the GP model performs slightly better than the local kinematic error model. Nonetheless, both local kinematic error model and GP approach, based upon the real CMM performance, have the difference of percentage errors at the low level which can be assumed that they are essentially the same as the actual CMM measurement.

The inconsistency may be due to the insufficient information when the simulated CMM sampling points are small, the GP approach suffers from this case meaning more uncertainty, but to a less degree. While the local kinematic error model is capable of performing with a small sample point due to concentrating only on the particular region.

In the simulations, we observed that the numerical simulation process of the GP model makes the mathematical calculations less-time consuming comparing to the local kinematic error model. The numerical simulation process, as shown in Chapter 4, the local kinematic error model has calculated under more complicated mathematical calculations than the GP approach e.g. Cheby-shev polynomial approach, Gauss-Newton algorithm, QR factorisation approach, and Jacobian matrix etc. In contrast to the GP method, it has basically used a GPML toolbox as a demonstrated matlab code as well as providing a mean and covariance functions to train the simulated sampling data.

Chapter 8 Conclusions and recommendations for future work

This thesis comprises four parts. The first part is divided into: “Introduction” (Chapter 1), “Literature Review” (Chapter 2), and “CMM verification approach” (Chapter 3). The second part is divided into: “Simulation of CMM local, kinematic errors model” (Chapter 4) and “Simulation of Gaussian Process model” (Chapter 5), which evaluate the uncertainty and calculate the errors of the CMM measurements; the validation of the simulations, “CMM calibration using a ball plate” (Chapter 6), is also examined here. The third part – “Data analysis” (Chapter 7) – is focused on the comparative case study between the simulations and the experimentation. The final part – “Conclusions and recommendations for future work” (Chapter 8) – provides the conclusions of this study, including contributions and recommendations for future research. In this chapter, we draw distinctive conclusions of a comparative performance study, highlight the contributions to knowledge, and recommend work for future studies.

8.1 Conclusions

Within this thesis, there are two approaches: local, kinematic error simulation and a GP model to improve the precision and accuracy of coordinate measurements using numerical simulations has been investigated. In order to achieve the objectives of better characterisation and uncertainty evaluation, the simulation and experimental results are implemented, analysed, compared, and discussed in the previous chapters. The important conclusions can be summarized as below:

- Prompted by the continuingly rising demand for measurement efficiency and accuracy in a rapid developing manufacturing industry, CMM and its related technologies has become a central research field. Among other approaches, the numerical simulation is a category of CMM tool that enables the planning of an optimal inspection path programme and the error analysis and uncertainty evaluation associated with the CMM measurement results. There are two approaches to numerical simulations: a local, kinematic error model and a GP model have been generated for a comprehensive integrated coordinate system in the existing solutions.
- Kinematic errors, errors in the machine components due to imperfect manufacturing or alignment during assembly, have been derived. There are 21 sources of CMM

kinematic errors consisting of a positioning error (one positional deviation in the direction of motion along three axes), straightness errors (two linear deviations orthogonal to the direction of motion along three axes), rotational errors (three angular deviations: roll, pitch, yaw along three axes), and squareness errors (three squareness errors between pairs of axes).

- A local, simplified kinematic error model has been enabled to improve the capability and CMM performance to simulate the measurement process and error compensation and uncertainty evaluation without the need to perform a large number of the measurement in a real physical CMM measurement. The numerical simulation procedures comprise a Gauss-Newton algorithm implemented for solving the linear least-square problem. QR factorisation can solve the problem of possible rank deficiency, while parametric error components can be generated based on the Cheby-shev polynomial and uncertainty is assessed by using a Jacobian matrix.
- The proposed GP model for modelling and assessing the parametric errors is presented. A GP method provides a probability distribution over functions which help in assessing the kinematic errors in the measurements of a CMM. A covariance function is defined to incorporate more specific prior distributions of the model. Our goal here is to study the GP model reconstruction in terms of error compensation and uncertainty evaluation, which helps to assess the kinematic errors better than traditional methods.
- In this thesis, both a theoretical approach in the case of simulations and experiments with a real CMM calibration study, enabling new approaches to improve performance for error and uncertainty evaluation, have been compared. As can be seen, the GP model can predict the distribution over function to perform the error assessment and uncertainty evaluation with fewer mathematical algorithms to calculate than the local, kinematic error model. However, both models show good results of the evaluation leading to confirmation of their effective performance regarding the quality of the inspection path.

8.2 Contributions to knowledge

A number of contributions to knowledge have been enabled in this work, which are summarized below:

- Mathematical model development for making effective choices regarding the local, kinematic error model and GP model is performed and formulated; this is verified by particular kinematic errors of the CMM measurements, presenting high accuracy and reliability of the error and uncertainty evaluation performance.
- The improvement achieved by the proposed method over the traditional approaches between the simulated datasets and actual CMM data measurements has been demonstrated.
- The numerical simulations with a well-designed strategy providing accurate estimates of the CMM kinematic errors using only a nominal CMM calibration with a ball plate have been validated and evaluated in both approaches.
- The influences of kinematic errors affected through the measurement process of the CMM on the calibration have been investigated.

8.3 Recommendations for future work

An investigation within this thesis intends to provide a complete effective approach to improve the techniques for error and uncertainty of CMM measurement evaluation. To make the most effective use of the current research, there are still certain areas that have not been thoroughly investigated due to the limitations of time and available facilities. Therefore, the following suggestions for future improvements are made:

- The uncertainty evaluation from the physical CMM measurements is needed in assessment and comparison to the simulations for a validation.
- The uncertainty evaluation of the GP model is required.
- More specific issues of the local, kinematic error model and the GP model for better completed challenging and accurate model, for instance, the three-dimensional and four-dimensional, can be further performed in the model in relation to the CMM kinematic errors evaluation.
- Further measurement strategies and other different types of reference artefacts (e.g. hole plates, step gauge, etc.) will be additional areas for study, with particular consideration of numerical stability. Consideration of thermal errors model will also be interesting for investigation due to their importance.
- An application of a spline function embedded with the model approach of kinematic errors evaluation can be further investigated for a better accurate performance of the model.

References

ANSI/ASME B89.1.12M, Methods for Performance Evaluation of Coordinate Measuring Machines, The American Society for Mechanical Engineering, New York, 1989.

Anthony, G. T., Anthony, H. M., Cox, M. G. and Forbes, A. B. (1991). "The parametrization of geometric form". CEC report EUR 13517 EN, Luxembourg.

Balsamo, A. et al. (1997). "Results of the CIRP-Euromet intercomparison of ball plate based techniques for determining CMM parametric errors", *Ann. CIRP*, 46(1), pp. 463-466.

Balsamo, A. et al., (1999) Evaluation of CMM uncertainty through Monte Carlo simulations. CIRP Annals - Manufacturing Technology, 48(1), pp.425-28.

Barakat, N. A., Elbestawi, M.A. and Spence, A. D. (2000). "Kinematic and geometric error compensation of a coordinate measuring machine". *International Journal of Machine Tools and Manufacture*, 40(6), pp. 833–850.

Barker, R. M., Cox, M. G., Forbes, A. B. and Harris, P. M. (2007). "Software support for metrology best practice guide no.4 – Discrete modelling and experimental data analysis". *NPL Report DEM-ES 018.*

Bauza, M. B., Hocken, R. J., Smith, S. T. & Woody, S. C., (2005). "The development of a virtual probe tip with application to high aspect ratio microscale features". *Review of Scientific Instruments*, 76(9), p.095112.

Beaman, J. & Morse, E., (2010). "Experimental evaluation of software estimates of task specific measurement uncertainty for CMMs". *Precision Engineering*, 34(1), pp.28-33.

Belforte, G., et al. (1987). "Coordinate measuring machines and machine tools self-calibration and error correction", *Annals of the CIRP*, 36(1), pp. 359-363.

Bohez, E. L. J., et al. (2007). “Systematic geometric rigid body error identification of 5-axis milling machines”, *Computer-Aided Design*, 39, pp. 229-244.

Brahim-Belhouari, S. and Bermak, A. (2004). “Gaussian process for nonstationary time series prediction”, *Computational Statistics&Data Analysis*, 47, pp.705-712.

Bringmann, B., Kung, A., and Knapp, W. (2005). “A Measuring Artefact for true 3D Machine Testing and Calibration”. *Annals of the CIRP - Manufacturing Technology*, 54(1), pp. 471–474.

British Standards Institution, (1987). “BS 6808-1:1987 Coordinate measuring machines — Part 1: Glossary of terms. London”: British Standards Institution.

Bryan, J.B. (1979). “The Abbe Principle revisited”, *Precision Engineering*, 1 (3), pp. 129-132.

Bryan, J.B. (1990). “International status of thermal error research”. *Ann. CIRP*, 39(2), pp. 645–656.

BS 6808: Part 1:1987, Coordinate Measuring Machines, Part 1: Glossary of Terms, British Standards Association, 1987.

BS 6808: Part 2:1987, Coordinate Measuring Machines, Part 2: Methods for Verifying Performance, British Standards Association, 1987.

BS 6808: Part 3: 1989, Coordinate Measuring Machines. Part 3: Code of Practice, British Standards Association, 1989.

Busch, K., Kunzmann, H. and Wäldele, F. (1985). "Calibration of coordinate measuring machines", *Precision Engineering*, 7(3), pp. 139-144.

Cauchick-Miguel, P., King, T. and Davis, T. (1996). “CMM verification: a survey”, *Measurement*, 17(1), pp. 1-16.

Chang, T.C., (1990). “Expert Process Planning for Manufacturing”. Reading, Massachusetts, USA: Addison-Wesley.

Chapman, M. A. V. (2013). “Calibration of machine squareness”. *Renishaw apply innovation.*

Chen, Y. H., Yang, Z. Y. & Lian, L. L. (2005). “On the development of a haptic system for rapid product development”. *Computer-Aided Design*, 37(5), pp.559-69.

Chen, Y.H., Wang, Y.Z. & Yang, Z.Y. (2004). “Towards a haptic virtual coordinate measuring machine”. *International Journal of Machine Tools & Manufacture*, 44(10), pp.1009-17.

Cheng, Y. & Cai, F., (1995). “Automated fixturing planning for inspection on coordinate measuring machine”. In Proceedings of the SPIE - The International Society for Optical Engineering. International Conference on Intelligent Manufacturing. Wuhan, China, 1995. SPIE - The International Society for Optical Engineering. no full text.

Chu, W. and Ghahramani, Z. (2005). “Gaussian Processes for Ordinal Regression”, *Journal of Machine Learning Research*, 6, pp. 1019-1041.

CMMA, “Accuracy Specification for Coordinate Measuring Machines”, Coordinate Measuring Machine Manufacturers Association, London, 1982.

COORD3 Metrology (2016) Available from: http://www.coord3-cmm.com/used-coord3-kronos-cmm-machine/ (accessed 01 February 2016).

Cox, M. G., Forbes, A. B., Harris, P. M. and Peggs, G. N. (1998). “Determining CMM behaviour from measurements of standard artefacts”. *NPL Report CISE 15/98*.

Ebden, M. (2008). “Gaussian Process for Regression: A Quick Introduction”.

Forbes, A. B. (1991). “Least-squares best-fit geometric elements”. *NPL Report DITC 140/89.*

Forbes, A. B. (1996). “Model parametrization. In Advanced Mathematical Tools in Metrology II”, (P. Ciarlini, M. G. Cox, F. Pavese and D. Richter, Eds.),World Scientific, Singapore, pp 28-37.

Forbes, A. B. (2015). “Empirical functions with pre-assigned correlation behaviour”, *Advanced mathematical and computational tools in Meterology and testing X*. United Kingdom: World Scientific Publishing Company.

Gu, P., (1994). “A knowledge-based inspection process planning system for coordinate measuring machines”. Journal of Intelligent Manufacturing, 5(5), pp.351-63.

Hocken, R., et al. (1977). “Three dimensional metrology”. *Annals of the CIRP*, 26(2), pp. 403-408.

Hu, Y., Yang, Q. P., Sun, X. (2012). “Design, implementation, and testing of advanced virtual coordinate-measuring machines”. *IEEE Transactions on Instrumentation and Measurement*, 61(5), pp. 1368-1376.

International Organization for Standardization, (1993), corrected and reprinted in 1995. ISO/IEC Guide 98:1995 Guide to the expression of uncertainty in measurement (GUM). Geneva, Switzerland: International Organization for Standardization.

International Organization for Standardization, (1993). International vocabulary of basic and general terms in metrology. second edition ed. Geneva, Switzerland: International Organization for Standardization.

International Organization for Standardization, (1997). ISO/IEC 14772-1:1997 Information technology -- Computer graphics and image processing -- The Virtual Reality Modelling Language -- Part 1: Functional specification and UTF-8 encoding. Geneva, Switzerland: International Organization for Standardization.

International Organization for Standardization, (2000). ISO 10360-1:2000 Geometrical Product Specifications (GPS) — Acceptance and reverification tests for coordinate

measuring machines (CMM) — Part 1: Vocabulary. Geneva, Switzerland: International Organization for Standardization.

International Organization for Standardization, (2004). ISO/TS 15530-3:2004(E) Geometrical product specifications (GPS) — Coordinate measuring machines (CMM): Technique for determining the uncertainty of measurement — Part 3: Use of calibrated workpieces or standards. Geneva, Switzerland: International Organization for Standardization.

International Organization for Standardization, (2006). ISO/TS 23165:2006(E) Geometrical product specifications (GPS) — Guidelines for the evaluation of coordinate measuring machine (CMM) test uncertainty. Geneva, Switzerland: International Organization for Standardization.

International Organization for Standardization, (2008). ISO/IEC GUIDE 98-3:2008(E) Uncertainty of measurement — Part 3: Guide to the expression of uncertainty in measurement (GUM: 1995). Geneva, Switzerland: International Organization for Standardization.

International Organization for Standardization, (2008). ISO/IEC Guide 98-3:2008/Suppl 1:2008 Propagation of distributions using a Monte Carlo method. Geneva, Switzerland: International Organization for Standardization.

International Organization for Standardization, (2008). ISO/TS 15530-4:2008(E) Geometrical product specifications (GPS) — Coordinate measuring machines (CMM): Technique for determining the uncertainty of measurement — Part 4: Evaluating task-specific measurement uncertainty using simulation. Geneva, Switzerland: International Organization for Standardization.

ISO 10360-2 Coordinate Metrology, Part 2: Performance Assessment of Coordinate Measuring Machines, International Organization for Standardization, 1994.

ISO 10360-2: (2002). Geometric Product Specifications Acceptance & Reverification tests for coordinate measuring machines (CMM) – Part 2: CMMs used for measuring size. International Organization for Standardization.

JIS B 7440, "Test Code for Accuracy of Coordinate Measuring Machines", Japanese Standards Association, Japan, 1987.

Jouy, F. and Clement, A. (1986). "Theoretical modelisation and experimental identification of the geometrical parameters of coordinate-machines by measuring a multi-directed bar". *Annals of the CIRP*, 35(1). pp. 393-396.

Kim, K. -D. and Chung, S. -C. (2001). "Synthesis of the measurement system on the machine tool". *International Journal of Production Research*, 39(11), pp. 2475-2497.

Knapp, W. (1988). "Accuracy of length measurement and positioning statistical measurement and contouring mode", *Annals of the CIRP*, 37(1), pp. 511-514.

Knapp, W. and Matthias, E. (1983). "Test of the three-dimensional uncertainty of machine tools and measuring machines and its relation to the machine errors", *Annals of the CIRP*, 32(1), pp. 459-462.

Knapp, W., et al. (1991). "Comparison of different artefacts for interim coordinate measuring machine checking", *Precision Engineering*, 13(4), pp. 277-291.

Kruth, J. P., Vanherck, P. and De Jonge, L. (1994). "Self-calibration method and software error correction for three-dimensional coordinate measuring machines using artefact measurements", *Measurement*, 14(2), pp. 157–167.

Kunzmann, H., Trapet, E. and Wäldele, F. (1990). "A Uniform Concept for Calibration, Acceptance Test, and Periodic Inspection of Coordinate Measuring Machines Using Reference Objects". *Ann. CIRP*, 39(1), pp. 561–564.

Kurfess, T.R., (2006). "What can CMMs do? They can measure almost anything". *Manufacturing Engineering*, 136(3), pp.173.

Liebrich, T., Bringmann, B. and Knapp, W. (2009) 'Calibration of a 3D-ball plate', *Precision Engineering*, 33(1), pp. 1–6.

Lu, C. G., Morton, D., Wu, M. H. & Myler, P. (1999). "Genetic algorithm modelling and solution of inspection path planning on a coordinate measuring machine (CMM)". *International Journal of Advanced Manufacturing Technology*, 15(6), pp.409-16.

Lu, C. G., Wu, M.H., Mylar, P. & Healey, R. (1995). "Developing an information model for LINDO software input-optimal path planning for CMM". In Proceedings of 1st World Congress on Intelligent Manufacturing Processes and Systems. Mayaguez/San Juan, Puerto Rico, 1995. University of Puerto Rico.

Lu, C.G., Myler, P. & Wu, M.H. (1995). "An artificial intelligence path planning system for multiple tasks inspection on co-ordinate measuring machine". In Proceedings of the 31st International MATADOR Conference. Manchester, UK, 1995. Macmillan Press.

Mackay, D. J. C. (1998). "Introduction to Gaussian processes".

McMurtry, D. R. (1979). US Patent 4153998 - Probes. United States.

Miguel, P. A. C., King, T. G. and Davis, E.J. (1995). "CMM: Higher Accuracy, Lower Cost and Increased Productivity?". *Quality World Technical Supplement*. pp. 48-52.

Mitutoyo. (2016) Available from: http://ecatalog.mitutoyo.com/FALCIO-Apex-G-Series-355-High-Accuracy-Large-CNC-CMM-C1627.aspx (accessed 01 February 2016).

Neal, R. M. (1997). "Monte Carlo Implementation of Gaussian Process Models for Bayesian Regression and Classification". *Technical report 9702*, Department of Statistics, University of Toronto. http://www.cs.toronto.edu/~radford.

NF E 11-150. (1986). "Instruments de Measurage Dimensionnel. Machines à Mesurer", AFNOR.

Okafor, A. C. and Ertekin, Y. M. (2000). “Derivation of machine tool error models and error compensation procedure for three axes vertical machining center using rigid body kinematics”. *International Journal of Machine Tools and Manufacture*, 40, pp. 1199-1213.

ONORM M 1385. (1989). “Koordinatenmesstechnik, Methode zur Naehprufung yon Koordinatenmessgeraten”, ON a-1021, Wien.

Pahk, H. J., Burdekin, M. and Peggs, G. N. (1998). “Development of virtual coordinate measuring machines incorporating probe errors”, *Proceedings of the Institution of Mechanical Engineers, Part B: Journal of Engineering Manufacture.* 212, pp. 533–548.

Phillips, S. D., et al. (1997). “The calculation of CMM measurement uncertainty via the method of simulation by constraints”. In *Proceedings of the 12th Annual Meeting of the American Society for Precision Engineering*. Norfolk, VA.

Rasmussen, C. E. & Williams, C. K. I. (2006). “Gaussian Processes for Machine Learning”. Cambridge: MIT Press.

Rasmussen, C. E. (2004). “Gaussian Processes in Machine Learning; Advanced Lectures on Machine Learning”, *Lecture Notes in Computer Science*, 3176, pp. 63-71.

Rasmussen, C. E. (2010). “Gaussian Processes for Machine Learning (GPML) Toolbox”, *Journal of Machine Learning Research,* 11, pp.3011-3015.

Rugbani, A. and Schreve, K. (2014), “Design and Structure of a Novel 3-DOF Micro-CMM”. In *Proceedings of the International Conference on Mechanical Design, Manufacture and Automation Engineering (MDMAE 2014).* Phuket, Thailand.

Sartori, S. and Zhang, G. X. (1995). “Geometric Error Measurement and Compensation of Machines”. *Ann. CIRP*, 44(2), pp. 599-609.

Schellekens, P., et al. (1998). “Design for Precision: Current Status and Trends”. *CIRP Annals-Manufacturing Technology*, 47(2), pp. 557-586.

Schultschik, R. and Matthias, E. (1977). “The components of the volumetric accuracy”, *Annals of the CIRP*, 26(1), pp. 229-233.

Schwenke, H., et al. (2008). “Geometric error measurement and compensation of machines—an update”. *Ann. CIRP*, 57(2), pp. 660–675.

Seeker, M. (2004). “Gaussian processes for machine learning”, *International Journal of Neural Systems*, 14(2), pp. 69-106.

Shen, Y.L. & Zhang, X. (1997). “Modelling of pretravel for touch trigger probes on indexable probe heads on coordinate measuring machines”. *The International Journal of Advanced Manufacturing Technology*, 13(3), pp. 206-13.

Silva, J. B. A., et al. (2009). “Approach for uncertainty analysis and error evaluation of four-axis co-ordinate measuring machines”, *International Journal of Advanced Manufacturing Technology*, 41, pp. 1130-1139.

Soons, J., et al. (1992). “Modeling the errors of multi-axis machines: a general methodology”, *Precision Engineering*, 14/1.

Sprauel, J.M., Linares, J.M., Bachmann, J. & Bourdet, P. (2003). “Uncertainties in CMM measurements, control of ISO specifications”. *CIRP Annals - Manufacturing Technology*, 52(1), pp. 423-26.

Spyridi, A. J. and Requicha, A. A. G. (1990). “Accessibility analysis for the automatic inspection of mechanical parts by coordinate measuring machines”. In *Proceedings of 1990 IEEE International Conference on Robotics and Automation*. Los Angeles, CA, USA.

Trapet, E. and Wiudele, F. (1991). “A reference object based method to determine the parametric error components of coordinate measuring machines and machine tools”, *Measurement*, 9(1), pp. 17–22.

Trenk, M., Franke, M. and Schwenke, H. (2004). “The ‘virtual CMM’ a software tool for uncertainty evaluation—Practical application in an accredited calibration lab”. *in Proc. ASPE Summer Top. Meeting Uncertainty Anal.*

Umetsu, K., Furutnami, R. and Osawa, S. (2005). “Geometric calibration of coordinate measuring machine using a laser tracking system”. *Meas. Sci. Technol.*16, pp. 2466-2472.

Van Dorp, B., Haitjema, H., Delbressine, F., Bergmans, R., and Schellekens, P. (2001). “Virtual CMM using Monte Carlo methods based on frequency content of the error signal,” *Proc. SPIE* 4401.

VDI/VDE 2617. (1986). “Accuracy of Coordinate Measuring Machines, Characteristics and their Checking. Part 1: Generalities”, Dusseldorf.

VDI/VDE 2617. (1986). “Accuracy of Coordinate Measuring Machines, Characteristics and their Checking. Part 2.1: Measurement Task Specific Measurement Uncertainty and Length Measurement Uncertainty”, Dusseldorf.

VDI/VDE 2617. (1989). “Accuracy of Coordinate Measuring Machines, Characteristics, Parameters and their Checking. Part 3: Components of Measurement Deviation of the Machine”.

VDI/VDE 2617. (1989). “Accuracy of Coordinate Measuring Machines, Characteristics and their Checking Part 4: Rotary Tables on Coordinate Measuring Machines”, Dusseldorf.

VDI/VDE 2617. (1991). “Genauigkeit yon Koordinatenmessgeraten, Kenngrossen und deren Prufung Blatt 5: Uherwachung dureh Prufkorper”, Dusseldorf.

Virtual Environments, Human-Computer Interfaces and Measurements Systems (VECIMS 2009). Hong Kong, China, 2009. IEEE.

Wang, C. (2003). “What is 3D volumetric positioning accuracy and How to define and measure it”, pp. 1–4.

Wang, Y. et al., (2009). “Accessibility analysis for CMM inspection planning by means of haptic device and STL representation”. In 2009 IEEE International Conference on *Virtual Environments, Human-Computer Interfaces, and Measurements Systems, VECIMS 2009.*

Wang, Y., Chen, Y., Nan, Z. & Hu, Y., (2006). Accessibility analysis for CMM inspection planning using haptic device. In IEEE International Conference on Robotics and Biomimetics - ROBIO2006. Kunming, China, 2006. IEEE.

Wilhelm, R.G., Hocken, R. and Schwenke, H. (2001). “Task specific uncertainty in coordinate metrology”. *Annals of the CIRP*, 50(2). pp. 553-563.

Wilson, A., Larsen, E., Manocha, D. & Lin, M.C., (1999). Partitioning and handling massive models for interactive collision detection. Computer Graphics Forum, 18(3), pp.C327-29.

Xia, H., Ding, Y. and Wang, J. (2008). “Gaussian process method for form error assessment using coordinate measurements”, *IIE Transactions*, 40, pp. 931-946.

Yang, Q., (1992). “A high precision probe system for three dimensional coordinate measurement”. PhD Thesis. London: Brunel University.

Yang, Q., Butler, C. & Baird, P., (1996). “Error compensation of touch trigger probes”. *Measurement*, 18(1), pp. 47-57.

Yang, Z. and Chen, Y. (2005). “Inspection path generation in haptic virtual CMM”. *Computer-Aided Design and Applications*, 2(1-4), pp. 273-82.

Zhang, G. X. and Zang, Y. F. (1991). “A method for machine geometry calibration using 1-D ball array”, *Annals of the CIRP*, 40/1, pp. 519-522.

Zhang, G., et al. (1985). “Error compensation of coordinate measuring machines”. *Ann. CIRP*, 34(1), pp. 445-448.

Zhang, G., et al. (1988). “A displacement method for machine geometry calibration”, *Annals of the CIRP*, 37/1, pp. 515.

Ziemian, C. W. and Medeiros, D. J. (1997). “Automated feature accessibility algorithm for inspection on a coordinate measuring machine”. *International Journal of Production Research*, 35(10), pp. 2839-56.

Ziemian, C. W. and Medeiros, D. J., (1998). “Automating probe selection and part setup planning for inspection on a coordinate measuring machine”. *International Journal of Computer Integrated Manufacturing*, 11(5), pp. 448-60.

Appendices

Appendix 1:

Summary of Facilities in the Research

Facilities	Performance Specifications	Calibration Equipment
CMM	Range: *X* x *Y* x *Z* (1200 x 1000 x 700) mm Uncertainty (k=2): $\sqrt{(0.52)^2 + (1.4x10^{-3}x\ l)^2}$ µm *l* being indication length of the CMM in mm Accuracy: 0.6 µm + L/600 Software: Quindos 6	Mfr. : Brown & Sharpe Model : PMM-C700P S/N. : 161
Ball plate	Range: up to 620 x 620 mm Number of Spheres : 25 Uncertainty (k = 2): $\sqrt{(0.26)^2 + (1.9x10^{-3}x\ l)^2}$ µm *l* being length of the ball plate in mm	Model : KOBA-check® Sphere Plate
Digital Thermometer	Uncertainty (k = 2) : 0.02 ^{o}C, 1.1 %RH	Mfr. : AHLBORN Model : H06100193 S/N : 2390-8

Appendix 2:

Part of the Simulation: Local, kinematic error model

```
% ------------------------------------------------------------------------
----
% R_BALLPLATE_1.M  Simulation of a ball plate calculation of kinematic
error
%                  model.
%
%                  Measurements with a number of probes.
%                  Three plate positions, 6 probes.
%                  Plate positions on a diagonal
%
%
% v1A 2012-07-27
% v1A 2009-07-27   ABF
% Author A B Forbes, NPL, www.npl.co.uk. (c) Crown copyright.
% ------------------------------------------------------------------------
----
clear all:
clc;

write_fig = 0;

rand('seed',0);
   format compact;

% Assign ballplate.
   Y = ballplate3;

   nY = size(Y,1);

% CMM dimensions in metres.
   Xdim = [0 1; 0 1; 0 1];

   yx = Y(:,1);
   yy = Y(:,2);

   yyy = Y';
   yyy = yyy(:); %[x1 y1 z1 x2 y2 z2...]' 3nYx1

% Ballplate locations in three positions.
   X1 = [ yx yy    0.5*ones(nY,1)];  %z=0.5
   X2p = [yx-0.5 zeros(nY,1) yy-0.5]*[1 -1 0; 1 1 0; 0 0
sqrt(2)]/sqrt(2);
   X2 = X2p+0.5;
   X3p = [yx-0.5 zeros(nY,1) yy-0.5]*[1 1 0; -1 1 0; 0 0
sqrt(2)]/sqrt(2);
   X3 = X3p+0.5;

% Order of polynomials; translation, rotation
   nt = 2;
   nr = 3;

   a = zeros(9*(nt+nr),1);
   na = length(a);
```

```
% Find transfromation parameters tt.
   %[x01,R01,X1h]=lsptm(Y,Y); %
   [x02,R02,X2h]=lsptm(X2,Y);
   %[x03,R03,X3h]=lsptm(Y,Y);
   %R0 = [R02;R01;R03];
   tt = [x02;zeros(3,1)];%;x02;zeros(3,1)];%x03;zeros(3,1)];
   nT = 1;
   R0=R02;

% Probe offsets.
   PO = [ 0 0  0.05;
          0 0 -0.05;
          0.05 0 0;
         -0.05 0 0;
          0 0.05 0;
          0 -0.05 0];

   nP = size(PO,1);

   p = PO';
   p = p(:);

% Total set of model parameters.
   aa = [yyy;tt;a;p];
  %load aa1g;
  %aa(3*nY+1:3*nY+6*nT)=tt;
   naa = length(aa);

% Index specifying measurement strategy.
   IX = [(1:nY)' 1*ones(nY,1) 3*ones(nY,1);
         (1:nY)' 1*ones(nY,1) 4*ones(nY,1);
         (1:nY)' 1*ones(nY,1) 5*ones(nY,1);
         (1:nY)' 1*ones(nY,1) 6*ones(nY,1)];
       % (1:nY)' 3*ones(nY,1) 3*ones(nY,1);
       % (1:nY)' 3*ones(nY,1) 4*ones(nY,1);
       % (1:nY)' 3*ones(nY,1) 5*ones(nY,1);
       % (1:nY)' 3*ones(nY,1) 6*ones(nY,1)];

   mX = size(IX,1);

% Approximate CMM measured coordinates.
   X0 = [X2;X2;X2;X2];%X3;X3;X3;X3]; %corresponding to IX

   wX = ones(mX,3);
   [f0] = fgfbpkempp(aa,nY,nT,nP,X0,IX,wX,R0,Xdim,nt,nr);
   X0 = X0-reshape(f0,3,mX)';
   sigma = 0.5e-6;
   error=ones(mX,1)*[1e-5 0 0];
   Xa=X0+error+sigma*randn(mX,3);

% Probe qualification.
    y0 = [ 0.5 0.5 0.5 ]';

    nY0 = 1;

    IX0 = [ ones(nP,1) (1:nP)' ];

    X0b = ones(nP,1)*y0';
```

```
    wX0 = ones(nP,3);

    aa0 = [y0;a;p];
     [fpc0, Jpc ] = fgfpqkempp(aa0,nY0,nP,X0b,IX0,wX0,Xdim,nt,nr);

% Exact data for probe qualification.
    X0b = X0b - reshape(fpc0,3,nP)';

    Xb=X0b+sigma*randn(nP,3);

     tol = 1e-7; %%
   normp = 1; %%
   niter = 1; %%

   while niter < 10 & normp > tol  %%
   niter
% Determine exact measurements.

   [f,J] = fgfbpkempp(aa,nY,nT,nP,Xa,IX,wX,R0,Xdim,nt,nr);
   normf=norm(f)

   if niter==1
       f1=f;
   end

    [ fpc, Jpc ] = fgfpqkempp(aa0,nY0,nP,Xb,IX0,wX0,Xdim,nt,nr);
     normfpc=norm(fpc)

      [mpc,npc] = size(Jpc);

% Jacobian matrix for ballplate measurements and probe qualification.
      Ja = [zeros(3*mX,3) J; ...
           Jpc(:,1:3) zeros(mpc,3*nY+6*nT) Jpc(:,4:npc)];

    d=[f;fpc];   %%

       pa = -lsqr(Ja,d);

    aa = aa + pa(4:naa+3);  %%
    aa0 = [y0;aa(3*nY+6*nT+1:naa)]; %%

    normp = norm(pa)  %%
    niter = niter + 1; %%
    end

  %save aa1 aa;

  reshape(aa(1:3*nY),3,nY)'
  reshape(aa(3*nY+1:3*nY+6*nT),3,2*nT)'
  reshape(aa(3*nY+6*nT+1:naa-3*nP),nt+nr,9)'
  reshape(aa(naa-3*nP+1:naa),3,nP)'

% Constraint matrices.

% All 18 functions zero at the origin and
% dxy(1) = dxz(1) = dyz(1) = 0;
```

```
  Ca = zeros(21,na);

  for k = 1:9
      Ca(k,(k-1)*nt+1) = 1;
      Ca(k+9,(k-1)*nr+9*nt+1) = 1;
  end
  c1 = cheb2(1,nt,0,1);

  Ca(19,      (nt+1:2*nt)) = c1;
  Ca(20,    (2*nt+1:3*nt)) = c1;
  Ca(21,    (5*nt+1:6*nt)) = c1;

    Ka = [zeros(21,3+3*nY+6*nT) Ca zeros(21,3*nP)];

    naa = size(Ja,2);

% Constrain t1 to be zero.
  Ct = zeros(6,naa);
  Ct(1:6,3*nY+4:3*nY+9) = eye(6);

   Ka = [Ka; Ct];

% Scale of Y.

  Cy = zeros(1,naa);
  Cy(1,4) = 1;
  Cy(1,4+24) = -1;

   Ka = [Ka; Cy];


% Constrain the centroid of p.

  Cp = zeros(3,naa);
  for h = 1:nP
     Cp(:,naa-3*h+1:naa-3*h+3) = eye(3);
  end

  Ka = [Ka; Cp];

  [mK,nK] = size(Ka');

% Determine the orthogonal constraint matrix.
  [Q,RKa]=qr(Ka');

  QK = Q(:,nK+1:mK);

% Jacobian matrix for the constrained parameters.
  Jred = Ja*QK;

% Assign sigma for random noise (in metres)
%
% 0.5e-6 is 0.5 micron
  % sigma = 0.5e-6;

% Uncertainty matrix for fitted parameters.
   K=36; %sum(diag(S)>1.5);
  [U,S,V] = svds(Jred, K);
```

```
 Z1=V*inv(S)*inv(S)*V';
Vaa = sigma*sigma*QK*Z1*QK';

 uaa = sqrt(diag(Vaa));

 VY = Vaa(4:3*nY+3,4:3*nY+3);

 [VYzs,VYp] = xux2uzsp(Y,VY);

 uyy = sqrt(diag(VYzs));

 Vap = Vaa(3*(nY+1)+6*nT+1:naa,3*(nY+1)+6*nT+1:naa);

 uap = sqrt(diag(Vap));

% Uncertainties associated with CMM error at random locations.

 Xr = 0.1+ 0.8*rand(200,3);

IXr = ones(200,1);

wXr = ones(200,3);

 naaa=length(aa);
aa0 = aa(3*nY+6*nT+1:naaa); %%

[fer,Jer] = fgkempp(aa0,Xdim,nt,nr,Xr,IXr,wXr);
 Ver = Jer*Vap*Jer';

 uer = sqrt(diag(Ver));

 [VEr,VEpr] = xux2uzsp(Xr,Ver);

 uerzs = sqrt(diag(VEr));

 Uerzs =  reshape(uerzs,3,200)';

% Uncertainty calculations for accurate ball plate and probe vectors.

naa = size(Ja,2);
Kaa = zeros(3*(nY+nP),naa);

Kaa(1:3*nY,4:3+3*nY) = 10*eye(3*nY);

Kaa(3*nY+1:3*nY+3*nP,naa-3*nP+1:naa) = 10*eye(3*nP);


Jreda = [Ja;Kaa]*QK;

[U,S,V] = svds(Jreda, K);
 Z1=V*inv(S)*inv(S)*V';
Vaaa = QK*sigma*sigma*Z1*QK';

uaaa = sqrt(diag(Vaaa));
Vaap = Vaaa(3*(nY+1)+6*nT+1:naa,3*(nY+1)+6*nT+1:naa);
```

```
  [fer,Jer] = fgkempp(aa0,Xdim,nt,nr,Xr,IXr,wXr);
  Ver = Jer*Vaap*Jer';

  uer = sqrt(diag(Ver));

  [VEar,VEap] = xux2uzsp(Xr,Ver);

   uearzs = sqrt(diag(VEar));

   Uearzs =  reshape(uearzs,3,200)';


%% Error Calculations

write_fig = 0;

e1=reshape(f1,3,2*18)'; %initial error after 1st iteration
e=reshape(f,3,2*18)';   %final error after 1st iteration
e0=reshape(f0,3,2*18)'; %error before 1st iteration
t=1:2*18;

plot(t, e(:,1),'b',t,e1(:,1),'r'); %pause;

plot(t, e(:,1),'b',t,e1(:,1)-1e-5,'r')

%% prediction
n = 3*nY+6*nT+9*(nt+nr)+3*nP;
a  = aa(3*nY+6*nT+1:n);
[fp1] = fgfbpkempp(aa,nY,nT,nP,X0,IX,wX,R0,Xdim,nt,nr); %X0 with probe
er removed, not the raw X0
%[fp2] = fkempp(a,Xdim,nt,nr,Xa,IX(:,3),wX);
ep1=reshape(fp1,3,2*18)';    %ep1=e
%ep2 = reshape(fp2,3,18)';
for i=1:3
%plot(t, e0(:,i),'y',t, e1(:,i),'b',t,ep1(:,i),'g',t,ep2(:,i),'r')
%plot(t, e1(:,i),'g',t,e(:,i),'b',t,ep1(:,i),'r');

plot(t, e1(:,i),'g',t,-ep1(:,i),'r');
axis auto
%axis([0 200 0 2e-6]);
disp('press Return to continue'); pause;
end

m=2000;
t=1:9;
Xp=X0-ep1*m;
er=(Xa-X0); %simulated errors.  X0,Xa from bp*.m programs. X0:true;
Xa:simulated measurements
Xc=X0+m*er;

figure, hold on
box on
plot(X0(t,1),X0(t,3),'*');
plot(Xc(t,1),Xc(t,3),'og');
plot(Xp(t,1),Xp(t,3),'+r');
axis([0.35 0.6 0.35 0.65]);
hold;
xlabel('X (m)');
ylabel('Z (m)');
title('X axis positioning error (magnified 2000 times)');
```

```
%title('Z axis rotational errors (magnified 2000 times), Z=0.5m)');

pause;
figure, hold on
box on
plot(X0(t,2),X0(t,3),'*');
plot(Xc(t,2),Xc(t,3),'og');
plot(Xp(t,2),Xp(t,3),'+r');
axis([0.4 0.6 0.35 0.65]);
hold;
xlabel('Y (m)');
ylabel('Z (m)');
title('Y axis straightness error (magnified 2000 times)');

pause;
figure, hold on
box on
plot3(X0(t,1),X0(t,2),X0(t,3),'*b')
plot3(Xc(t,1),Xc(t,2),Xc(t,3),'og')
plot3(Xp(t,1),Xp(t,2),Xp(t,3),'+r')
axis([0.35 0.6 0.35 0.65]);
xlabel('X (m)');
ylabel('Y (m)');
zlabel('Z (m)');
title('Z axis yaw errors (magnified 2000 times)');
hold
```

Appendix 3:

Part of the Simulation: Gaussian Process model

```
clear all, close all ,clc
write_fig = 0;


%% T1
n = 9;

% a) Assign ballplate.

  % Inputs
   Y = ballplate2;
   nY = size(Y,1);

  % CMM dimensions in metres.
   Xdim = [0 1; 0 1; 0 1];

   yx = Y(:,1);
   yy = Y(:,2);

   yyy = Y';
   yyy = yyy(:);

  % Ballplate locations in three positions.
   X1 = [ yx yy    0.5*ones(nY,1)];
   X2p = [yx-0.5 zeros(nY,1) yy-0.5]*[1 -1 0; 1 1 0; 0 0
sqrt(2)]/sqrt(2);
   X2 = X2p+0.5;
   X3p = [yx-0.5 zeros(nY,1) yy-0.5]*[1 1 0; -1 1 0; 0 0
sqrt(2)]/sqrt(2);
   X3 = X3p+0.5;

  % Plot Figure 1: 3x3 matrix
   X = X1(:,1);
   Y = X1(:,2);

   figure, hold on
   plot(X,Y,'o')
   title('{\bf Figure 1: Training data X- and Y-coordinates in Location
X1}')
   xlabel ('X (mm)'), ylabel('Y (mm)')
   axis ([0.35 0.65 0.35 0.65])
   pause(1)


% b) Assign sigma for random noise (in m.)
  % 1.0e-6 is 1 micron

   sigma_n = 0.01;
   format compact
   randn('seed',0);
```

```
   ii = 2;
   jj = 2;
   kk = 2;

  %noisex =
[0.01*ii;0.01*ii;0.01*ii;0.01*jj;0.01*jj;0.01*jj;0.01*kk;0.01*kk;0.01*k
k]
   noise = gpml_randn(sigma_n,nY,1);

  % Calculate adding noise
  for i = 1:9
    xx(i) = (noise(i)*0.1*0.2)/max(noise);
  end
  adjnoise = xx';

% c) Assign y (y is the random errors; unit: mm)
  y = adjnoise;

  XT = X + adjnoise;
  YT = Y + adjnoise;
  x = [XT YT];

% d) Plot Figure 2: Y versus X including random errors
  figure, hold on
  plot(XT,YT,'o')
  title('{\bf Figure 2: Plot of Y versus X including random errors}')
  xlabel ('X (mm)'), ylabel('Y (mm)')
  axis ([0.35 0.65 0.35 0.65])
  hold on
  pause(1)


  %% T2

% e) Set the initialization steps
  % Mean function
    meanfunc={@meanZero};

  % Likelihood function
    likfunc = @likGauss;

  % Covariance function
    covfunc=@covSEiso; % choosing SE covfunc

  % Inference function
    hyp.cov = [0;0];
    hyp.mean = [];
    hyp.lik = log(0.1); % If we do not have the optimal parameter
values,
                        % we employ the minimise function based on CG
method

    hyp = minimize(hyp, @gp, -500, @infExact, meanfunc, covfunc,
likfunc, x, y);
                        % to get the optimal parameters

% f) Estimate the whole domain: z (unit: mm)
    z1= 0.4:0.01:0.6; z1 = z1';
```

```
    z2= 0.4:0.01:0.6; z2 = z2';
    z = zeros(441,2);
    for i=1:1:21;
        for j=1:1:21;
            z((i-1)*21+j,1)=z1(j);
            z((i-1)*21+j,2)=z2(i);
        end
    end

% Plot Figure 3: X-,Y-,Z-coordinates with zero mean regression
[m s2] = gp(hyp, @infExact, meanfunc, covfunc, likfunc, x, y, z);
                                                    % m is the
estimation
                                                    % s2 is the
variance
z_temp0=reshape(m,21,21);
i=0.4:0.01:0.6; j=0.4:0.01:0.6;
figure;
mesh(j,i,z_temp0)
title('{\bf Figure 3: Training data X- and Y-coordinates (Mean Zero)}')
xlabel ('x (mm)'), ylabel('y (m)'), zlabel('Errors (mm)')
pause(1)

%% T3

meanfunc = {@meanMylinear_2D};
likfunc = @likGauss;
covfunc = {@covSEiso};
hyp.cov = [-2.013712762984104;-4.082864313671445];
hyp.mean = [-0.179669833204103;0.778362671986138;-0.863234577981942];
hyp.lik = -4.485943839204587;

hyp = minimize(hyp, @gp, -500, @infExact, meanfunc, covfunc, likfunc,
x, y);
                                % -500 can be changed to -5000 if
necessary
                                % get the optimal parameters

% Plot Figure 4: X-,Y-,Z-coordinates with nonzero mean
[m s2] = gp(hyp, @infExact, meanfunc, covfunc, likfunc, x, y, z);
z_tempmx = reshape(m,21,21);
i = 0.4:0.01:0.6; j = 0.4:0.01:0.6;
figure;
mesh(j,i,z_tempmx)
title('{\bf Figure 4: Training data X- and Y-coordinates (Mean
Linear)}')
xlabel ('x (mm)'), ylabel('y (m)'), zlabel('Errors (mm)')
pause(1)

%% T4
% Error Calculation

errors = abs(z_temp0 - z_tempmx);

figure;
mesh(j,i,errors)
title('{\bf Figure 5: Errors}')
xlabel ('X (mm)'), ylabel('Y (mm)'), zlabel('Errors (mm)')
pause(1)
```

Appendix 4:

Part of the Simulation: Error Comparisons

```
% Comparison between the local kinematic error model, GP model, and
% Experiment

%Experiment from CMM measurement using a ball plate:unit m.

Xe = [0.000006922632   0.379402548
      0.000005095517   0.388789432
      0.000003309287   0.389297331
      0.000001580293   0.490356429
      0.000001049189   0.500484984
      0.000006911419   0.501178156
      0.000005093238   0.597454154
      0.000003327074   0.595485484
      0.000001586738   0.604187517];

% Local kinematic error model: unit m.

Xl = [0.0000040021350965496   0.398473436911506
      0.0000047010216799123   0.398778665263544
      0.0000053977379546273   0.399299664074415
      0.0000039863552288421   0.500039501421911
      0.0000046958953204060   0.500958638571635
      0.0000054092190130473   0.500164320182017
      0.0000039814982232220   0.600002286960399
      0.0000047004785837555   0.600433343017248
      0.0000054110551496922   0.600309271707133];

% GP model: unit m.

Xg = [0.000005900052321235   0.389402464616161
      0.000004695421843564   0.398789432126833
      0.000003380998511044   0.399297331201631
      0.000001666197099004   0.500356429388448
      0.000003292403033542   0.500652635669063
      0.000005400359572624   0.500215671160708
      0.000004680076346875   0.599736103814207
      0.000003220329300165   0.601802440235066
      0.000002106791591668   0.599357015828094];

figure, hold on
box on
plot(Xe(:,2),Xe(:,1),'r*','linewidth',2);
xlabel('X (m)');
ylabel('Z (m)');
title('Errors from the CMM measurements :
(unit:m)','fontweight','bold','fontsize',11');
axis([0.35 0.65 0.0000005 0.000008]);
pause(1)

figure
plot(Xl(:,2),Xl(:,1),'og','linewidth',2);
```

```
box on
xlabel('X (m)');
ylabel('Z (m)');
title('Errors from local kinematic model :
(unit:m)','fontweight','bold','fontsize',11');
axis([0.35 0.65 0.0000005 0.000008]);
pause(1)

figure
plot(Xg(:,2),Xg(:,1),'+b','linewidth',2);
box on
xlabel('X (m)');
ylabel('Z (m)');
title('Errors from GP model :
(unit:m)','fontweight','bold','fontsize',11');
axis([0.35 0.65 0.0000005 0.000008]);
pause(1)

figure, hold on
box on
plot(Xe(:,2),Xe(:,1),'m*','linewidth',2);
plot(Xl(:,2),Xl(:,1),'og','linewidth',2);
plot(Xg(:,2),Xg(:,1),'+b','linewidth',2);
axis([0.35 0.65 0.0000005 0.000008]);
xlabel('X (m)');
ylabel('Z (m)');
title('A comparison of errors :
(unit:m)','fontweight','bold','fontsize',11);
```

Appendix 5:

Data from the Certification of the CMM calibration using a ball plate

Ball No.	X (mm)	Y (mm)	Z (mm)
1	0.00000	0.00000	0.00000
2	133.00290	-0.00227	0.02431
3	266.00507	-0.00105	0.03647
4	399.01133	-0.00135	0.02500
5	532.01177	0.00000	0.00000
6	-0.02315	133.01424	0.03210
7	132.97946	133.01362	0.03260
8	265.98404	133.01369	0.01655
9	398.98772	133.01312	0.01506
10	531.98615	133.01594	0.01290
11	-0.02972	266.02582	0.02500
12	132.97166	266.02073	0.05020
13	265.97498	266.02321	0.01598
14	398.97817	266.02608	0.01873
15	531.97721	266.02716	0.01955
16	-0.03190	399.03716	0.02817
17	132.94964	399.03716	0.04030
18	265.94964	399.03716	0.02091
19	398.94976	399.03716	0.04080
20	531.94935	399.03959	0.04205
21	-0.06060	532.04455	0.00000
22	132.94081	532.04455	0.02600
23	265.94029	532.04455	0.05323
24	398.93874	532.04455	0.06065
25	531.93735	532.04455	0.04558